Communications
Research
Centre

COHERENT SUB-APERTURE PROCESSING TECHNIQUES FOR SYNTHETIC APERTURE RADAR

by

K.H. Wu and M.R. Vant

This work was sponsored by the Department of National Defence, Research and Development branch under Project No. 33C06.

CRC REPORT NO. 1388
OTTAWA, JANUARY 1984

Government of Canada
Department of Communications

Gouvernement du Canada
Ministère des Communications

Canada

85-6482/

COMMUNICATIONS RESEARCH CENTRE

DEPARTMENT OF COMMUNICATIONS
CANADA

COHERENT SUB-APERTURE PROCESSING TECHNIQUES FOR SYNTHETIC APERTURE RADAR

by

K.H. Wu and M.R. Vant

(Radar and Communications Technology Branch)

CRC REPORT NO. 1388

January 1984
OTTAWA

This work was sponsored by the Department of National Defence, Research and Development Branch under Project No. 33C06.

CAUTION

The use of this information is permitted subject to recognition of proprietary and and patent rights.

TABLE OF CONTENTS

		Page
ABSTRACT		1
1.	INTRODUCTION	1
2.	BASIC CONCEPT OF COHERENT SUB-APERTURE PROCESSING VIA MATCHED FILTERING	4
3.	GENERAL FORM OF RECEIVED SIGNAL	8
3.1	Spatial-to-Spectral Mapping in Azimuth	10
4.	ONE-DIMENSIONAL AZIMUTH PULSE COMPRESSION WITHOUT RANGE CURVATURE COMPENSATION	13
4.1	Mainlobe Broadening in the Azimuth Dimension	13
4.2	Mainlobe Broadening in the Range Dimension	20
5.	A PIECEWISE QUADRATIC APPROXIMATION - COHERENT SUB-APERTURE PROCESSING	21
6.	COMPUTER SIMULATIONS OF COHERENT SUB-APERTURE PROCESSING WITH PIECEWISE CORRECTION	27
6.1	Form of the Received Signal	28
6.2	Continuous Range Curvature Compensation	29
6.3	Cubic Phase Term Effect	32
6.4	Sub-aperture Processing Computer Simulations	32
7.	ERROR ANALYSIS OF THE EFFECTS OF PHASE AND AMPLITUDE DISTORTIONS, CAUSED BY THE PIECEWISE APPROXIMATION	36
7.1	Spectrum Envelope Distortion	36
7.2	Residual Phase Error	44
7.3	Overall Paired-echo Magnitude	46
7.4	Degradation of Integrated Sidelobe Ratio due to Paired-echoes	46
7.5	Range Invariance of the Piecewise Solution	46
8.	DERAMPING TECHNIQUES	47
8.1	Spectral Analysis Method	51
8.2	Step Transform	56
8.2.1	Formulation of the Step Transform	61
8.2.2	Effect of Weighting on the Step Transform	67
8.2.3	Computer Simulation Results	73
8.2.4	Effects of the Cubic Phase Term on the Step Transform	74
8.2.5	Range Curvature Compensation	79

Page

9. COMPUTATIONAL REQUIREMENTS..... 79

9.1 Computational Requirements for Single Look Cases without Range Curvature and Cubic Term Compensation..... 80

9.1.1 Examples of Cases Without Range Curvature and Cubic Phase Term Compensation..... 85

9.2 Computational Requirements for Single Look Cases with Range Curvature Compensation..... 89

9.3 Computational Requirements for the Coherent Multi-look Cases with Range Curvature and Cubic Phase Compensations..... 91

10 SUMMARY..... 95

11. ACKNOWLEDGEMENT..... 95

12. REFERENCES..... 95

APPENDIX A - Polynomial Truncations of the Taylor Expansion of the Radar Received Signal..... 97

APPENDIX B - Azimuth Resolution..... 99

COHERENT SUB-APERTURE PROCESSING TECHNIQUES FOR SYNTHETIC APERTURE RADAR

by

K.H. Wu and M.R. Vant

ABSTRACT

Coherent sub-aperture techniques for processing synthetic aperture radar (SAR) signals are described. The techniques involve partitioning the full aperture data, in either the time or the frequency domain. Each partition or sub-aperture is then processed independently by the application of a conventional matched filter, or the equivalent. The low resolution images formed by this process are then coherently recombined to form a full resolution image. Such a processing scheme has the advantage of high computational efficiency and provides the capability for the compensation of low frequency spurious motions, even when the SAR is operating in a highly squinted, high resolution imaging situation.

A detailed description of two coherent sub-aperture techniques namely, the multi-look matched filtering approach and the step transform, are presented. The techniques are characterized and the normal computational requirements are evaluated. Computer simulations, which were performed to verify the feasibility of the processing schemes, are also described.

1. INTRODUCTION

In this report two coherent sub-aperture schemes, for compressing synthetic aperture radar (SAR) azimuth data are described. One scheme is based on matched filtering and the other on the step transform. The processing involves breaking up an aperture data set into pieces, in either the spatial or the frequency domain. Each piece, or sub-aperture, which has a fraction of the original bandwidth, is processed individually and then the processed pieces are recombined coherently to restore the original bandwidth and hence the original resolution. As opposed to the usual non-coherent sub-aperture processing, where the major purpose is to smooth out speckle noise at the expense of resolution, the technique described herein is aimed at improving the processing efficiency, within the constraint of having to produce high resolution imagery at high squint

angles. The additional requirements that low frequency spurious target motion must be corrected, and that the whole system performs with limited processor memory, are also imposed. It is also assumed in the following discussions that the angle of the antenna, with respect to the aircraft or satellite velocity vector, remains fixed, i.e., the target is not spotlighted. Most of the techniques can also be applied to spotlight SARs, but that problem is not considered here.

In the first technique, matched filtering via fast convolution, the bandwidth of the recorded data is partitioned in the frequency domain. Each partition, or "sub-aperture", or "look", is extracted by an FIR filter. (The terms "look" and "sub-aperture" are used interchangeably).

Each look is then compressed by a linear FM matched filter specially tailored to overcome the complexities associated with large squint angle and high resolution. In synthesizing each sub-aperture matched filter, a piecewise approximation of its exact phase characteristic at the centre of the look is used. It is assumed that there is little phase deviation over the entire cross-range extent of the look.

As described later in the report, the processing requires that each sub-aperture data be shifted in range to correct for the effects of range curvature. The shifting, which must be done by means of an interpolation operation, requires that a certain minimum number of rows or range cells be in memory simultaneously. Since each sub-aperture is shorter than the full aperture it was extracted from, it is frequently possible to meet the minimum number of rows requirement with sub-aperture processing whereas with full aperture processing it is not. Even in situations where the minimum number of rows requirement is met with the full aperture, it may be advantageous to use sub-apertures to increase the interpolation efficiency.

In situations in which target motion must be compensated, the sub-aperture approach allows, at least in theory, for piecewise compensation of the target motion over the number of sub-apertures. This of course assumes a suitable motion spectrum for the target.

The second technique, known as the step transform [6-9], is a modified form of the deramping technique, wherein small deramp references, whose lengths are a fraction of the full aperture, are used to extract sub-apertures. Upon deramping each look, the data set becomes an ensemble of CW signals whose frequencies correspond to the relative spatial locations of the targets. Then, the target spectra can be extracted using a filter bank, which can be realized by the discrete Fourier transform. The process is repeated for the other sub-apertures, and the extracted spectra, from the sub-apertures that are associated with a given target, are added coherently to form an image of the target at full resolution. The major advantages of this technique include a small requirement for memory and a smaller signal loss than with the conventional deramping technique. This report extends the original concept of the step transform [6-9] and shows how such effects as range curvature and cubic phase error can be overcome.

In the following sections details of the different principles underlying the technique of sub-aperture processing via matched filtering is given. Then, the general form of the radar return, including such effects as range curvature and cubic phase error is formulated, followed by a description of the image quality degradations that result if these effects are left uncompensated. Next, the general form of the sub-aperture (multi-look) matched filter is synthesized, using a piecewise approximation. This is followed by an analysis of the projected performance of the technique, based on the computer simulation. Next, an overview of the various deramping techniques is given and finally, the computational requirements for the approaches are calculated, and their efficiencies compared.

2. BASIC CONCEPT OF COHERENT SUB-APERTURE PROCESSING VIA MATCHED FILTERING

The principle of sub-aperture processing is based on the fact that, provided the frequency variation with respect to time is monotonic, and the amplitudes in the data change gradually, there is a one-to-one mapping between the time and the frequency domains. This phenomenon is known as the principle of stationary phase [3]. How this principle relates to SAR processing is explained next. Point targets paraded on a straight line parallel to the radar flight path will give exactly the same phase history, and will differ only in their respective time delays. If the collected target return ensemble is Fourier transformed, the frequency responses of all targets will be superimposed on the same frequency range, but within the return from each target there will be embedded a linear phase term (in addition to other inherent higher order phase terms), which signifies its spatial location. A look extraction process in the frequency domain is equivalent to simultaneous look extractions for all targets illuminated by the same portion of the antenna pattern. The portion of the spatial look thus extracted depends on the frequency-space relationship, which in turn is governed by the geometrical complexity of the imaging scenario. The relationship between frequency and space is greatly simplified, indeed it is one-to-one, if the principle of stationary phase holds.

In order to facilitate the illustration of the concept, we assume that the Doppler phase history traced by a point target is purely quadratic (i.e. linear FM) over a full aperture, of duration T. This typifies the side-looking, low resolution case. The form of this one-dimensional signal is

$$\mu(t) = \text{rect}\left[\frac{t}{T}\right] e^{j\frac{\pi B t^2}{T}}, \qquad (1)$$

where B is the bandwidth in Hz, and rect $\left[\frac{t}{T}\right]$ is a rectangular function of duration T. Assuming the time-bandwidth product is sufficiently large, the Fourier transform of $\mu(t)$ can be approximated, using the principle of stationary phase [3] as:

$$U(f) = F\{\mu(t)\} = \sqrt{\frac{T}{B}}\,\mathrm{rect}\left[\frac{f}{B}\right] e^{-j\frac{\pi Tf^2}{B} + \frac{\pi}{4}} \qquad (2)$$

where $F\{\}$ denotes the Fourier transform operation. The first and the last factors are of no importance to our formulation, and hereafter are dropped.

The spectrum can be broken up into N_L (even) equal looks as shown in Figure 1 and the signal spectrum in (2) is partitioned to give:

$$U(f) = \left\{ \sum_{q=-N_L/2}^{N_L/2-1} \mathrm{rect}\left[\frac{f - \frac{2q+1}{2N_L}B}{B/N_L}\right] \right\} e^{-j\frac{\pi Tf^2}{B}} . \qquad (3)$$

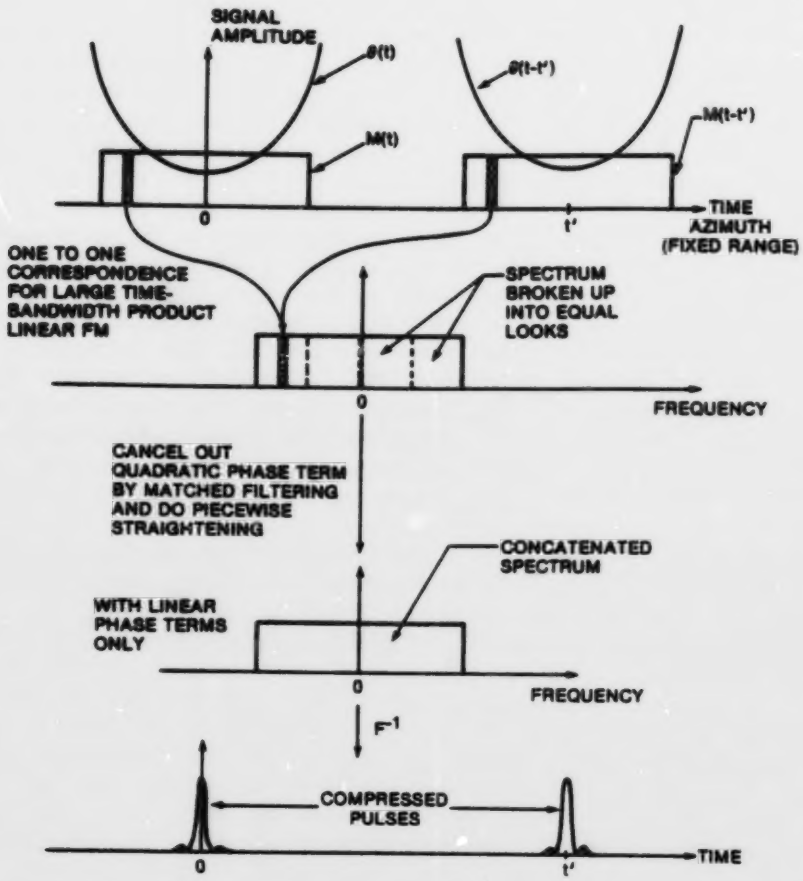

Fig. 1 - Basic principle of coherent sub-aperture processing for two ideal linear FM signals.

The rect[ ] can be thought of as an ideal low pass extraction filter with bandwidth B/N_L and centred at $\frac{2q+1}{2N_L}B$.

If the q^{th} look spectrum is shifted to baseband by substitution

$$f \to f' + \frac{2q+1}{2N_L}B, \tag{4}$$

it becomes,

$$U'_q(f) = U_q\left(f + \frac{2q+1}{2N_L}B\right),$$

$$= \text{rect}\left[\frac{N_L f'}{B}\right] e^{-j\frac{\pi T}{B}\left(f'+\frac{2q+1}{2N_L}B\right)^2},$$

$$= \text{rect}\left[\frac{N_L f'}{B}\right] e^{-j\frac{\pi T}{B}f'^2} e^{-j\frac{2\pi T}{B}\left(\frac{2q+1}{2N_L}B\right)f'} e^{-j\frac{\pi T}{B}\left(\frac{2q+1}{2N_L}\right)^2 B^2}. \tag{5}$$

The last two exponential factors are look dependent and deterministic, so they must be taken out before the universal matched filter is applied. When this is done,

$$U''_q(f) = U'_q(f') e^{j\frac{2\pi T}{B}\left(\frac{2q+1}{2N_L}B\right)f' + j\frac{\pi T}{B}\left(\frac{2q+1}{2N_L}\right)^2 B^2},$$

$$= \text{rect}\left[\frac{N_L f'}{B}\right] e^{-j\frac{\pi T}{B}f'^2}, \tag{6}$$

is obtained. The matched filter for $U''_q(f')$ is

$$M(f') = \text{rect}\left[\frac{N_L f'}{B}\right] e^{j\frac{\pi T}{B}f'^2}. \tag{7}$$

After multiplication by the matched filter in the frequency domain, the compressed signal is

$$R_q(f') = U''_q(f')\, M(f') = \text{rect}\left[\frac{N_L f'}{B}\right]. \tag{8}$$

After frequency shifted back to its orignal frequency position, using (4) for the relationship between f and f', the correlated signal becomes

$$R_q(f) = \text{rect}\left[\frac{N_L}{B}\left(f - \frac{2q+1}{2N_L}B\right)\right]. \tag{9}$$

The same process can be applied to all the other looks, and then the looks can be summed or concatenated together to form the original bandwidth signal,

$$R(f') = \sum_{q=-\frac{N_L}{2}}^{\frac{N_L}{2}-1} \text{rect}\left[\frac{N_L}{B}\left(f - \frac{2q+1}{2N_L}B\right)\right],$$

$$= \text{rect}\left[\frac{f'}{B}\right]. \qquad (10)$$

The compressed pulse, or the point spread function of the point target, is obtained by taking the inverse Fourier transform of R(f'), i.e.,

$$r(t) = B\,\text{sinc}(Bt). \qquad (11)$$

Alternatively, the summation can be performed in the time domain

$$r(t) = \sum_{q=-\frac{N_L}{2}}^{\frac{N_L}{2}-1} \mathcal{F}^{-1}\left\{\text{rect}\left[\frac{N_L}{B}\left(f - \frac{2q+1}{2N_L}B\right)\right]\right\},$$

$$= \sum_{q=-\frac{N_L}{2}}^{\frac{N_L}{2}-1} \frac{B}{N_L}\,\text{sinc}\left(\frac{Bt}{N_L}\right) e^{j2\pi\left(\frac{2q+1}{2N_L}\right)Bt},$$

$$= B\,\text{sinc}(Bt). \qquad (12)$$

The above analysis is illustrated in Figure 1, where two point targets located at t=0 and t=t' and at the same slant range are assumed to be present. A Fourier transform over the entire time domain results in superimposed spectra of the two targets, since they both have the same phase characteristic. Moreover, there is a one-to-one correspondence between the time and the frequency domains, as illustrated by the mapping of two corresponding strips of the time signals into a single superimposed strip in the frequency domain. The spectrum is then partitioned into equal looks. Each look is individually processed. All the processed look spectra are then concatenated and inverse Fourier transformed to form the final compressed pulses. Since the system is linear, an ensemble of target returns can be processed simultaneously. The processing procedure is summarized in Figure 2, where the coherent look summation takes place in the time domain.

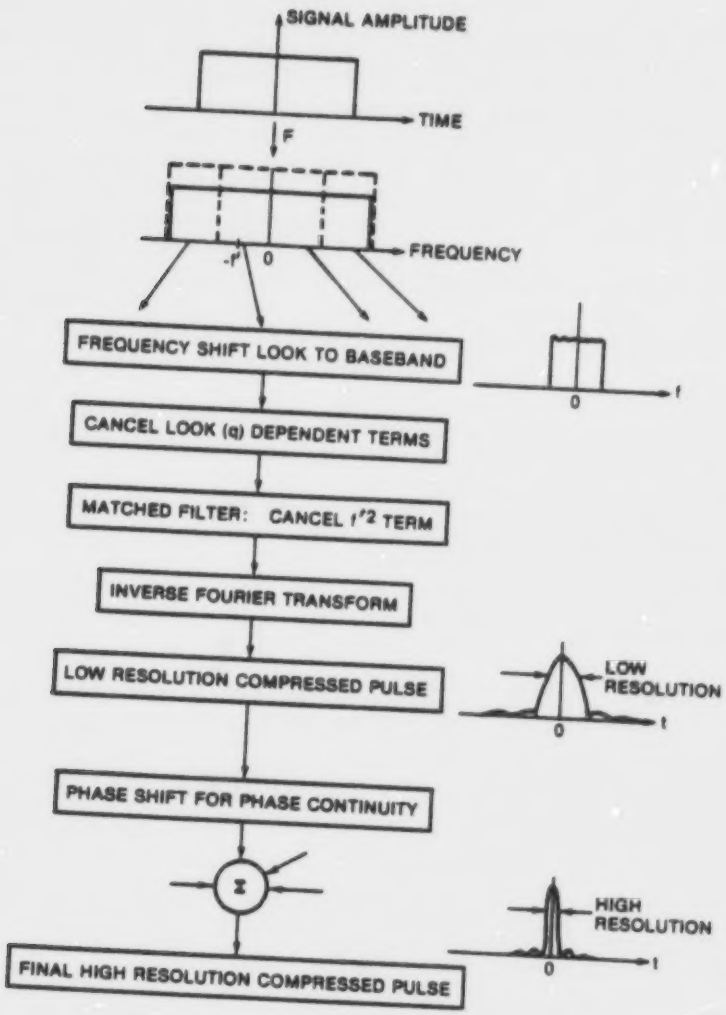

Fig. 2 - Coherent sub-aperture processing procedure for an ideal linear FM signal.

Other than the fact that the foregoing approach can ease the computer memory requirement in some cases, it is obvious that such a processing scheme would be redundant if the input signal is as simple as that given by (1). However, complications arise under different operating conditions such as: high squint angles, long integration periods, and spurious target motions. In order to combat these complications, with little loss of processing efficiency and small increase in memory requirements, it may be necessary to fine-tune a matched filter for each segment (look or sub-aperture) of the input data. The inter-relationship between the sub-aperture and this fine-tuning procedure will be discussed further in the following sections.

3. GENERAL FORM OF RECEIVED SIGNAL

The received signal in the azimuth dimension, encompasses more complications than the one-dimensional linear FM signal described in the previous section. When the antenna is squinted away from the side-looking position, abnormalities in phase and time of arrival of the radar return signal become a problem. In general, higher order phase terms (e.g. the cubic term) may severely degrade the compressed pulse width and the integrated sidelobe ratio. If the time of arrival of the radar return signal and the digitization timing are not synchronized then the range compressed target history associated with a point target is no longer confined to a single row of digitized azimuth data, but instead spans several range cells. This phenomenon is commonly known as range migration. A thorough treatment of these effects can be found in [2].

Next, we will describe, in terms of the slant range and squint angle, a general form of the received signal. This formulation will provide for a better understanding of the various complications and hint at ways to suppress image quality degradations, while still maintaining a reasonable degree of computational efficiency.

With reference to the flight geometry depicted in Figure 3, the distance, r(s), between the radar and a point target on the ground, for a flat Earth model, is

$$r(s) = \sqrt{s^2 + r_p^2 - 2sr_p\cos\eta_p}, \qquad (13)$$

where s is the distance along the radar flight path, r_p (=r(o)) is the

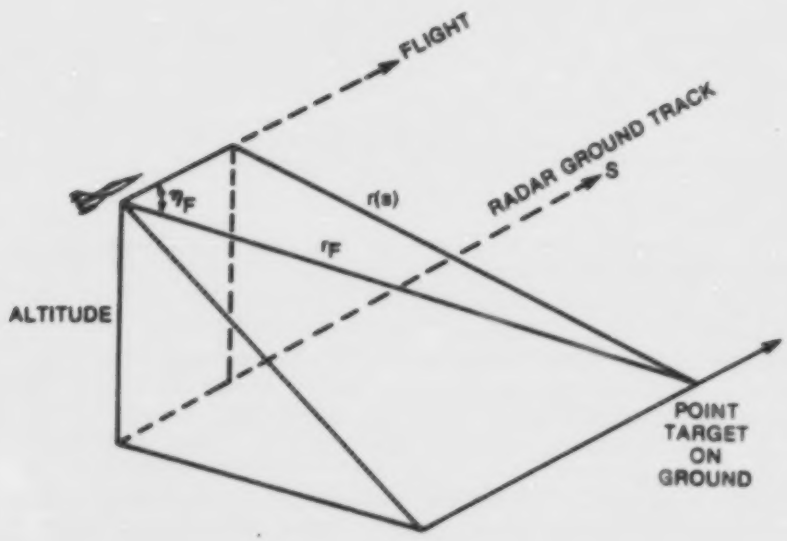

Fig. 3 - Airborne SAR geometry with fixed antenna squint angle (assuming flat Earth).

slant range at the centre of the aperture, and η_p is the squint angle, measured between the slant range and the aircraft velocity vector, as shown in Figure 3.

For ease of analysis, the right hand side of (13) is expanded into a Taylor's series, i.e,

where $a_0 = r_p$,

$$a_1 = -\cos\eta_p,$$

$$a_2 = \frac{\sin^2\eta_p}{2r_p^2},$$

$$a_3 = \frac{\cos\eta_p\sin^2\eta_p}{2r_p^2},$$

and,

$$a_4 = \frac{\sin^2\eta_p(5\cos^2\eta_p-1)}{r_p^3},$$

and the form of the received signal can be expressed as a two-dimensional function, i.e.,

$$g_D(t',s) = \psi\left[t' - \frac{2}{C}\,r(s)\right] e^{-j\frac{4\pi}{\lambda}r(s)}, \qquad (15)$$

where C is the velocity of propagation,

$$t' = t - m\Delta,$$

is the time measured from the start of the m^{th} pulse, and represents the along range dimension,

$$s = mV_{eq}\Delta,$$

is the distance travelled by the sub-aircraft point along the sub-aircraft track during m interpulse periods of length Δ sec., and represents the azimuth (cross-range) dimension, V_{eq} is the radar platform velocity, λ is the transmitted carrier wavelength in metres, and $\psi(t)$ is the compressed range profile. The time delay embedded in ψ signifies the range curvature variation over the aperture. The scattering magnitude and the antenna pattern are assumed to be unity.

The series given in (14) converge. In most practical cases, when calculating the amount of range migration in ψ, only the terms up to the quadratic need to be included. However, when calculating the phase term, which must be accurate to within 0.75π at aperture edge with heavily

windowed data, the cubic term sometimes has to be included (see Appendix A). With these modifications the general form of the received signal becomes

$$g_D(t',s) = \psi\left[t' - \frac{2}{c}(a_o + a_1 s + a_2 s^2)\right] e^{-j\frac{4\pi}{\lambda}[a_o + a_1 s + a_2 s^2 + a_3 s^3]} \quad (16)$$

The envelope term in (16) shows that the locus of the ridge of the range compressed data is defined by a parabola, $t' = \frac{2}{c}(a_o + a_1 s + a_2 s^2)$, in the (t',s) domain. The tilted linear locus, due to the $a_2 s^2$ term, is known as range curvature [9]. In squinted mode SAR, the amount of range walk can span several range cells, thereby prohibiting the use of one-dimensional processing. In practice, range walk can be avoided by acquiring data along the line $a_o + a_1 s$, this simplifies the argument of ψ; and by demodulating the data in azimuth to remove the $a_1 s$ phase term. Thus $g_T(t',s)$ can be rewritten as

$$g_T(t',s) = \psi\left[t' - \frac{2}{c} a_2 s^2\right] e^{-j\frac{4\pi}{\lambda}[a_o + a_2 s^2 + a_3 s^3]} \quad (17)$$

The acquisition scheme is implemented by triggering the A/D conversion $\frac{2}{c}(a_o + a_1 s)$ sec. after an FM pulse is transmitted. As the radar platform advances in the s-dimension, the A/D triggering delay time also changes accordingly. In doing so, individual target data are placed on arectangular grid of a two-dimensional computer memory array, and thereby minimizes range migration in the range dimension. This is shown in Figure 4. The recorded data look as if they were taken in the side-looking position ($\eta_p = 90°$). However, there is a major complication: targets with different true ranges, r_p, and thus requiring different phase compensation, are mapped into the same processing cell. The processing scheme outlined here does not allow different compensation to be applied to the various targets if they lie in the same cell. Therefore, the region, over which the same compensation can be used, must be large enough to accommodate the change in true range with azimuth as we move from one end of the cell to the other.

3.1 Spatial-to-Spectral Mapping in Azimuth

Since the look extraction and matched filtering are performed in the frequency domain, it is necessary to know the form of the range curvature in that domain. The mapping of range curvature between space and frequency will not alter the overall parabolic shape of the curvature significantly. Based on the principle of stationary phase, it can be seen

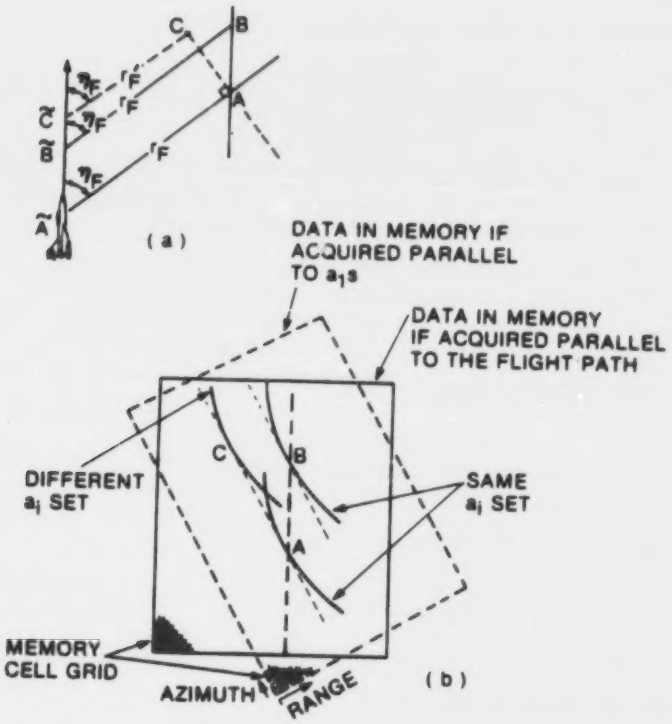

Fig. 4 - Two data acquistion schemes, (i) parallel to flight path, (ii) parallel to $a_1 s$. (a) Shows flight geometries for three targes, A, B, C. (b) Shows the corresponding data memory arrangement for the two schemes.

that the most important term in the mapping is the quadratic phase term, $\frac{4\pi}{\lambda} a_2 s^2$. This reinforces our notion that the shape is parabolic. However, it is not that simple. The cubic phase term, $\frac{4\pi}{\lambda} a_3 s^3$, introduces a non-linearity into the mapping, which slightly distorts the parabolic shape of the range curvature. The form of the mapping is discussed in the next paragraph.

The point-to-point correspondence between the two domains is obtained by differentiating the phase term, $\theta(s)$, given in (17):

$$\theta(s) = -\frac{4\pi}{\lambda}\left(a_o + a_2 s^2 + a_3 s^3\right), \tag{18}$$

so

$$f = f(s) = \frac{1}{2\pi}\frac{d\theta(s)}{ds} = -\frac{2}{\lambda}\left(2a_2 s + 3a_3 s^2\right), \tag{19}$$

or

$$3a_3 s^2 + 2a_2 s + \frac{\lambda f}{2} = 0. \tag{20}$$

The solution to this quadratic equation in s is

$$s = \begin{cases} \dfrac{-2a_2 + \sqrt{4a_2^2 - 6a_3\lambda f}}{6a_3}, & \text{for } a_3 \neq 0; \\ -\dfrac{\lambda f}{4a_2}, & \text{for } a_3 = 0. \end{cases} \tag{21}$$

The f-s curve given by (19) is sketched in Figure 5.

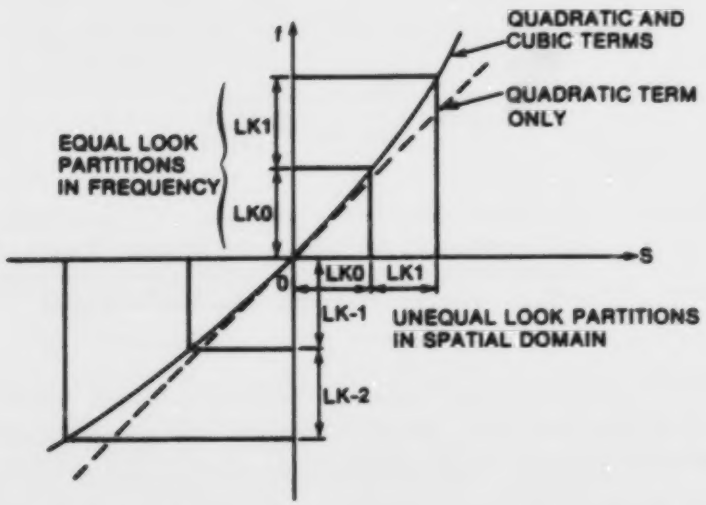

Fig. 5 - Dependence of frequency f on distance s. Look partitions, denoted by LK-2, LK-1, LK0, LK1.

$$d_1(f) = \begin{cases} \dfrac{2a_2}{CT}\left[\dfrac{-2a_2 + \sqrt{4a_2^2 - 6a_3\lambda f}}{6a_3}\right], & \text{for } a_3 \neq 0; \\ \dfrac{\lambda^2}{8a_2 CT} f^2, & \text{for } a_3 = 0. \end{cases} \tag{22}$$

where T is the range sampling interval. In general, a_3 is small, and d_1 can be approximated as

$$d_1(f) \approx \frac{\lambda^2}{8a_2CT} f^2, \qquad (23)$$

which is a parabola, as noted before.

4. ONE-DIMENSIONAL AZIMUTH PULSE COMPRESSION WITHOUT RANGE CURVATURE COMPENSATION

The exact matched filter for the SAR given by (17) is two-dimensional [2]. Two-dimensional data processing is characterized by its massive data size, and its efficiency is contrained by the available computer memory space. Therefore it would be advantageous if one-dimensional processing could be used instead. This can be achieved under either of two circumstances:

(i) if the range and azimuth signals can be decoupled by breaking up the aperture into small pieces, each one exhibiting negligible curvature,

or

(ii) if the range curvature is small enough to be disregarded.

In this section, we will assess the degradation due to uncompensated range curvature and in Section 5 we will consider the decoupling approach.

The dominant deterioration caused by range curvature is the broadening of the mainlobe of both the azimuth and the range compressed pulse. We will attempt to characterize the mainlobe broadening effects in range and azimuth in a simple manner, while still keeping the description general. Because of the non-linear and three-dimensional nature of the scenario, namely, range, azimuth and signal amplitude, a more precise characterization can only be obtained by empirical means, and then only for a limited set of parameters.

4.1 Mainlobe Broadening in the Azimuth Dimension

A typical range compressed profile exhibiting range curvature is shown in Figure 6. Profiles of the uncompressed azimuth signal in the spatial and the frequency domains are shown in Figures 7(a)-(c). The envelopes of these profiles are shaped by coupling between the range and azimuth signals. Antenna pattern effects have been neglected. Provided that a Hamming (or similar) window is used during range compression and that the range curvature is approximately parabolic, the overall shape of the profiles will be insensitive to practical parameter variations.

In this characterization, the azimuth profile passing through the origin (i.e. at s=0, and f=0) was found to be the major energy contributor (see Figure 7(a)). This centre profile was used to examine the effects of range curvature. A generalized parameter R was used to characterize the extent of the cuvature. R is the ratio of the full bandwidth, N_p cells, measured along the range curvature locus, to the -6dB (half amplitude)

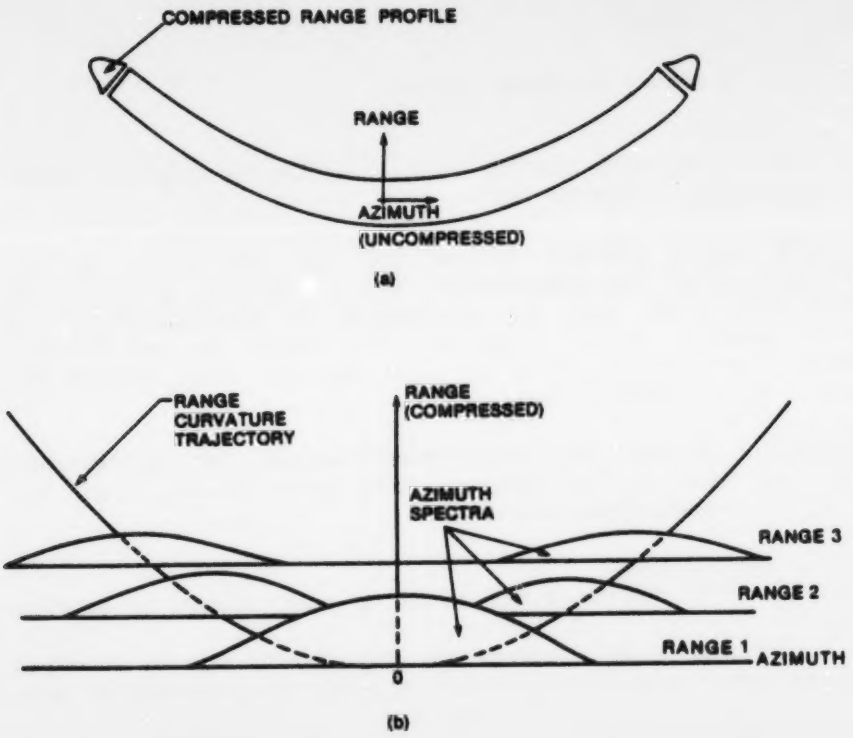

Fig. 6 - Signal history of a point target. (a) Range curvature with compressed range profile. (b) Perspective view of range curvature.

bandwidth, 2n' cells, measured along the middle of the range cell, i.e.,

$$R = \frac{N_p}{2n'}. \tag{24}$$

The parameters R and n' are shown in Figure 8. Note that n' locates the -6dB points in range and azimuth. The offset of the range profile is given by d, which is measured from the centre of curvature (see Figure 8). The parameter d can be used to relate n' to the other parameters. First, d is expressed in terms of the number of range cells of curvature:

$$d = \frac{1.81\gamma_R \Delta S_R}{2}, \tag{25}$$

where the 1.81 factor is the -6dB mainlobe width of a Hamming weighted pulse, expressed in terms of range resolution bins (see [4], p.55), γ_R is

$$\gamma_R = \frac{\text{sampling frequency}}{\text{range signal bandwidth}}; \quad \text{where } \gamma_R > 1, \tag{26}$$

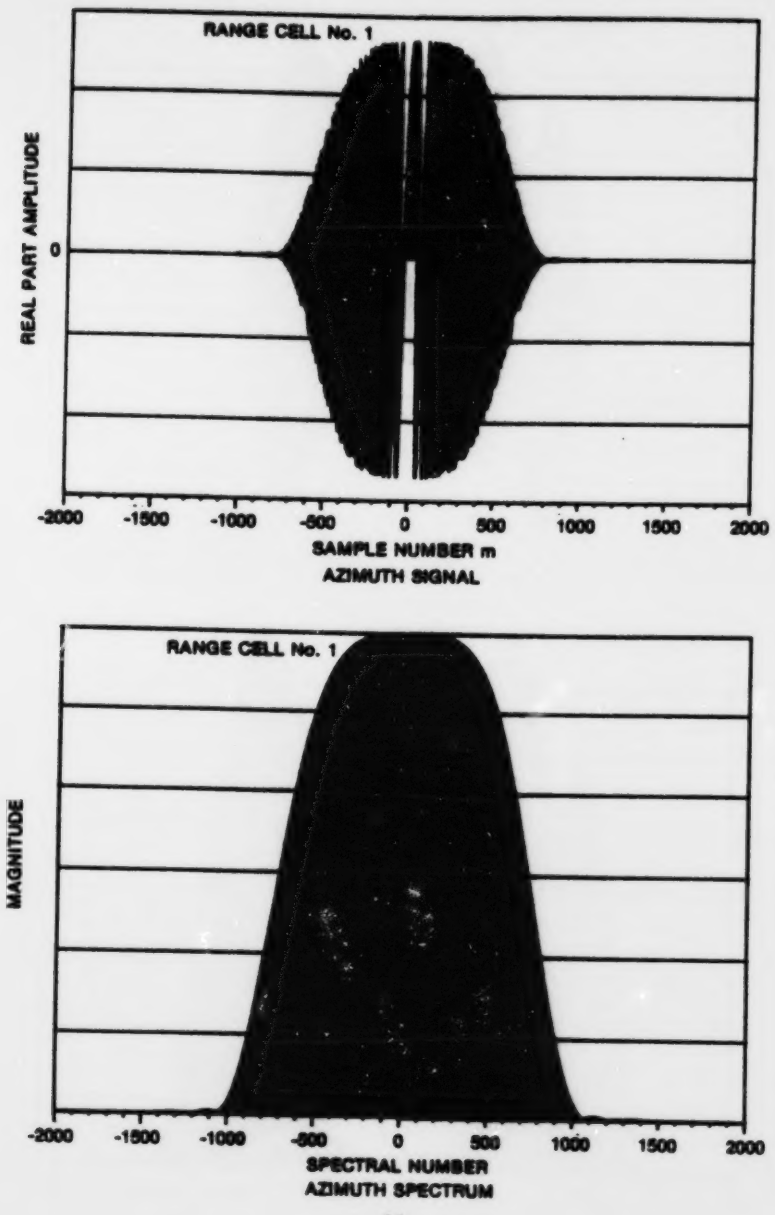

Fig. 7 - Slices of uncompressed azimuth profiles (compressed in the range dimension) in space and frequency domains. In the signal profiles, the horizontal axes denote the samples collected at the pulse repetition frequency. The vertical axes denote the real part of the signal. The azimuth spectra are obtained by taking FFT (4096 points in this...

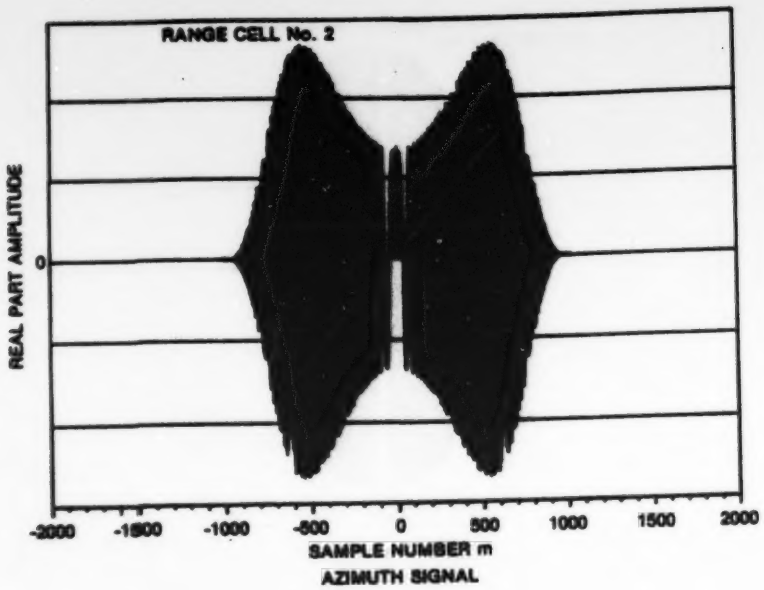

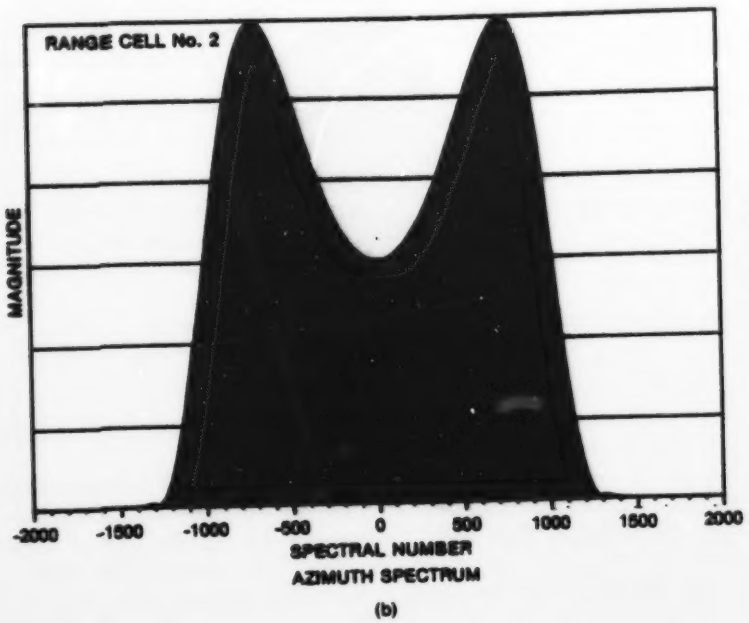

(b)

Fig. 7 (cont.) - case) on the received complex signal. The vertical axes denote the magnitudes of the spectra. (a) corresponds to the profiles through the centre of the range curvature signal (see Figure 6), (b) and (c) are the profiles in the next two adjacent range cells.

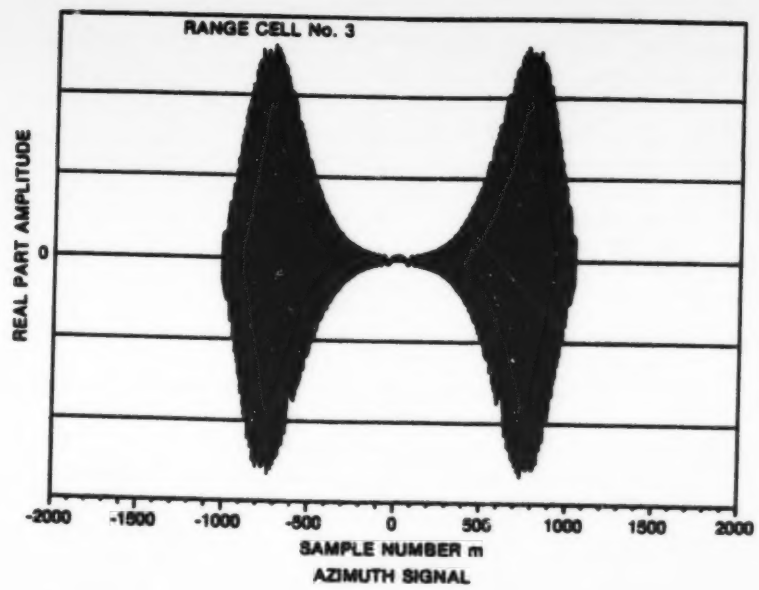
RANGE CELL No. 3
REAL PART AMPLITUDE
0
-2000
-1500
-1000
-500
0
500
1000
1500
2000
SAMPLE NUMBER m
AZIMUTH SIGNAL

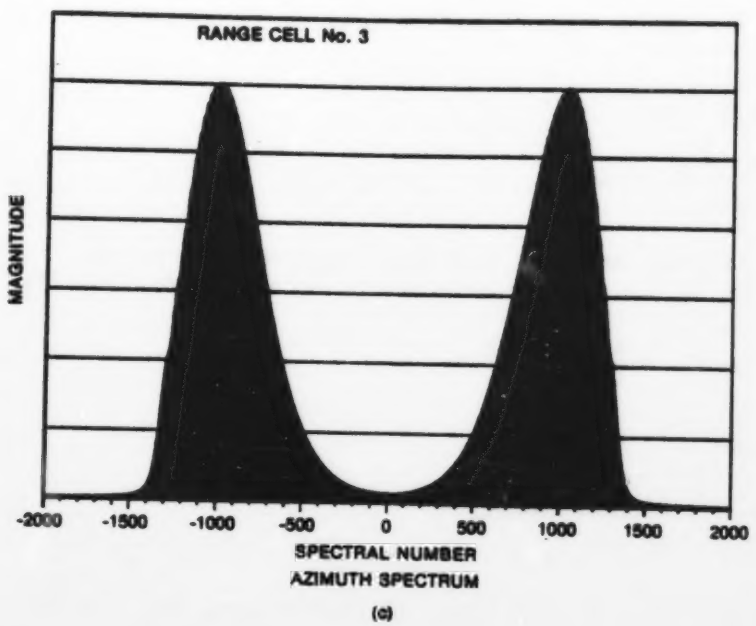
RANGE CELL No. 3
MAGNITUDE
-2000
-1500
-1000
-500
0
500
1000
1500
2000
SPECTRAL NUMBER
AZIMUTH SPECTRUM

(c)

Fig. 17 (cont.) -

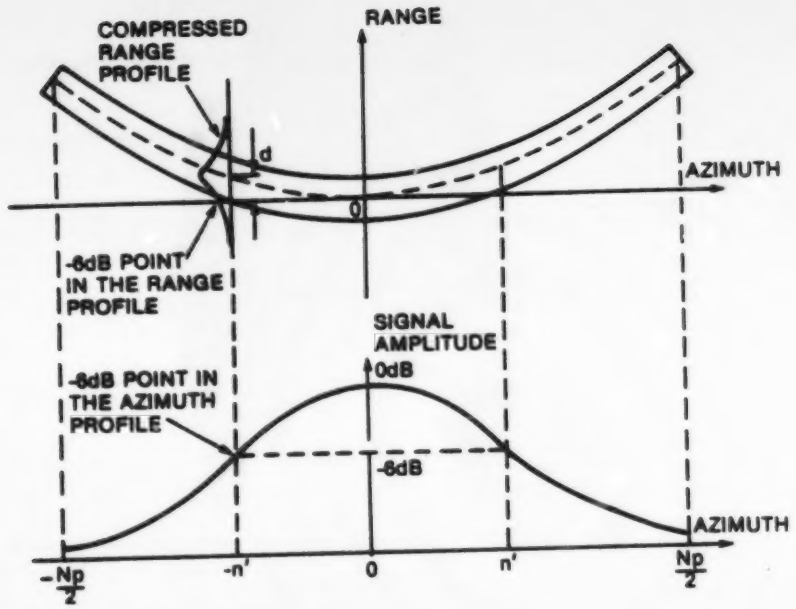

Fig. 8 - Range (compressed) - azimuth (uncompressed) couping.

$$d = a_2 n'^2 \Delta S_A^2$$

$$= \frac{\sin^2 \eta_F}{2r_F} n'^2 \Delta S_A^2, \qquad (27)$$

where ΔS_A is the azimuth sampling interval in metres. The desired expression for n' can now be obtained by equating (25) and (27), i.e.,

$$0.905 \gamma_R \Delta S_R = \frac{\sin^2 \eta_F}{2r_F} n'^2 \Delta S_A^2 , \qquad (28)$$

and solving for n':

$$n' = \sqrt{\frac{1.81\ \gamma_R r_F \Delta S_R}{\Delta S_A^2 \sin^2 \eta_F}} . \qquad (29)$$

This expression for n' can then be substituted in (24) to obtain the desired expression:

$$R = \frac{N_p \Delta S_A \sin\eta_F}{2\sqrt{1.81\ \gamma_R r_F \Delta S_R}}, \qquad (30)$$

The azimuth resolution, as derived in Appendix B, is given by

$$\rho = \frac{1.4\ \lambda r_p}{2N_p \Delta S_A \sin\eta_p} \quad . \tag{31}$$

This can be substituted in (30) to further simplify the expression for R, i.e.,

$$R = \frac{0.26\lambda}{\rho}\sqrt{\frac{r_p}{\gamma_R \Delta S_R}} \quad . \tag{32}$$

The larger the curvature, the larger the value R will be. For small curvature (R<1), the -6dB point is beyond the ends of the azimuth aperture bounded by $\frac{N_p}{2}$, i.e., $|n'| \leq \frac{N_p}{2}$. However, even in this situation, R remains a valid parameter for the characterization.

Computer simulations of the amount of mainlobe broadening were performed for different values of R. The results are plotted in Figure 9. The percent broadening of the compressed mainlobe width, measured at the -10dB points, was defined as

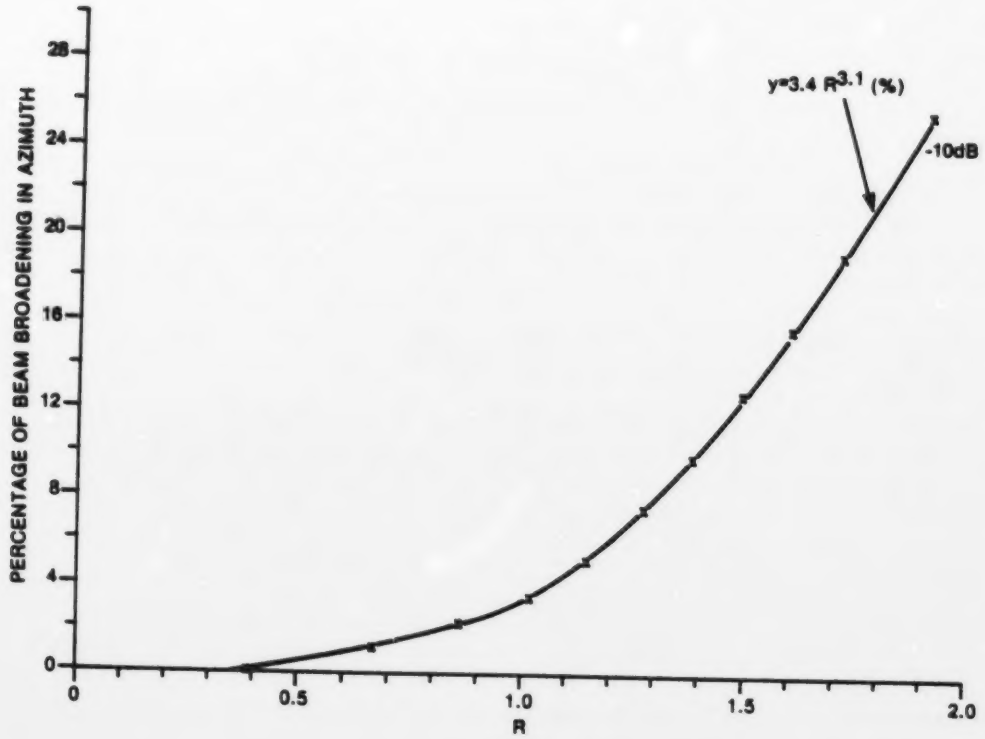

Fig. 9 - Empirical azimuth beam broadening.

$$W_A = \frac{W_u - W_c}{W_c} \times 100\% \qquad (33)$$

where W_u is the mainlobe width without range curvature compensation, and W_c is the mainlobe width with range curvature compensation. Before W_u and W_c were measured, the compressed mainlobes were interpolated by a factor of 100. An empirical equation relating W_A and R, was developed to fit the measurements:

$$W_A = 3.4R^{3.1}, \text{ for } R < 2, W_A < 2.7\%. \qquad (34)$$

In the above computer simulations, a Hamming window was applied in the frequency domain over the uncompensated range curvature azimuth data set before the inverse Fourier transform was taken. Therefore, N_p is no longer a measure of the bandwidth associated with a single point target but is instead a measure of the length of the weighted aperture.

4.2 Mainlobe Broadening in the Range Dimension

With significant range curvature, energy is spilled over onto the concave side of the range curvature thereby broadening the already compressed range profile. If a Hamming window is applied in the frequency domain in azimuth, energy at the end of the curvature is highly attenuated, and the spill-over in the range dimension is small. Computer simulations were used to demonstrate that under normal operating conditions the rate of mainlobe broadening in range is slower than that in azimuth.

A parameter x, which is the number of range cell crossings at the end of the aperture, normalized by the -6dB range mainlobe width, was used as a simple and effective way of characterizing the range broadening. This parameter x is given by:

$$x = \frac{\text{number of range cell crossings}}{1.81\gamma_R},$$

$$= \frac{a_2 \Delta S_A^2 \left(\frac{N_p}{2}\right)^2}{1.81\gamma_R},$$

from (31),

$$x = \frac{0.0338\lambda^2 r_p}{\gamma_R \rho^2}. \qquad (35)$$

Computer simulations of the amount of range mainlobe broadening, expressed as a percentage, were performed for different values of x; the results are plotted in Figure 10. An empirical equation

$$W_R = 1.46x^{2.562}, \text{ for } x < 2, w_R < 9\%, \qquad (36)$$

was found to fit the curve.

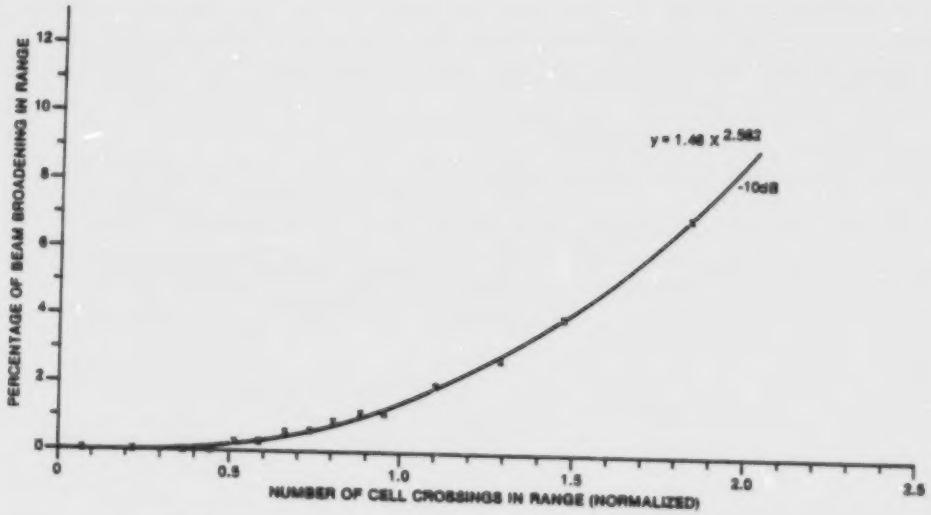

Fig. 10 - Empirical range beam broadening.

5. A PIECEWISE QUADRATIC APPROXIMATION - COHERENT SUB-APERTURE PROCESSING

In this section, a generalized coherent sub-aperture processing technique is described. This technique overcomes the processing problems caused by the non-linearities that arise when imaging at a high squint angle and/or to a high resolution. The reasons for favouring the sub-aperture approach over the continuous straightening approach [11] are two-fold:

i) spurious low frequency motion effects, if they exist, can be corrected over small areas by applying different compensation, e.g. azimuth FM rates, to each sub-aperture; and

ii) The sub-aperture technique, with its piecewise correction, requires much shorter row-lengths than the continuous straightening approach, thus the across-row operations required for the interpolation during range curvature correction can be much more easily accommodated, i.e., more rows can be fit in memory simultaneously.

The major goal is to devise a sub-aperture processing scheme that can remove, without resorting to two-dimensional processing, the distortions attributed to the non-linear effects previously described. As with most problems involving non-linearities, piecewise approximation was deemed to be the simplest approach. Each piece of the signal was assumed to be linear up to a certain degree of error tolerance. Figure 11 illustrates a slant range plane containing the flight path and a point target of interest. The fight path is broken up into several segments to signify different sub-apertures. Each sub-aperture is extracted by an FIR filter

and is then demodulated by a matched filter, especially designed for it. The extraction filtering and the matched filtering can be combined in the frequency domain and the two processes performed simultaneously. All the sub-apertures, except the two end ones, which may only be partly filled, have equal bandwidth.

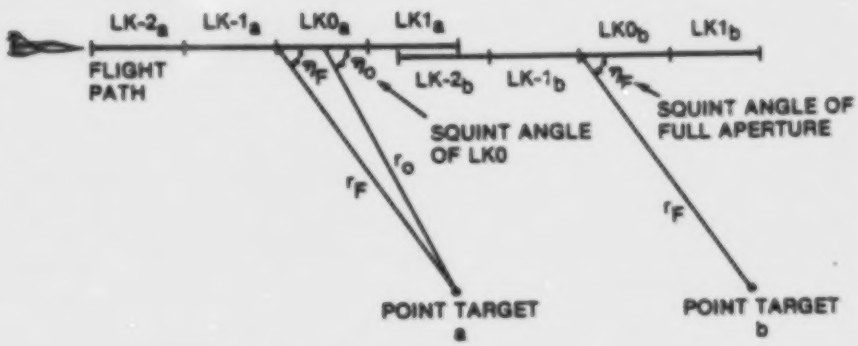

Fig. 11 - A slant plane containing flight path and two point targets, a and b. Note the corresponding look designations (denoted by LK) are displaced by the same amount as the separation between two targets. The look geometries are congruent.

In order to define the matched filters for each sub-aperture several other things must first be done. The look centres in the frequency domain must be located, and their frequency domain locations translated into corresponding spatial domain ones. This ties down the values of effective squint angle, η_q, of the q^{th} look, and slant range to the look centre, r_q, which are required to define the matched filter. Next the phases, over the look and over the local section of the full aperture, are matched. The look phase contains terms of up to quadratic order, whereas the full aperture phase contains terms of up to cubic order. The phase matching must be done in order to maintain coherency over the phase jumps between the looks. Range curvature compensation must also be applied; in this case, as already discussed, the curvature compensation is to be piecewise. Finally, the demodulation which removed the $a_1 s$ term during data acquisition must be accounted for. After all these operations are completed the matched filter can be defined.

Referring back to Figure 11, each look can be thought as independent, with its own look centre, slant range and squint angle. The locations of the look centres are based on the number of looks required, or equivalently, the bandwidth of the extraction filter. In the present scheme, the entire frequency axis is extracted even though part of the spectrum has no signal.

In the frequency domain, the look centre of a sub-aperture is given by,

$$f_q = \frac{2q-1}{2N_L} B_e, \quad -\frac{N_L}{2} - 1 < q < \frac{N_L}{2}, \ N_L \text{ is even}, \tag{37}$$

where q denotes the look index, and B_e is the bandwidth of a pre-designed extraction filter. B_e is a function of the number of looks, N_L, such that $B_e N_L = 0.9 f_s$, where f_s is the sampling frequency. A bandwidth of 0.1fs is reserved as guard-band near the Nyquist frequency.

The look centre in the spatial domain can be calculated using (21):

$$a_q = \begin{cases} \dfrac{-2a_2 + \sqrt{4a_2^2 - 6a_3 \lambda f_q}}{6a_3}, & \text{for } a_3 \neq 0; \\ -\dfrac{\lambda f_q}{4a_2}, & \text{for } a_3 = 0. \end{cases} \tag{38}$$

Once a_q is known, the slant range r_q, to the q^{th} look centre, from the point target of interest, and the squint angle η_q, can be calculated. Referring back to Figure 11, we have,

$$\frac{\sin(180° - \eta_q)}{r_p} = \frac{\sin(\eta_q - \eta_p)}{a_q},$$

$$\text{or,} \quad \eta_q = \tan^{-1}\left[\frac{\sin\eta_p}{\cos\eta_p - \dfrac{a_q}{r_p}}\right]. \tag{39}$$

$$\text{Also,} \quad \frac{\sin\eta_p}{r_q} = \frac{\sin(180° - \eta_q)}{r_p},$$

$$\text{so that } r_q = r_p \frac{\sin\eta_p}{\sin\eta_q}. \tag{40}$$

Equipped with η_q and r_q, and the previously derived quadratic approximation, we can synthesize the phase of the acquired data. Within the q^{th} sub-aperture, the phase is,

$$\theta_q(s') = -\frac{4\pi}{\lambda}(a_{oq} + a_{1q}s' + a_{2q}s'^2), \tag{41}$$

where s' is the spatial co-ordinate with its origin located at the sub-aperture centre,

$$a_{oq} = r_q, \tag{42}$$

$$a_{1q} = -\cos\eta_q, \tag{43}$$

$$\text{and} \qquad a_{2q} = \frac{\sin^2\eta_q}{2r_q} \,. \tag{44}$$

From (16), the phase of the original data is given by,

$$\theta(s) = -\frac{4\pi}{\lambda}\,(a_o + a_1 s + a_2 s^2 + a_3 s^3). \tag{45}$$

The phases $\theta_q(s')$ and $\theta(s)$ must match very closely over the look, i.e.,

$$\theta_q(s') = \theta(s), \text{ for } s = s_q,\ s' = 0,$$

and (46)

$$\theta_q(s') = \theta(s), \text{ for } s_q - \frac{L_s}{2N_L} \le s \le s_q + \frac{L_s}{2N_L}, \text{ i.e., } -\frac{L_s}{2N_L} \le s' \le \frac{L_s}{2N_L},$$

where L_s is the full synthetic-aperture length. Since $s' = s - s_q$, $\theta_q(s')$ can now be written as,

$$\theta_q(s) = -\frac{4\pi}{\lambda}\,[a_{oq} + a_{1q}(s-s_q) + a_{2q}(s-s_q)^2]. \tag{47}$$

Because amplitude matching is unimportant, we can set the amplitude to be unity without piecewise approximation, and rewrite the piecewise synthesized phase signal over the sub-aperture as

$$g_q(t',s) = \psi\left[t' - \frac{2}{C}a_2 s^2\right] e^{j\theta_q(s)},$$

$$= \psi\left[t' - \frac{2}{C}a_2 s^2\right] e^{-j\frac{4\pi}{\lambda}\,[a_{oq} + a_{1q}(s-s_q) + a_{2q}(s-s_q)^2]}. \tag{48}$$

$\psi(t)$ represents the profile of the range compressed pulse over the range dimension, and the variable $\left[t' - \frac{2}{C}\,a_2 s^2\right]$ represents the continuous range curvature, as a function of position in the azimuth aperture. As described in Section 3, range curvature correction is sometimes required to prevent range and azimuth broadening from occurring.

If range curvature compensation is needed, interpolation must be performed on the range compressed signal in the range dimension. The range interpolation can be done in the azimuth frequency domain, prior to azimuth fast convolution compression, or in the azimuth spatial domain, after azimuth compression. In the former approach, the range curvature can be fully compensated, whereas in the latter approach only a piecewise compensation can be done. The reason for this is as follows: once the

azimuth signal is compressed, the curvature phase is transformed into broadening of the range compressed pulse, and the trace of the range curvature is lost. The only way to correct for curvature after the azimuth signal is compressed (i.e. the post-compression scheme previously mentioned), is to use sub-apertures, each of which produces a pulse which is minimally distorted, but is displaced in range from the centre of the range cell. The displacement is equal to the amount of range curvature at the sub-aperture centre. Range shifting of the sub-apertures, by means of interpolation, can be used to remove the curvature. Such interpolation is equivalent to performing a piecewise correction along a single azimuth array in the frequency domain. This is shown in Figure 12. This piecewise curvature compensation is incomplete and causes paired-echoes in the final image, see Sections 6 and 7 for further details.

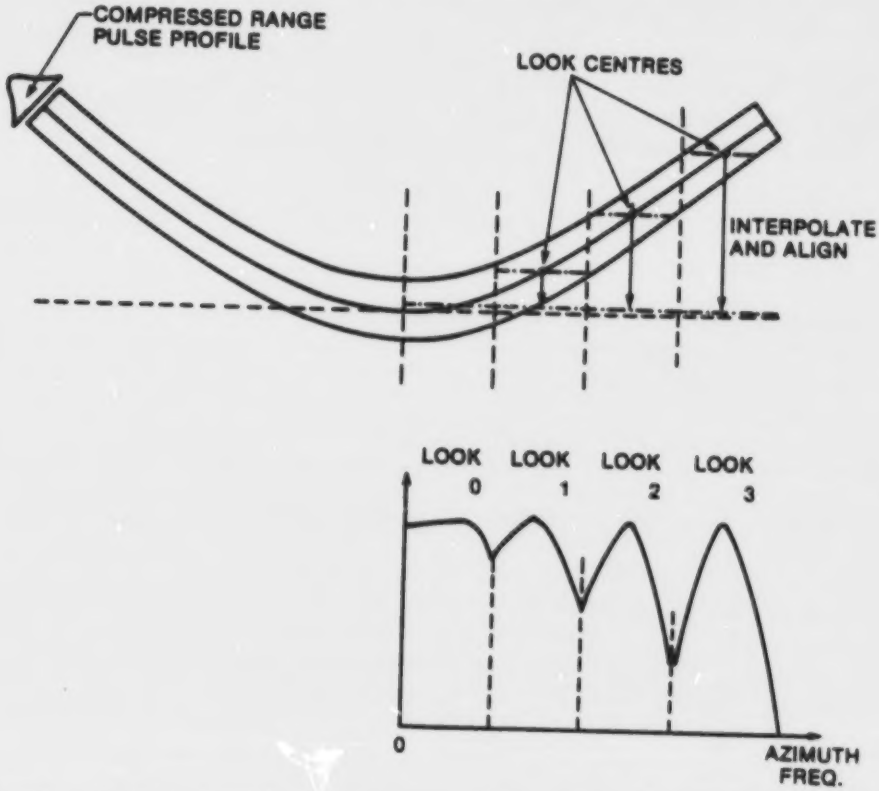

Fig. 12 - Look extraction with range curvature. (a) Signal history of a point target. (b) Look extraction with piecewise range curvature correction (only the positive frequency axis is shown).

Despite these paired-echoes, post-compression interpolation is preferred in the present scheme. This is because there is insufficient computer memory to do the cross-row interpolation operations on the long rows needed for full aperture correction in the range, azimuth-frequency

domain. In this case, the shorter rows required for the piecewise correction of the sub-apertures make the post-compression, range-azimuth spatial co-ordinate correction technique more attractive.

The range curvature profile $\psi(t)$, given in (48), will also be approximated in a piecewise fashion, namely,

$$g_q(t'_q,s) = \psi[t'_q - \frac{2}{c} a_2 s^2] \, e^{-j\frac{4\pi}{\lambda}[a_{oq} + a_{1q}(s-s_q) + a_{2q}(s-s_q)^2]} , \tag{49}$$

over the sub-aperture, where $t'_q = \frac{2}{c} a_2 s_q^2$ near the look centre. $\psi(t)$ now represents a coupled, slanted projection of the compressed range profile onto the uncompressed azimuth profile. This coupling only affects the spectrum magnitude, leaving the phase unaffected. For ease of illustration, $\psi(t)$ will be dropped, i.e., it will be assumed the curvature has been properly corrected. Thus, (49) becomes,

$$g_q(s) = e^{-j\frac{4\pi}{\lambda}[a_{oq} + a_{1q}(s-s_q) + a_{2q}(s-s_q)^2]} . \tag{50}$$

The phase of the original signal is

$$g(s) = e^{-j\frac{4\pi}{\lambda}[a_o + a_1 s + a_2 s^2 + a_3 s^3]} . \tag{51}$$

This signal is modified by removing the phase term $-\frac{4\pi}{\lambda} a_1 s$, during data acquisition, i.e. the recorded phase signal is

$$\tilde{g}(s) = g(s) \, e^{j\frac{4\pi}{\lambda} a_1 s} = e^{-j\frac{4\pi}{\lambda}(a_o + a_2 s^2 + a_3 s^3)} . \tag{52}$$

It now remains to define the matched filter for this signal. Setting $\tilde{g}(s) = \tilde{g}_q(s)$ over the sub-aperture q, we get

$$\begin{aligned} \tilde{g}_q(s) = \tilde{g}(s) &= g(s) \, e^{j\frac{4\pi}{\lambda} a_1 s} , \\ &= g_q(s) \, e^{j\frac{4\pi}{\lambda} a_1 s} , \\ &= e^{-j\frac{4\pi}{\lambda}[a_{oq} + a_{1q}(s-s_q) + a_{2q}(s-s_q)^2]} \, e^{j\frac{4\pi}{\lambda} a_1 s} , \end{aligned} \tag{53}$$

where $\tilde{g}_q(s)$ is a quadratic piecewise approximation to $\tilde{g}(s)$ over the

sub-aperture. Equation (5.17) can be regrouped as,

$$\tilde{g}_q(s) = e^{-j\frac{4\pi}{\lambda}[(a_{oq}-a_{1q}s_q) + (a_{1q}- a_1)s + a_{2q}(s-s_q)^2]}, \quad (54)$$

and the matched filter, m(s), can be derived from this regrouped $\tilde{g}_q(s)$, i.e.,

$$m(s) = \tilde{g}^*(-s),$$

$$= e^{j\frac{4\pi}{\lambda}[(a_{oq} - a_{1q}s_q) - (a_{1q}-a_1)s + a_{2q}(-s-s_q)^2]}. \quad (55)$$

The Fourier transform of m(s) is

$$M(f) = F\{m(s)\},$$

$$= e^{j\frac{4\pi}{\lambda}(a_{oq}-a_{1q}s_q)} \; e^{-j\frac{\pi\lambda}{4a_{2q}} h_o^2 + j2\pi s_q h_o}, \quad (56)$$

where $h_o = f + \frac{2}{\lambda}(a_{1q}-a_1)$. The amplitude of M(f) is normalized to unity, and the small amplitude variations from look to look are ignored. By completing the square of the phase of the second exponent, (5.20) can be rewritten as

$$M(f) = e^{j\frac{4\pi}{\lambda}(a_{oq} - a_{1q}s_q + a_{2q}s_q^2)} \; e^{-j\frac{\lambda\pi}{4a_{2q}}h^2}, \quad (57)$$

where $h = f + \frac{2}{\lambda}[(a_{1q} - a_1) - 2s_q a_{2q}]$.

The q dependent phase terms ensure phase continuity at the boundaries between adjacent looks in the concatenated spectrum. The frequency dependent phase terms cancel the quadratic and linear phase factors in the original data. The above matched filter can be applied directly onto the Fourier transformed data via fast convolution.

6. COMPUTER SIMULATIONS OF COHERENT SUB-APERTURE PROCESSING WITH PIECEWISE CORRECTION

In this section the digital form of the received signal from a unit amplitude point target, and the form of the continuously straightened spectrum of the signal are described; the effect of the cubic phase term is examined; and the results of a computer simulation of piecewise correction, i.e. sub-aperture processing, are presented.

It was assumed in the simulation that a Hamming window was applied to the range frequency data prior to range compression, and that the slope

of range curvature versus azimuth position in the aperture was small at either end of the aperture. It was also assumed that the linear component of range migration was removed during the data acquisition operation.

6.1 Form of the Received Signal.

The digital form of the received signal is

$$G(m,n) = R(m,n)\, e^{-j\frac{4\pi}{\lambda}r(m)}$$

where m,n are the running indices for azimuth and range respectively, R(m,n) is the amplitude profile of the recorded signal, and

$$r(m) = \sqrt{(m\Delta S_A)^2 + r_P^2 - 2m\Delta S_A r_P \cos\eta_P - a_1 m\Delta S_A},$$

$$= \sqrt{(m\Delta S_A)^2 + r_P^2 - 2m\Delta S_A r_P \cos\eta_P + m\Delta S_A \cos\eta_P}, \qquad (58)$$

where ΔS_A is the azimuth sampling interval in metres, and

$-\frac{L_S}{2\Delta S_A} < m < \frac{L_S}{2\Delta S_A}$, where L_S is the synthetic-aperture length in metres.

The last term in (58) accounts for the cancellation, during data acquisition, of the linear term $m\Delta S_A \cos\eta_P$. R(m,n) is the compressed range profile, which runs along the range curvature. It is given by the Fourier transform of the Hamming window [4], i.e.,

$$R(m,n) = D_1 + 0.426(D_2 + D_3), \qquad (59)$$

where $D_1 = \text{sinc}(\frac{x}{\gamma_R})$,

$$D_2 = e^{-j\frac{\pi}{N_W}} \text{sinc}(\frac{x}{\gamma_R} - 1) = \text{sinc}(\frac{x}{\gamma_R} - 1),$$

$$D_3 = e^{j\frac{\pi}{N_W}} \text{sinc}(\frac{x}{\gamma_R} + 1) = \text{sinc}(\frac{x}{\gamma_R} + 1),$$

and N_W is the range data length for compression, which is the same as the window length. The peak amplitude of R(m,n) has been normalized to unity. For large N_W, the phase terms, π/N_W, in D_2 and D_3 are negligible. The variable x is given by

$$x = n - N_O - \frac{r(m)}{\Delta S_R},$$

where ΔS_R is the range sampling interval in metres, γ_R is the

over-sampling factor in range, and N_o is an arbitrary offset for positioning the data in the middle of the two-dimensional computer memory. A profile of a compressed range pulse is shown in Figure 13. To obtain this figure, a set of typical operating parameters was used (see Table 1).

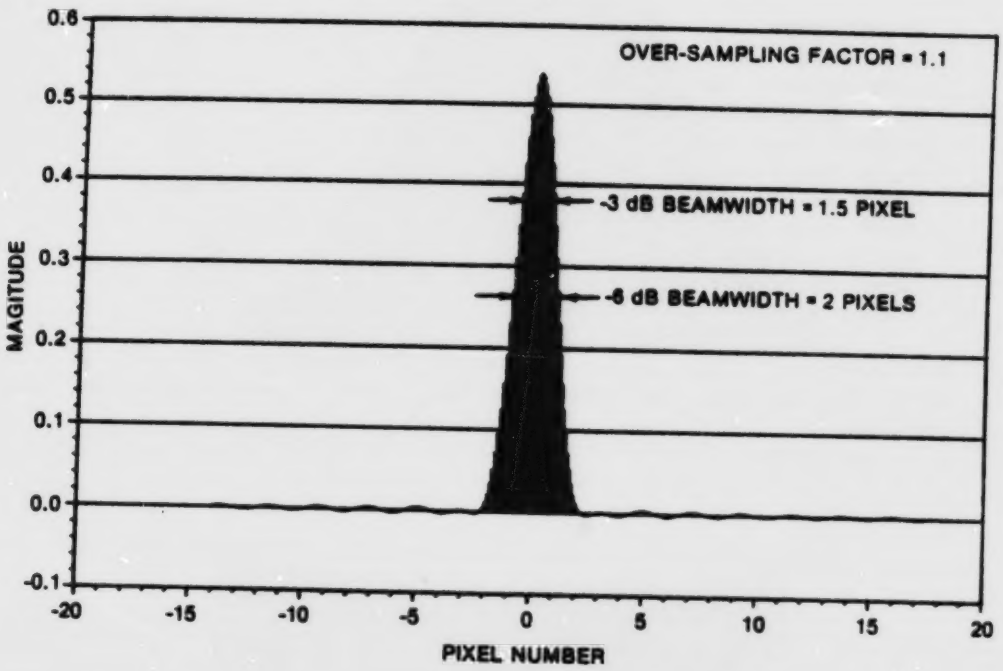

Fig. 13 - Compressed range pulse with Hamming weighting.

6.2 Continuous Range Curvature Compensation

As previously described, one way to remedy the energy spill-over effect caused by range curvature is to straighten out the curvature by continuous correction in the range-spatial, azimuth-frequency domain. An azimuth spectrum, straightened by this method is shown in Figure 14. It is virtually identical to what would be obtained if there were no curvature. The interpolator used in the straightening process was a modified four-point sinc function [5] given by

$$W(x) = \frac{\sin(\pi x)}{\pi x}\left(1 - \frac{x^2}{16}\right), \tag{60}$$

where $x = i + \text{INTEGER}(\ell_1) - \ell_1$, $i = -1, 0, 1, 2,$ (61)

and $\ell_1 = \dfrac{\lambda^2}{8CTa_2\Delta S_A^2 N_T^2} m^2 + n, \; -\dfrac{N_T}{2} \leq m < \dfrac{N_T}{2},$ (62)

TABLE 1

Processing Parameters for Computer Simulation Examples

Parameter	
Stant Range (r_p)	100 km
Wavelength (λ)	0.0321 m
-3dB azimuth resolution (ρ)	1.358 m
Azimuth sampling interval (ΔS_A)	1.617 m
Azimuth over-sampling factor (γ_A)	1.18
Range sampling intervals (ΔS_R)	0.75 m
Range sampling period (T)	5 nS
Range over-sampling factor (γ_R)	1.1
Squint angle (η_p)	30°
Range curvature at the end of the full aperture	2.33

N.B. For examples with squint angles (η_p) equal to 15° and 6°, ΔS_A will be changed accordingly, all other parameters are kept constant.

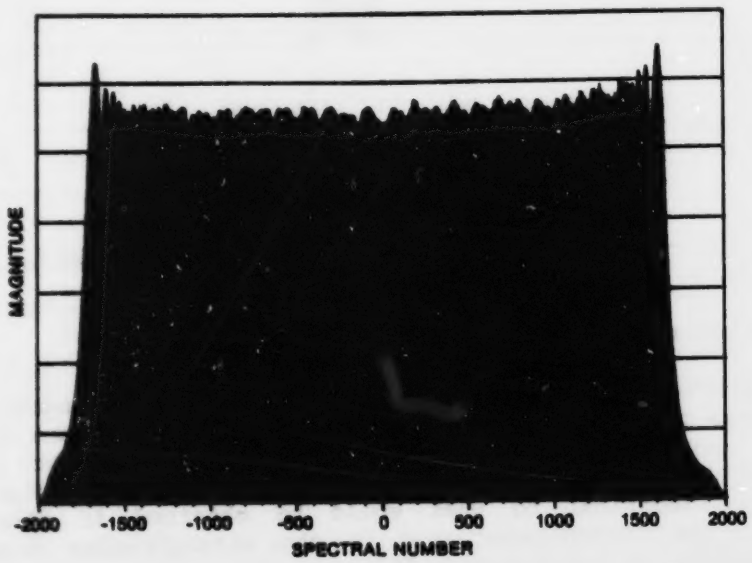

Fig. 14 - Azimuth spectrum continuous range curvature compensation.

where N_T is total number of data points used in processing. Equation (62) is the digital form of (23) with $f = m/N_T\Delta S_A$. The straightened spectrum shown in Figure 14 was then windowed to suppress spectral leakage and multiplied by a matched filter. The windowed spectrum is shown in Figure 15, and the final compressed pulse is shown in Figure 16.

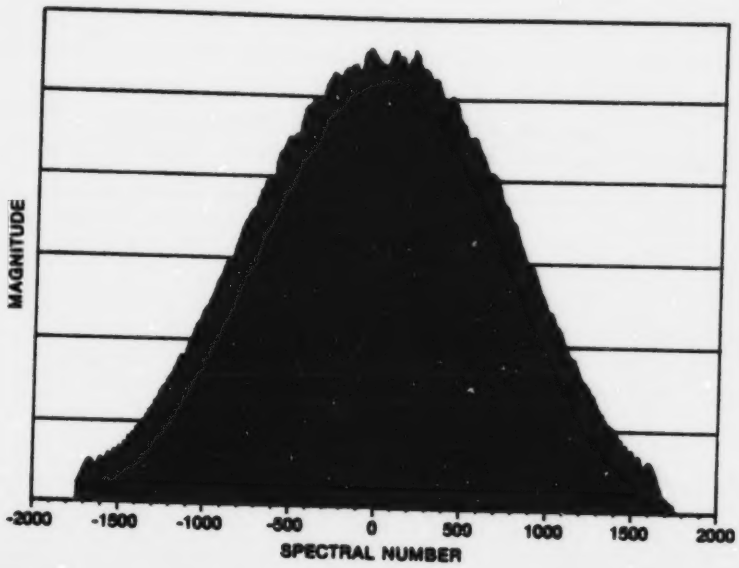

Fig. 15 - Spectrum of Figure 14 with Hamming weighting.

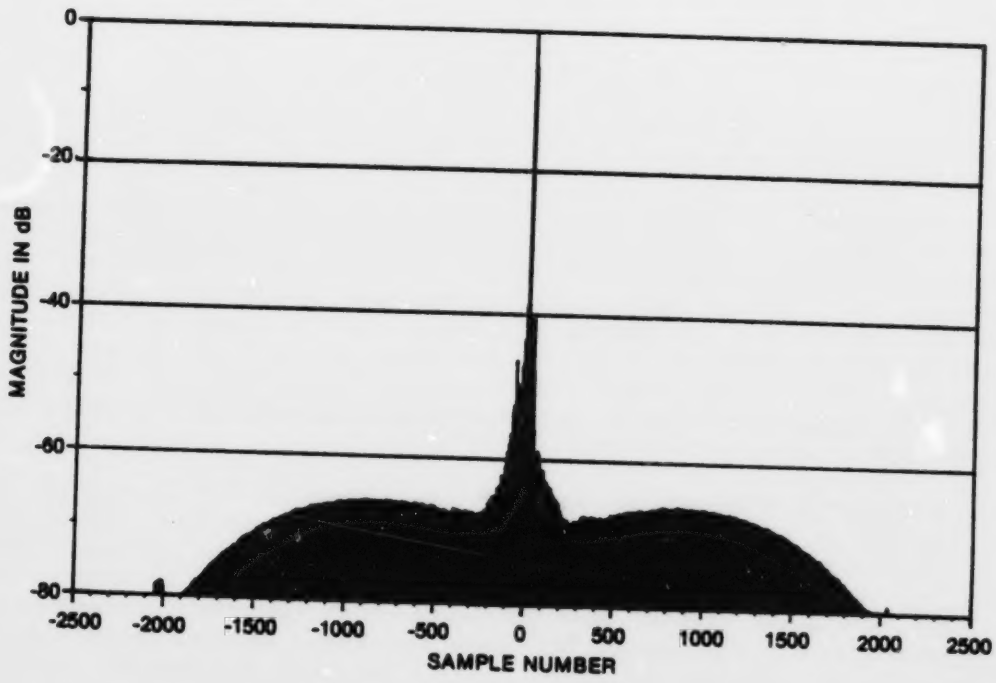

Figure 16 - Compressed pulse with continuous range curvature compensation, (a) overall,

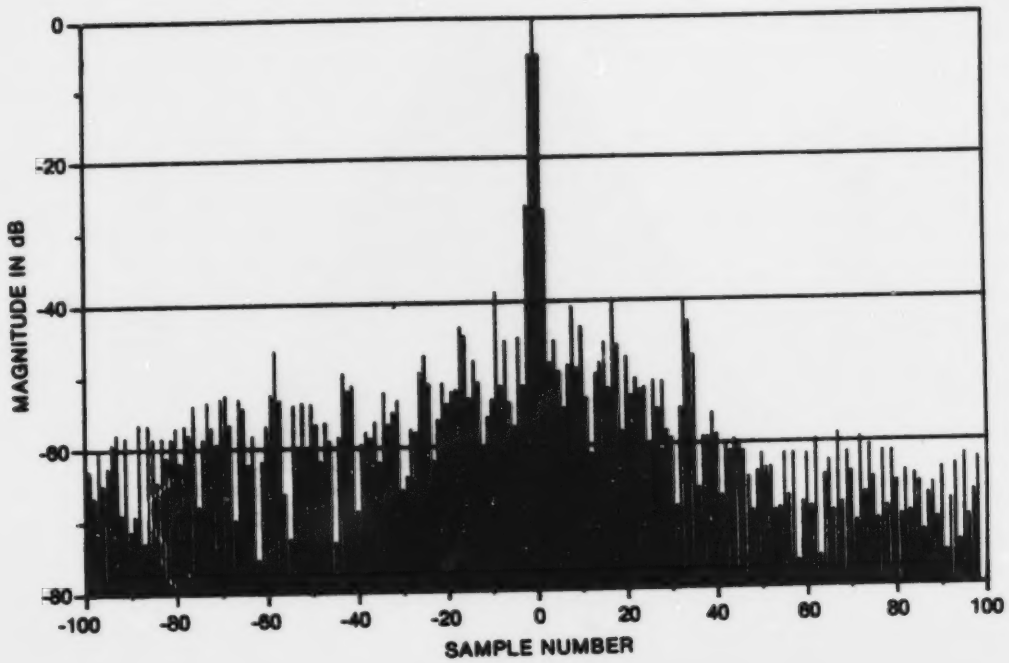

Fig. 16 - (b) zoom in.

6.3 Cubic Phase Term Effect

Aside from the range curvature problem, there may be a problem caused by the cubic phase term. If the cubic phase term is significant relative to the quadratic phase term, as in the highly squinted, high resolution case, a phase correction must be made in addition to the range curvature correction. An example of such a case is shown in Figure 17. In this situation there was a cubic phase error of 1102° at the end of the aperture. This cubic phase error can be eliminated by adding an appropriate cubic phase term in the matched filter, or by using the sub-aperture processing technique.

6.4 Sub-aperture Processing Computer Simulations

In sub-aperture processing, the spectrum is broken up into small pieces or sub-apertures, which are proportionally shorter in length, and can have their FM rates fine-tuned to that of the corresponding sub-aperture data. The form of the frequency domain matched filter is

$$M(n) = e^{j\frac{4\pi}{\lambda}(a_{oq}-a_{1q}s_q+a_{2q}s_q^2)} \; e^{-j\frac{\pi\lambda_w^2}{4a_{2q}}}, \qquad (63)$$

where, $\nu = n + \frac{2N_T \Delta S_A}{\lambda} [(a_{1q} - a_1) - 2s_q a_{2q}]$;

N_T is the FFT length;
ΔS_A is the azimuth sampling interval in metres;
ΔS_q is the spatial location of the look centre, given by (55);

$n = \frac{f}{\Delta f}$; and $\Delta f = \frac{1}{N_T \Delta S_A}$.

Equation (63) is the digital counterpart of (57).

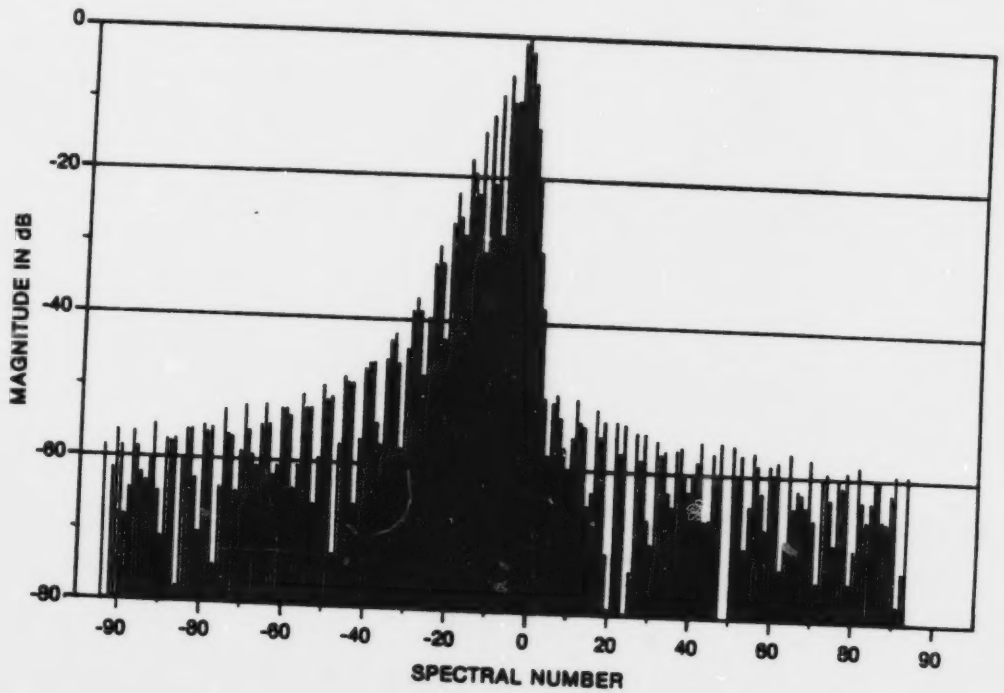

Fig. 17 - Compressed pulse with cubic phase uncompensated.

Each of the sub-apertures is filtered with its own M(n) and then the spectra for the sub-apertures are coherently summed by concatenating them together. An example of a coherently summed spectrum with eight looks is shown in Figure 18 where the left portion of the spectrum belongs to negative frequencies. Prominent gaps are evident between the adjacent sub-aperture spectra. As the frequency increases, the gaps go deeper. This is because the coupling between range and azimuth increases at the ends of the aperture, i.e., where the range curvature slope is steepest.

If a Hamming window, with the same bandwidth as that of the original spectrum is applied to the concatenated spectrum shown in Figure

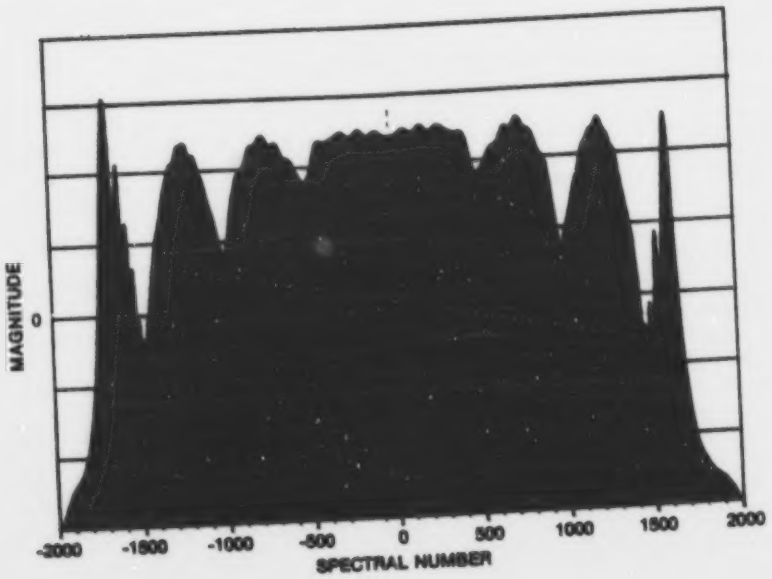

Fig. 18 - Azimuth spectrum with piecewise range curvature compensation (squint angle $\eta_y = 30°$).

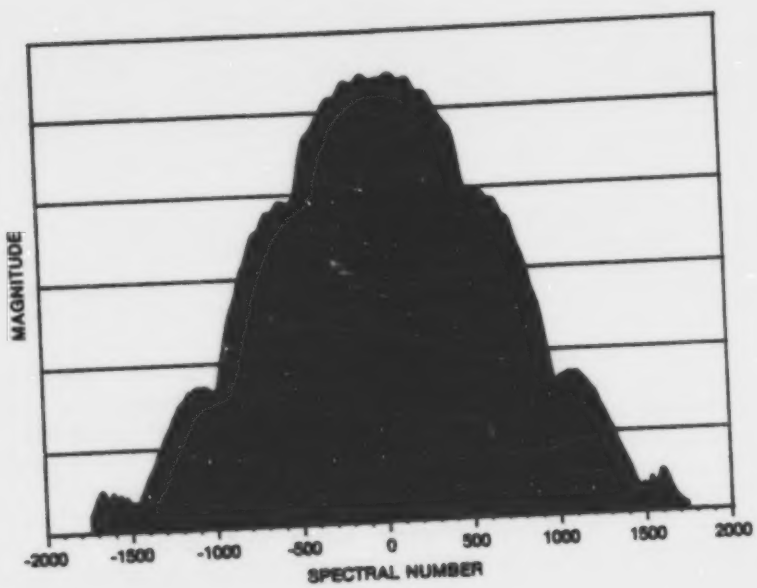

Fig. 19 - Spectrum of Figure 18 with Hamming weighting.

19, the spectral leakage is suppressed. In addition and perhaps more importantly, the amplitude of the gaps in the envelope are equalized. The gaps modulate the envelope intensity and cause distortion in its Fourier transform. The equalization effect of the window makes the envelope modulation almost sinusoidal. This means that "paired-echoes" will be produced in the other domain [1]. Without the equalization the modulation is non-sinusoidal, and a more complex, harder to analyze distortion is produced.

An output pulse from one sub-aperture is depicted in Figure 20. The mainlobe width is wider than that from a fully compensated full aperture. This is because the sub-aperture bandwidth is proportionally

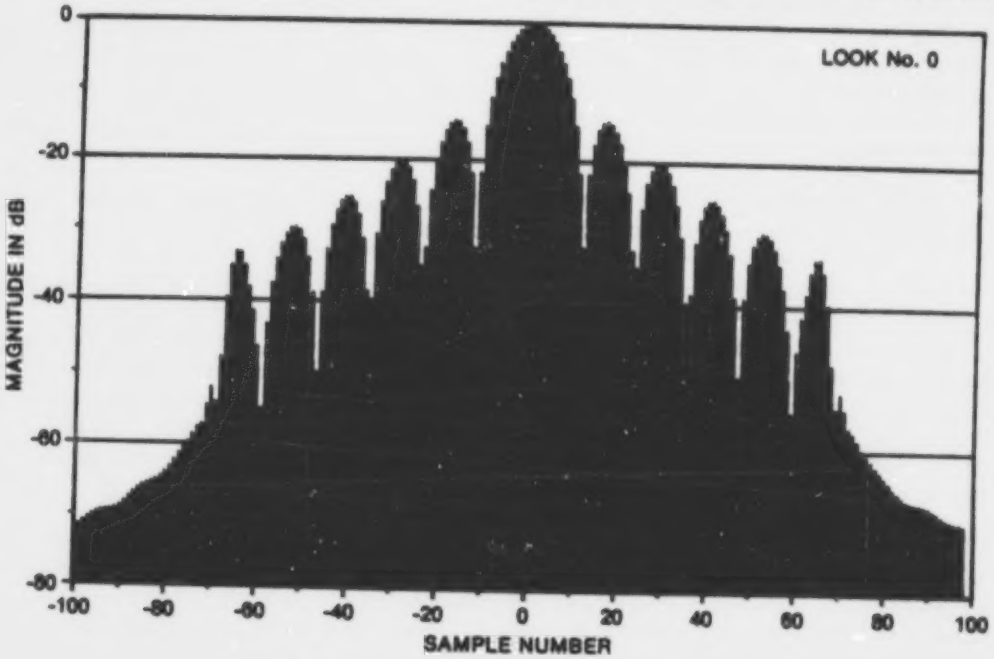

Fig. 20 - Compressed pulse of one look.

smaller than that of the full aperture. Also, there are prominent sidelobes . This is to be expected since the window was not applied to the sub-aperture spectrum. Instead the window will be applied later to the concatenated spectrum, and the high sidelobes will be cancelled out at that time.

Thus far only the effects of amplitude distortion have been considered. Phase errors near the boundaries of the adjacent looks also cause "paired-echo" type distortions. The phase cancellation during matched filtering is incomplete when a piecewise correction is used. This incomplete phase cancellation causes a nearly sinusoidal residual phase error in the frequency domain, which in turn causes paired echoes in the time domain. This effect is serious at high squint angles (e.g. 6°),

where the cubic phase term ($\frac{4\pi}{\lambda} a_3 s^3$) becomes very large and cannot be ignored. A plot of the residual phase errors for our present example, is shown in Figure 21.

In order to obtain the final compressed pulse, an inverse Fourier transform of the windowed, demodulated, concatenated spectrum is taken. The result is shown in Figure 22. Except for the presence of paired-echoes, the compressed pulse shape is identical to the case with continuous range curvature compensation. As has already been mentioned, these paired-echoes are the products of envelope and residual phase distortions.

Simulated compressed output pulses for two cases with high squint angles (η_p = 15°, 6°) are shown in Figure 23 and 24. As can be seen in the figures, the paired-echo magnitudes increase as the radar becomes more highly squinted (i.e., smaller η_p is used). The interrelationship between various radar parameters and the paired-echo magnitudes will be discussed in the next section.

7. ERROR ANALYSIS OF THE EFFECTS OF PHASE AND AMPLITUDE DISTORTIONS, CAUSED BY THE PIECEWISE APPROXIMATION

The piecewise correction for range curvature and cubic phase introduces phase and amplitude errors into the matched filtering process. In fact, exact matching occurs only at the look centres. Our goal here is to characterize, with respect to the number of sub-apertures and the other operating parameters, the form and magnitude of each of the distortions arising from these abnormalities. Because an exact description of the errors is extremely complicated and unnecessary, a combined deterministic and empirical estimation procedure will be used instead.

In this section the form of the magnitude and phase errors in the frequency domain, will be examined. Then, models will be developed that allow prediction of both the size of the errors, and the individual and combined paired echo levels that result from the errors. Next, a procedure for estimating the Integrated Sidelobe Ratio degradation, caused by the errors, will be described, and finally, the range independence of a given set of piecewise corrections will be examined.

7.1 Spectrum Envelope Distortion

In the following, we will describe a simplified approach for determining the gap size between adjacent looks in the frequency domain, as a function of look centre location, and then we will relate the gap sizes to the paired-echo magnitudes in the spatial domain.

When post-compression interpolation is used, the coupling between range and azimuth prevents the complete correction of the curvature, and gaps are left in the spectrum. The height and width of the gap, associated with each sub-aperture, depend on the compressed pulse width in range and the local slope of the range curvature versus azimuth position curve. The slope of the range curvature function in the frequency domain is given

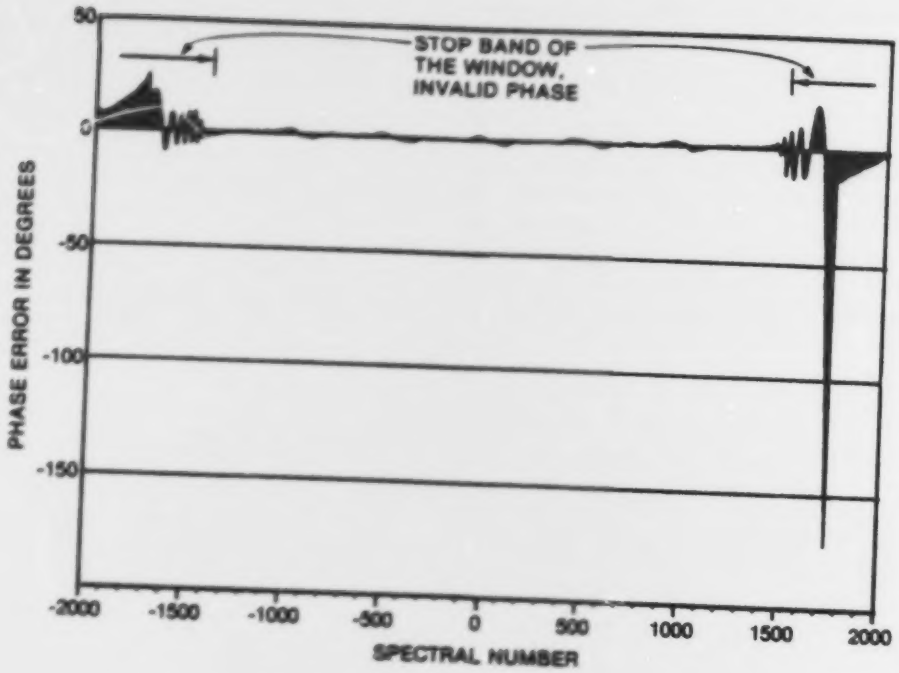

Fig. 21 - Residual Phase error (squint angle η_g = 30°).

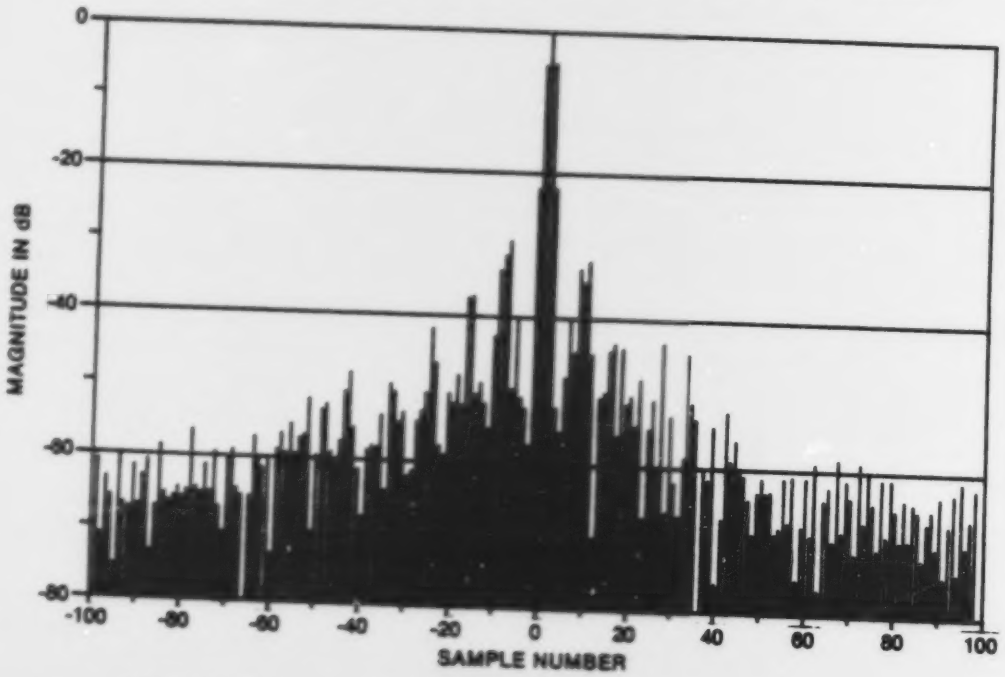

Fig. 22 - Compressed pulse with piecewise range curvature.

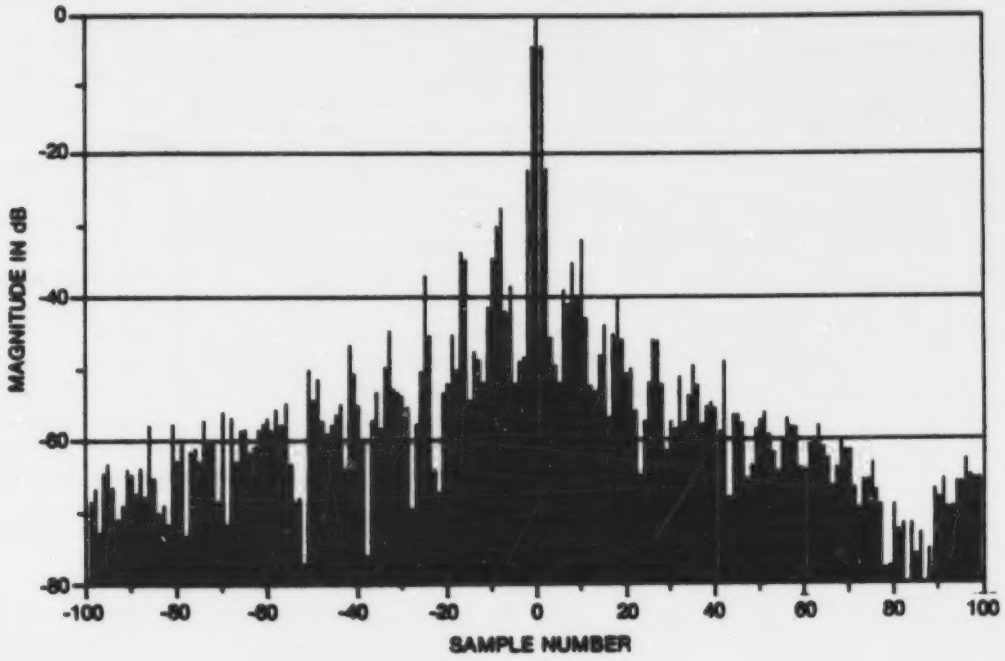

Fig. 23 - Compressed pulse with piecewise range curvature compensation (squint η_p = 15°).

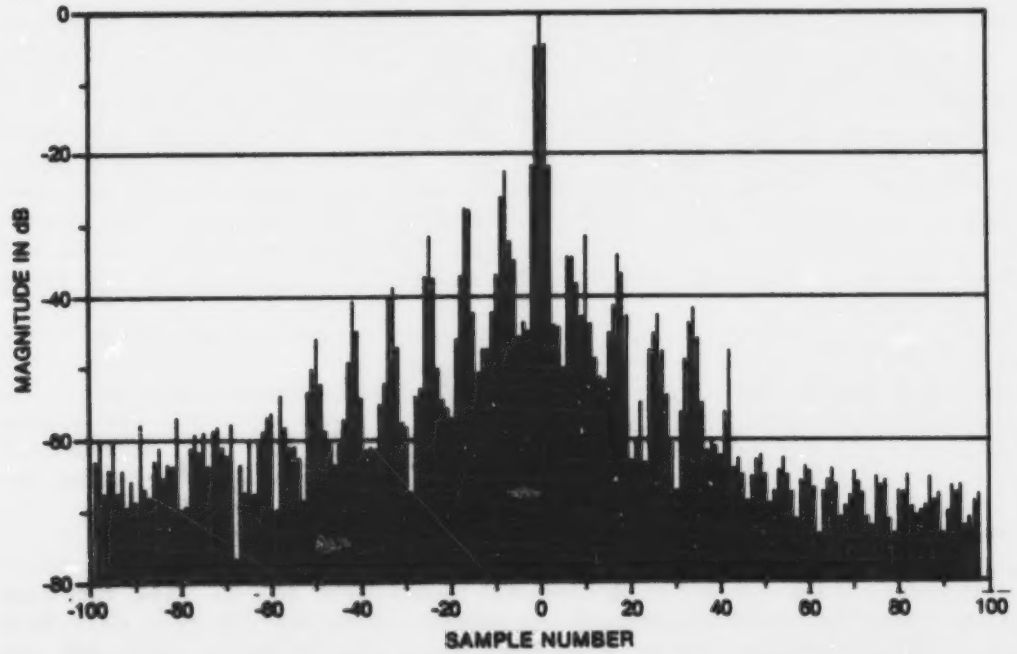

Fig. 24 - Compressed pulse with piecewise range curvature compensation (squint angle η_p = 6°).

by the derivative of the amount of range curvature (ℓ_1) as given in (62) with respect azimuth space (m), i.e.,

$$\text{slope} = \frac{d\ell}{dm} = \frac{\lambda^2}{4CTa_2\Delta S_A^2 N_T^2}\, m, \qquad (64)$$

where the slope is expressed in number of range cells shifted per azimuth cell. The parameters ℓ and m are the running indices in range and azimuth respectively. This slope is used to project the compressed range profile onto the azimuth spectrum. It is assumed that a Hamming window is used in range compression, and that therefore the compressed range profile is approximately the shape of the Fourier transform of the Hamming window, (see (59)).

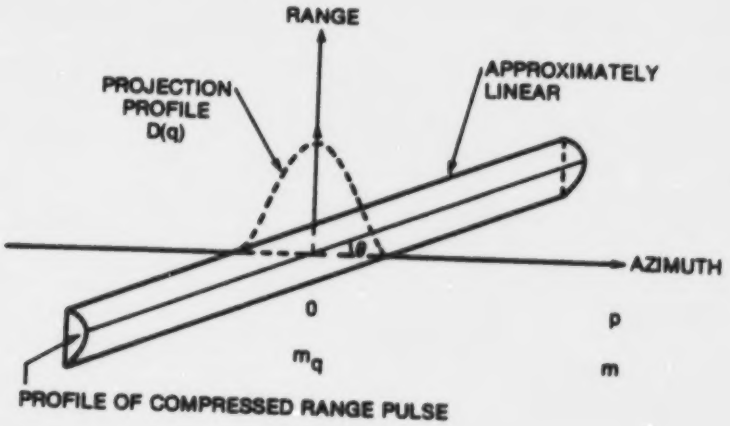

Fig. 25 - Range-azimuth coupling.

The coupled range-azimuth signal for one sub-aperture is shown in Figure 25. It is assumed that the sub-aperture is short, that the quadratic component of the curvature is negligible, and that the slope $(\frac{d\ell}{dm})$ of the sub-aperture segment s so small, and so constant over the sub-aparture, that $\theta(m)$ in Figure 25 can be approximated as:

$$\theta(m) \approx \tan\theta(m) = \frac{d\ell}{dm} = \frac{\lambda^2}{4CTa_2\Delta S_A^2 N_T^2}\, m. \qquad (65)$$

With this approximation, the normalized projection of the compressed range profile onto the azimuth frequency axis becomes,

$$W(m_q,p) = E_1(M_q,p) + 0.426[E_2(m_q,p)+E_3(m_q,p)], \qquad (66)$$

where,

$E_1(mq,p) = \text{sinc}\ (pk)$,
$E_2(m_q,p) = \text{sinc}\ (pk-1)$,
$E_3(m_q,p) = \text{sinc}\ (pk+1)$,

$$k = \frac{1}{\gamma_R}\frac{df}{dm}\bigg|_{m=m_q} = \frac{\lambda^2}{4CTa_2\Delta S_A^2 N_T^2 \gamma_R} m_q,$$

$$m_q = \frac{f_q}{\Delta f},$$

$$p = m - m_q,$$

and f_q is the location of the centre of look q. m_q denotes the centre of the q^{th} look in the m (global frequency) dimension. p is a new local frequency dimension, whose origin is at the centre of the q^{th} look.

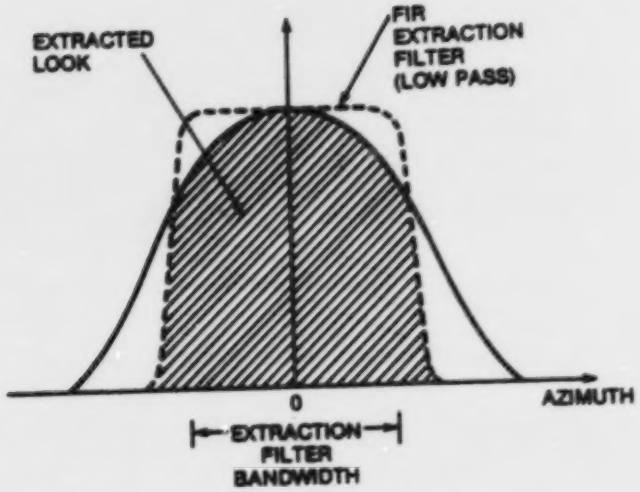

Fig. 26 - Look extraction using a low pass filter.

As shown in Figure 26 the desired sub-aperture is extracted, by means of an FIR filter, from an appropriately rotated version of the baseband spectrum. If the FIR filter shape is approximately rectangular, the spectral height at the filter edge ($p = \frac{N_F}{2}$) is

$$h_q = W(m_q, p) = E_1\left(m_q, \frac{N_F}{2}\right) + 0.426\left[E_2\left(m_q, \frac{N_F}{2}\right) + E_3\left(m_q, \frac{N_F}{2}\right)\right], \quad (67)$$

where N_F is the number of frequency cells covered by the bandwidth of the extraction filter.

For the looks extracted from the ends of the spectrum, the slope of the range curvature is steeper, and the area of the projected range

profile is narrower. As a result, the gap between adjacent sub-apertures is widened and deepened. In other words, the envelope distortion worsens towards either end of the full aperture. A typical coherently summed spectrum is sketched in Figure 27. As shown in the figure, the minima can be connected by a dotted line described by,

$$h(m) = F_1(m) + 0.426\left[F_2(m) + F_3(M)\right], \qquad (68)$$

where,

$F_1(m) = \text{sinc}\,(Km)$,
$F_2(m) = \text{sinc}\,(Km-1)$,
$F_3(m) = \text{sinc}\,(Km+1)$,

and,

$$K = \frac{\lambda^2 N_F}{8CTa_2 \Delta S_A^2 N_T^2 \gamma_R}.$$

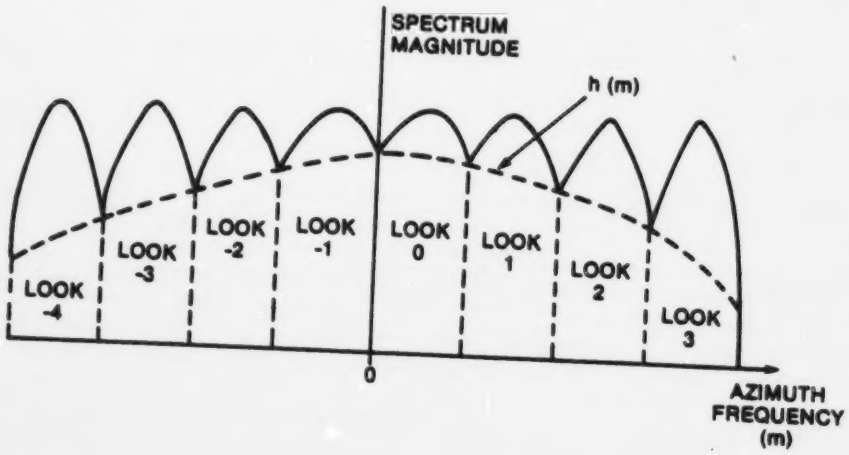

Fig. 27 - A typical coherent summed spectrum. The dotted line connecting all the minima is described by Eq. 68.

As mentioned previously, Hamming weighting is normally applied to the concatenated spectrum to suppress the spectral leakage that occurs during the calculation of the inverse Fourier transform. The weighting function has the same bandwidth as the summed spectrum. The weighted spectrum is sketched in Figure 28.

Besides suppressing spectral leakage, the weighting also helps reduce the size of the larger gaps at the ends of the concatenated spectrum. The gaps are now more or less equalized over the entire aperture. As shown in Figure 29, the weighted gaps can be thought of as ripples superimposed on an ideal smooth spectrum. The amplitude of the ripples at a distance of a quarter of the bandwidth from the aperture centre is estimated to be,

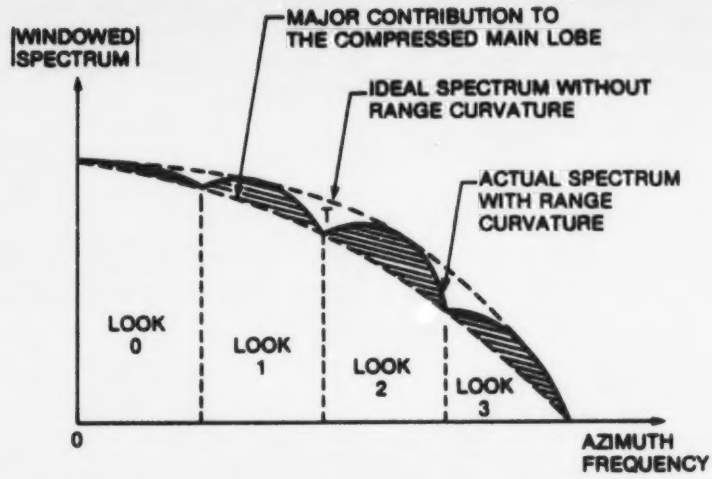

Fig. 28 - Spectral energy distribution.

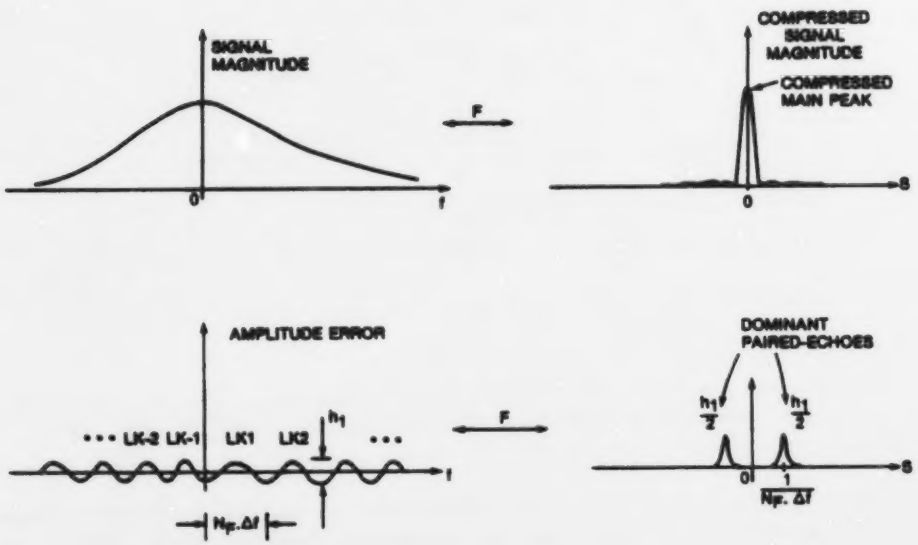

Fig. 29 - Envelope distortion (assume sinusoidal ripples) for coherent multi-look spectrum.

$$h_1 = \frac{\left[1-h\left(\frac{N_T}{4\gamma_R}\right)\right]}{2} \times 0.54, \qquad (69)$$

where h(m) is given by (29) and the 0.54 numerical factor accounts for the Hamming weighting. This ripple amplitude is taken to be representative of the ripple across the whole aperture.

The ripples shown in Figure 28 exhibit a periodic sinusoidal-like waveform. Assuming for now that the ripples are purely sinusoidal (which is not really true), the inverse Fourier transform, as shown in Figure 29, will give paired-echoes of magnitude $h_1/2$, on either side of the mainlobe of height approximately equal to 0.54.

The ratio of the magnitudes of the paired-echoes to that of the main peak is

$$\frac{\text{paired-echo magnitude}}{\text{mean peak}} = \frac{h_1/2}{0.54}$$

$$= \frac{\left[1-h\left(\frac{N_T}{4\gamma_R}\right)\right]}{4}$$

$$= \frac{1}{4}\left\{1-F_1(m')-0.426[F_2(m')+F_3(m')]\right\} \qquad (70)$$

where $m' = \frac{N_T}{4\gamma_R}$.

Unfortunately, the computer simulations did not produce paired-echoes of the predicted magnitude. One explanation for this disagreement is that the ripples on the summed spectrum are not purely sinusoidal. If this is the case, the first order harmonic coefficient should fairly closely represent the most dominant paired-echo. In the absence of an analytical expression for the ripple, it is impossible to prove this implication. Instead, a correction factor was established, which, when used in the simulation, caused paired-echoes of the correct magnitude to be produced. It was found that if a correction factor of one-half was used in (70), the results were reasonable in most cases. With a correction factor of one-half, (70) becomes

$$\frac{\text{dominant paired-echo magnitude}}{\text{main peak}} = \begin{cases} \frac{1-h'}{8}, & \text{for more than two looks;} \\ \frac{1-h'}{12}, & \text{for two looks.} \end{cases} \qquad (71)$$

A special provision is made for the two-look case, i.e., the correction factor is set to 1/3 instead of 1/2. This is required because the envelope ripple deviates more strongly from a sinusoidal shape in the two-look case than it does in the other cases.

These results are consistent with the fact that as the ripple shape deviates more and more from the sinusoidal, more energy is displaced into the higher order harmonics, and thus the magnitude of the dominant harmonic decreases.

With changes in the operating parameters, the general shape of the ripples is preserved, and the relative values of Fourier coefficients do not change. Equation (71) provides a good estimate of the paired-echo magnitudes when the magnitudes are between -20dB to -35dB. For ratios greater than -20dB, the aforementioned linear approximation assumptions break down gradually, with the estimated ratio increasing more rapidly than the actual ratio. For ratios less than -35dB, (71) also breaks down, this time because the pair-echo magnitude becomes so low that it merges with the shoulder of the main peak.

The location of the dominant paired-echo, which is related to the number of looks involved, is given by

$$n_{pe} = \frac{N_L}{p} \text{ cells}, \tag{72}$$

where N_L is the number of looks and p is the ratio of the overall extracted spectrum to the Nyquist bandwidth. In most cases,

$$p = \frac{N_P N_L}{N_T} \approx 0.9, \tag{73}$$

and thus

$$n_{pe} = \frac{N_T}{N_P} \approx 1.1\ N_L \text{ cells}. \tag{74}$$

In the above analysis and simulations, envelope distortion was considered to be the sole contributor to paired-echoes, and the phase was assumed to be perfectly matched. In the next section, the effects of phase errors are examined.

7.2 Residual Phase Error

The residual phase error originates from a phase mismatch between the piecewise quadratic matched filter and the data. This error causes paired-echoes.

The phase error, between the recorded data and the matched filter, at s=0, is taken to be representative of the phase error ripple across the entire aperture. This representative phase error is obtained by subtracting the phase in (45) from (47), and then setting s=0, and q=1, i.e.

$$\Delta\theta = \frac{4\pi}{\lambda} \left| a_{01} - a_{11}s_1 + a_{21}s_1^2 - a_0 \right|. \tag{75}$$

Based on the correspondence between the spatial and frequency domains described by (21) it is possible to find an f_1 for every s_1, such that the phase in the frequency domain at f_1 equals the phase in the spatial domain at s_1. If the principle of stationary phase holds, it also follows that the maximum phase error in the frequency domain is equal to the maximum phase error in the spatial domain. Therefore the residual phase error,

$\Delta\theta$, given by (75), is equal to the phase error at the boundary of the first look in the frequency domain.

It was assumed, and confirmed later by computer simulations, that the peak residual phase errors at the end of the sub-apertures are approximately equal.

A sketch of the typical residual phase error in a coherently summed spectrum is shown in Figure 30. The residual phase error is periodic in pattern. Because of the overlap (18 to 21%) of the transition bands of the look extraction filters, the residual phase errors at the look boundaries cancel each other out. This cancellation reduces the peak error ($\Delta\theta_p$), to about 2/3 of $\Delta\theta$, i.e.

$$\Delta\theta_p \approx \frac{2}{3}\Delta\theta$$
$$= \frac{8\pi}{3\lambda}\left| a_{o1} - a_{11}s_1 + a_{21}s_1^2 - a_o \right|. \qquad (76)$$

If the phase error is purely sinusoidal, with amplitude $\Delta\theta_p$, where $\Delta\theta_p$ < 0.4 radian, then the paired-echo magnitude is given by a Bessel function approximation [1], such that

$$\frac{\text{paired-echo due to phase error}}{\text{main peak}} \approx \frac{\Delta\theta_p}{2}. \qquad (77)$$

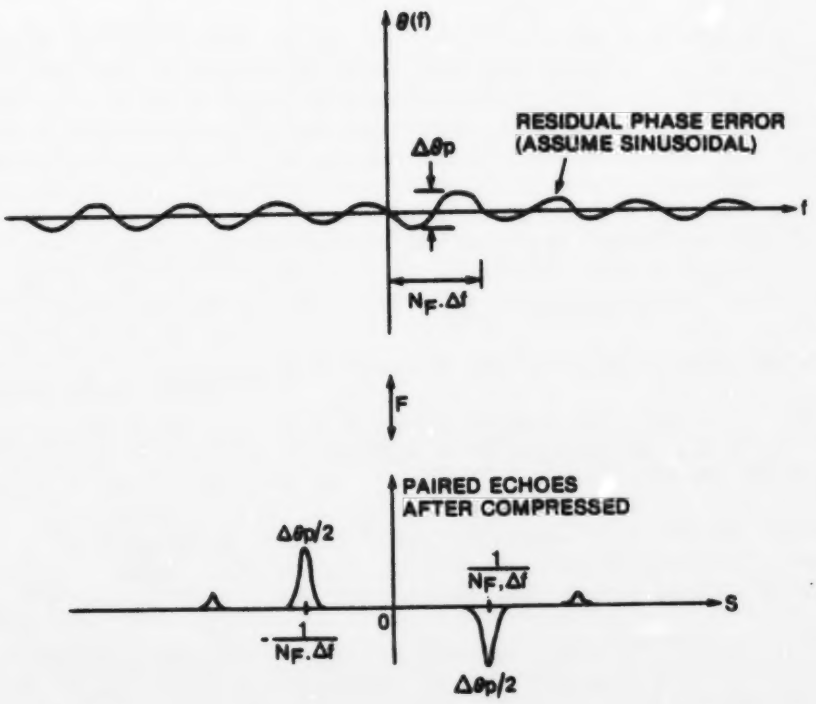

Fig. 30 - Residual phase error and paired echoes.

As was the case with the envelope distortion, the phase error is not exactly sinusoidal and no simple solution can be formulated. However, the size of the dominant first harmonic coefficient can be obtained by computar simulation. When this is done, and a 20% transition band is assumed, the magnitude of the first harmonic turns out to be only about half of that given by (77), i.e.,

$$p_p = \frac{\text{paired-echo due to phase error}}{\text{main peak}} = \frac{\Delta\theta_p}{4} \qquad (78)$$

Since the residual phase error in the frequency domain has the same period as that of the envelope distortion, the locations of the paired-echoes, caused by the phase distortion, coincide with the locations of the echoes produced by the envelope distortion.

7.3 Overall Paired-echo Magnitude

The first order paired-echo magnitudes are given by the sum and difference [1] of that contributed by envelope distortion (70) and residual phase error (78), i.e.,

$$\frac{\text{overall paired-echo}}{\text{main peak}} = \left|p_m \pm p_p\right|. \qquad (79)$$

7.4 Degradation of Integrated Sidelobe Ratio due to Paired-echoes

For a heavily weighted spectrum (e.g. Hamming), in the absence of additional phase errors, e.g. FM rate mismatch or motion errors, the integrated sidelobe level (everything outside the first minima from the main peak) is composed mainly of energy contributed by the paired-echoes, $\left|p_m \pm p_p\right|$. The integrated sidelobe ratio (ISLR) can be approximated as

$$\begin{aligned} ISLR &= 10\ \log_{10}[(p_m + p_p)^2 + (p_m - p_p)^2] \\ &= 10\ \log_{10}[2(p_m^2 + p_p^2)]. \end{aligned} \qquad (80)$$

7.5 Range Independence of the Piecewise Solution

The resultant piecewise solution can be regarded as a one-look matched filtering process with a distorted frequency transfer function. The amplitude versus frequency response is modulated with sinusiodal-like ripples in its passband, while the phase versus frequency response is composed of ripple-like residual phase errors superimposed on the usual linear and quadratic phase cont ributions. In both cases, the distortions are local in nature since they arise from mismatches within a look.

In a normal one-look azimuth matched filtering process, the filter is matched to the azimuth signal returned from a radar point target located at the centre of the processing swath. This matched filter is then applied to all the data in that processing swath. The quadratic or cubic phase mismatch between the data and the filter increases towards the

edges of the swath. The width of a swath is determined by the maximum amount of phase mismatch tolerable, at the end of the processing aperture. This swath width is known as the depth of focus [2].

During the application of the azimuth multi-look, frequency domain, matched filter to data at different ranges across the swath, the compressed frequency domain signal will suffer both local and global phase mismatches, as well as envelope distortion. The overall distortion in the frequency domain signal will be

$$\varepsilon(f) = A(f)\, e^{j\phi_e(f)+j\phi_g(f)},$$

$$= \left[A(f)\, e^{j\phi_e(f)}\right] e^{j\phi_g(f)}.$$

In the spatial domain the error will be

$$\varepsilon(s) = F^{-1}\{\varepsilon(f)\} = F^{-1}\{A(f)e^{j\phi_e(f)}\} * F^{-1}\{e^{j\phi_g(f)}\}, \tag{81}$$

where,

$A(f)$ is the envelope ripple as a function of frequency;
$\phi_e(f)$ is the local residual phase error as a function of frequency; and
$\phi_g(f)$ is the global phase mismatch as a function of frequency.

In (81), the local phase error can be combined with the envelope distortion and inverse Fourier transformed. The global phase can be inverse Fourier transformed separately. The first inverse Fourier transform gives rise to paired-echoes, whereas the second degrades the integrated sidelobe ratio. The convolution of the two inverse Fourier transforms describes the total effect. Thus, in evaluating the paired-echo magnitudes only the localdistortions need to be considered, whereas in evaluating the degradation in the integrated sidelobe ratio (separate from that contributed by the paired-echoes), only the global phase mismatch needs to be considered.

8. DERAMPING TECHNIQUES

This section is an overview of alternate forms of pulse compression for a linear FM signal. Instead of matched filtering, or fast convolution, a deramping (dechirping), spectral analysis approach can be used. In the conventional deramping method, the quadratic phase term in the incoming radar return signal is cancelled by multiplication with a reference signal, which has a phase term that is the conjugate of the returned signal. The process is shown diagramatically in Figure 31. The deramped signal becomes a CW signal, which has a frequency, f_1, directly proportional to the time separation, Δ, between the received signal and the reference. The CW signal is then Fourier transformed to give a compressed pulse as shown in Figure 31(c). The location of the pulse is directly proportional to the deramped CW frequency, f_1. As a result, the

target is resolved at its location of arrival, Δ. Figure 32 shows a multi-target environment, in which three targets are resolved at their respective locations.

The width and magnitude of the compressed pulse depend on the duration of the overlap (T_e) between the reference and the received signal, as shown in Figures 32(a) and (b). For targets which lie further away from the reference (i.e. smaller T_e), the deramped signals suffer more energy loss, and therefore, their pulse width and magnitude are degraded, as shown in Figure 32(c). In practice, there exists a threshold above which the amount of energy loss is intolerable. In order to stay within the threshold, it is necessary to overlap reference signals so as

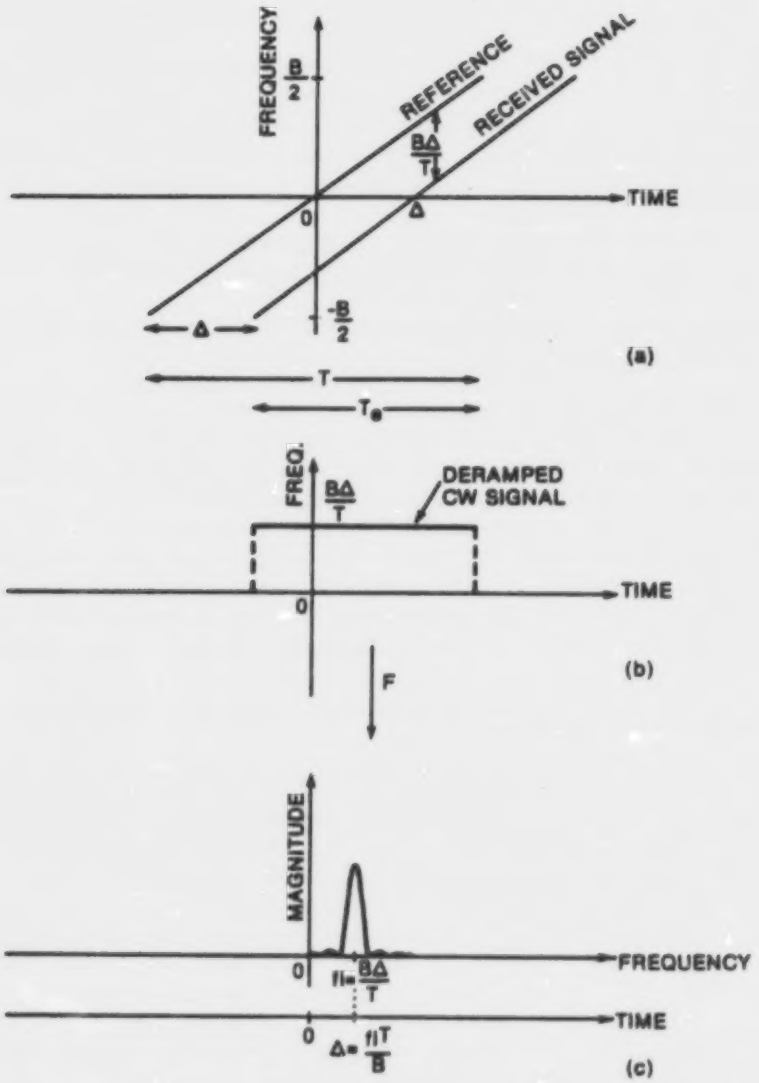

Fig. 31 - Conventional deramping technique for a point target.

to decrease the time separation between the received signal and the nearest reference. Such a scheme reduces the amount of energy loss, but at the expense of having the data repeatedly deramped by nearby reference signals. This is illustrated in Figure 33. The repetitions produce redundant data with energy loss above the tolerable threshold. Only data in the vicinity of the centre of a reference ramp are kept. The redundant data are discarded. The valid data derived from successive references are concatenated to form the final image.

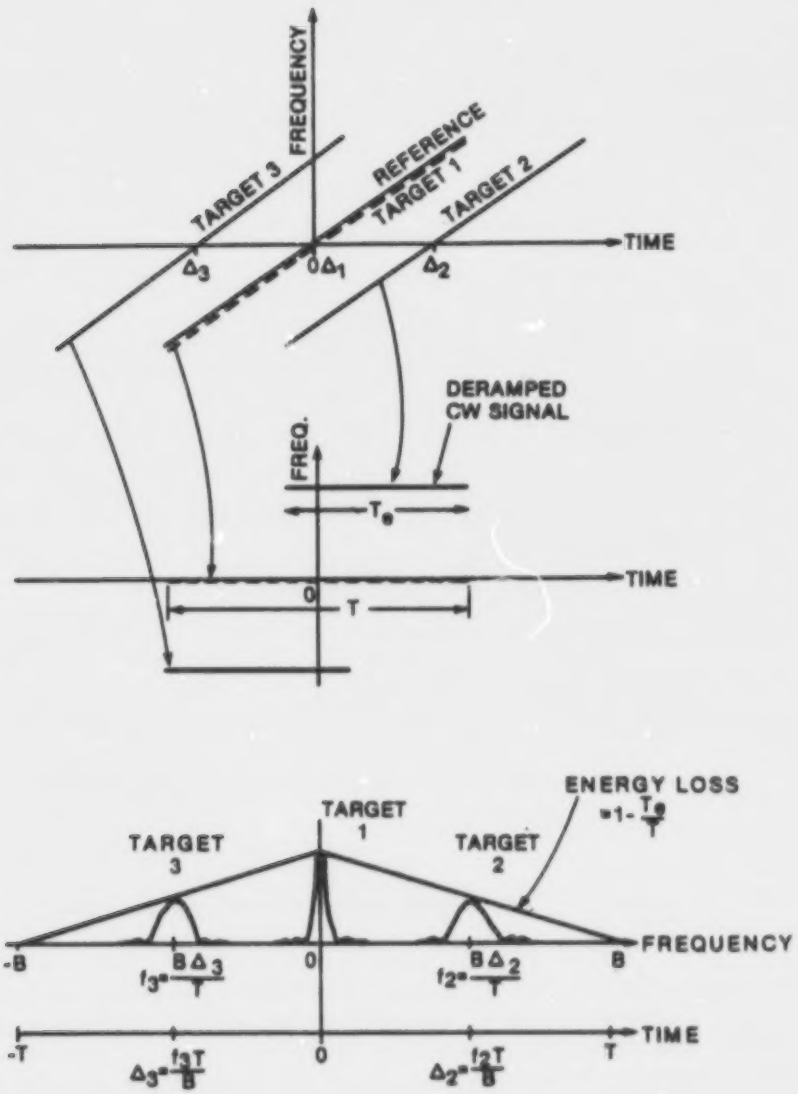

Fig. 32 - Conventional deramping technique for multi-targets.

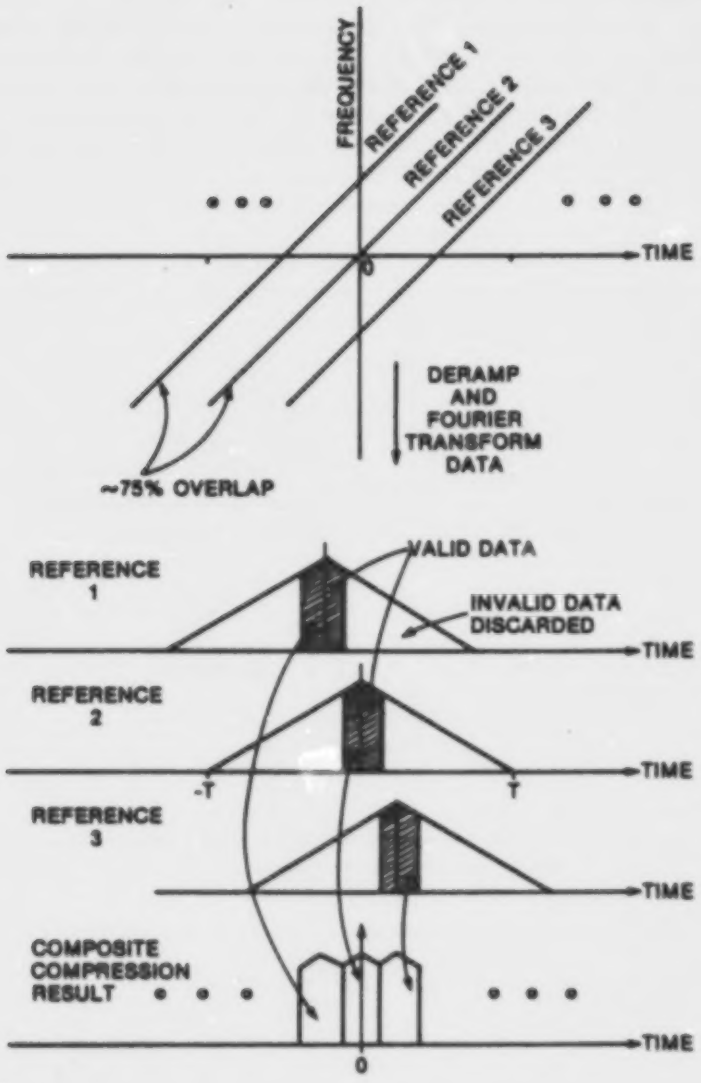

Fig. 33 - Overlap reference ramps to reduce collapsing loss .

In this section, we will overview two pulse compression techniques based on the aforementioned deramping approach, namely, the Spectral Analysis [10] and the Step Transform [6-9] Methods. Compared to the basic de-ramping approach both methods allow a reduction of the energy loss and/or an improvement in the processing efficiency. The following description forms a framework for the discussion, in Section 9, of the processing efficiency of the sub-aperture compression techniques.

8.1 Spectral Analysis Method [9,10]

The spectral analysis method attempts to reduce the energy lost, due to aliasing, during the deramping process. This is achieved by utilizing a continuous, non-overlapping deramp sawtooth reference with an FM rate of the same magnitude, but of opposite slope and longer duration, than the signal from a single point target. In addition, the phase at the end of one sawtooth is π and that at the beginning of the next sawtooth is $-\pi$, or vice versa (i.e. the phase at the boundary is circularly continuous and anti-symmetric). A signal ramp crossing a sawtooth boundary does not change its deramped CW frequency because aliasing causes the disjoint frequency to fold back in the spectrum and align with the unaliased portion. The phase is continuous at the boundary. This is illustrated in the frequency versus time diagram shown in Figure 34(a)-(c). It is therefore possible to employ a Fourier transform to extract the spectrum

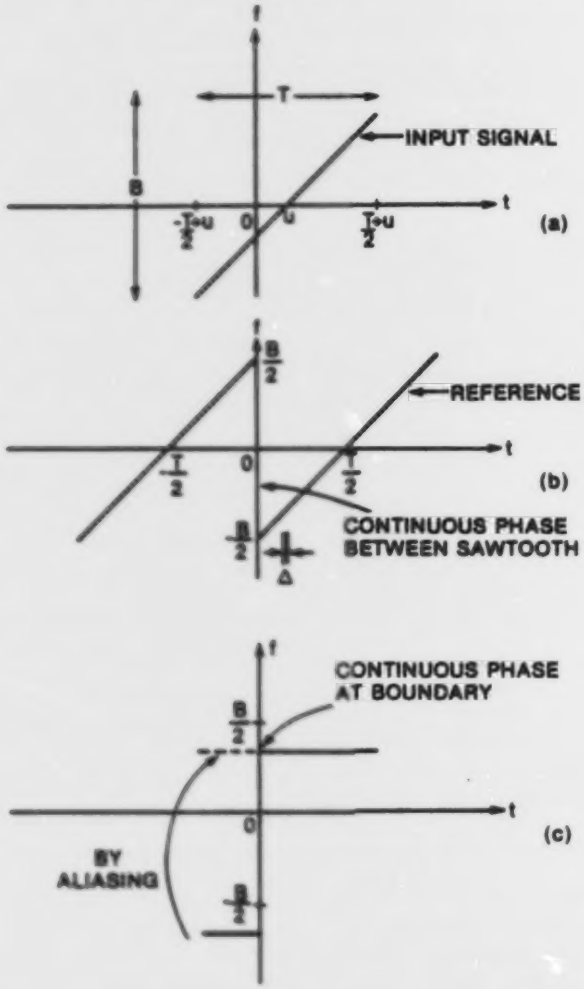

Fig. 34 - The spectral analysis method.

representing the point target.

For multiple targets, superimposed target returns can be uniquely resolved by the deramping - Fourier transform process. Figure 35(a) shows a parade of equally spaced target returns in the frequency versus time plane. Figure 35(b) shows the corresponding deramping reference signal. Note that it has opposite FM slope as the target signals. Upon mixing the target signals with the reference, the individual FM signals are translated into CW signals, with their frequencies corresponding to their positions relative to the reference. The resultant deramped signal ensemble is depicted in Figure 35(c).

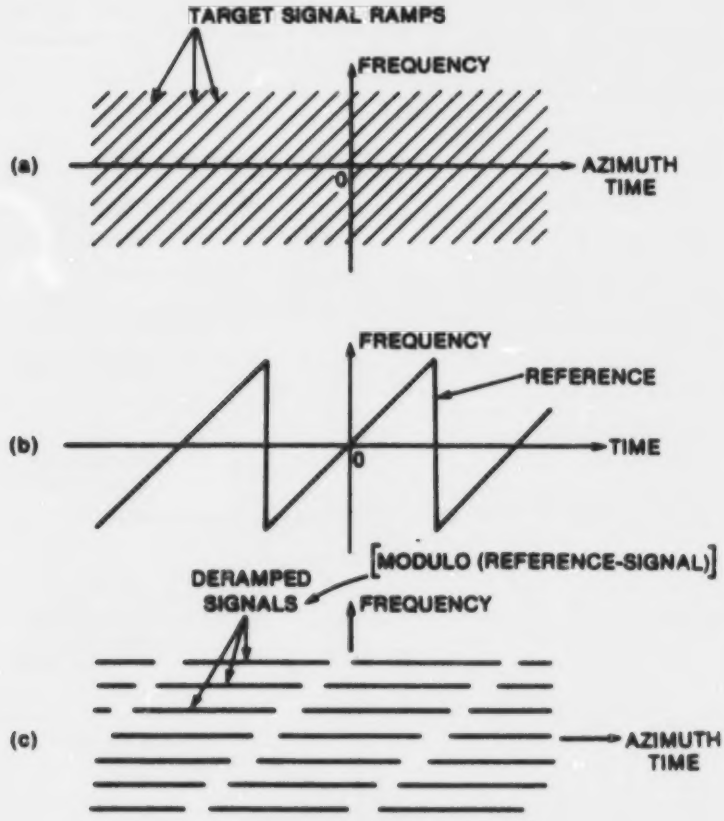

Fig. 35 - Deramping process via the spectral analysis method.

Signal ramps falling within a period of the sawtooth reference are grouped into a parallelogram in the frequency versus time plane. The oblique boundaries between parallelograms prohibit Fourier transformation of the full aperture data set. Processing can only be performed with shorter Fourier transforms that prevent data from the adjacent parallelogram from being drawn into the transform and getting mixed up with the

returns that belong there. It should be noted that the data are only directly accessible in the time-domain (i.e. column-wise in Figure 35(c)), because all the targets are superimposed. The frequency dimension (vertical axis) is accessible through either the DFT or filtering separations on the time domain data. As already mentioned, one way to avoid mixing up the data is to partition the parallelogram into narrow columns. Each column is centred in the neighbourhood where the target data are to be resolved. Each column of data (actually a superimposed one-dimensional time-domain data ensemble) is Fourier transformed along the time axis to resolve the target ensemble. A data column will inevitably cross a parallelogram boundary, thus mixing up data between the parallelograms. Compressed data in the vicinity of a boundary are invalid and must be discarded. The placement of one processing region is shown in Figure 36.

$$T' = \left[(1-\beta)\frac{B}{K} - \frac{\sigma N}{B}\right] \text{(SECONDS)}$$

$$g = T' K \text{ (Hz)}$$

$$G = \frac{g}{B} N = \left[(1-\beta - \frac{\sigma N K}{B^2}) N\right] \text{(SAMPLES)}$$

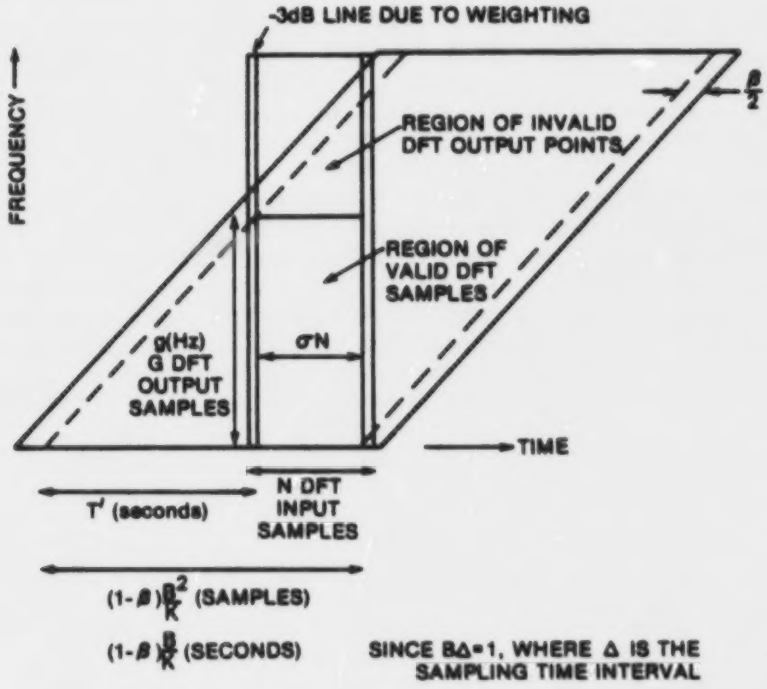

Fig. 36 - Placement of one processing region.

Because of the antenna aperture modulation, target signals compressed using this technique are subject to amplitude modulation. The amplitude modulation can be controlled by keeping the data of interest away from the edges of the parallelogram.

Targets in the remaining portions of the parallelogram can be similarly compressed by partitioning another processing column at the other end of the parallelogram as shown in Figure 37. Compressed data from the two processing regions within the parallelogram are concatenated to form a continuous image. In practice, a guard band of fractional width β is included to keep the valid processed data away from the oblique border. As mentioned previously, this is done to control amplitude modulation. A typical value of β should be 0.3 to 0.5 depending on the antenna pattern. The output of an N-point DFT computed along a processing column spans the entire frequency space of B Hz. When weighting is applied to the N-point DFT, the effective DFT length σN (where $\sigma < 1$) is chosen to be less than or equal to the -3dB width of the weighting function. This narrower processing column is then used to calculate the number of valid output points. With the aid of Figure 36, the number of valid points is found to be

$$G = \left(1-\beta - \frac{\sigma N k}{B^2}\right)N \quad \text{samples,} \tag{82}$$

where k is the azimuth linear FM rate;
B is the reference sawtooth bandwidth; and
N is the DFT length, which is fixed for all the processing columns.

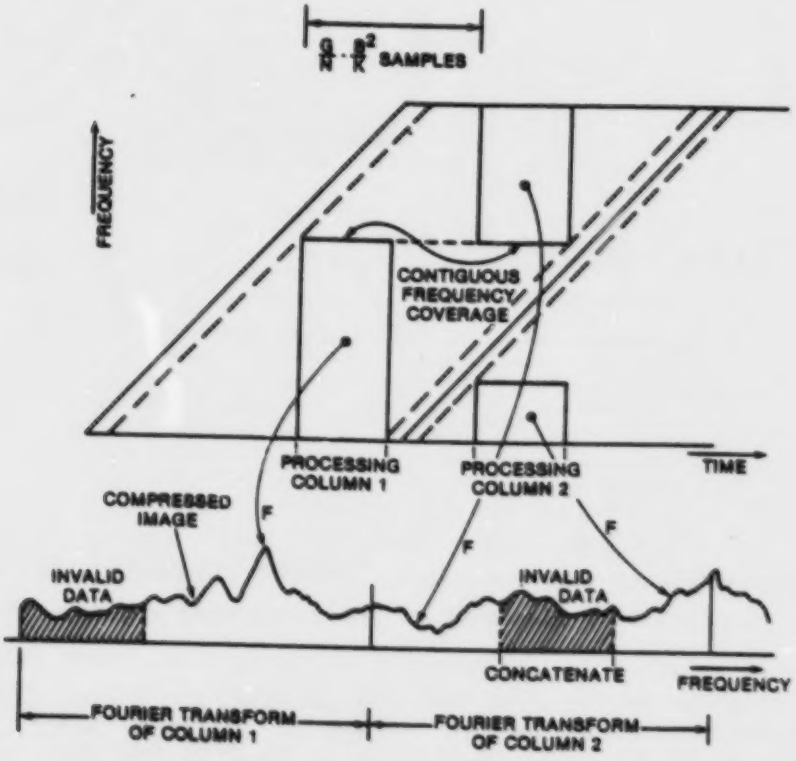

Fig. 37 - Placement of successive processing regions to ensure image continuity.

The invalid data, discarded because of the boundary crossing problem, can be regained by putting another processing column near the opposite end of the parallelogram, as shown in Figure 37. This second processing column has the same width (N points) as the first one. Its position is determined by the frequency at which the first column is cutoff. The second processing column encompasses both data left over from the first processing column and data from the succeeding parallelogram. Part of the output is invalid data corresponding to the frequencies which straddle the oblique boundary. In order to ensure image continuity, the second processing column is located such that the beginning of the region of valid output samples in the second DFT is at the same frequency as the end of the corresponding region of the first DFT. This is shown as a horizontal dotted line in Figure 37. From simple geometry, the required continuous frequency coverage is achieved if the second DFT is begun at

$$\tilde{N} = \frac{G}{N}\frac{B^2}{k} = \left(1-\beta - \frac{\sigma N k}{B^2}\right)\frac{B^2}{k} = (1-\beta)\frac{B^2}{k} - \sigma N \qquad (83)$$

input samples after the start of the first DFT.

Since N is not equal to the width of a parallelogram, the processing columns are not synchronized with the parallelogram boundaries. As the processing progresses, the boudnary cuts the processing columns at different frequencies, therefore the locations of the valid data regions must be updated for each processing column.

The above analysis assumes that two processing columns are sufficient to resolve the entire bandwidth with the prescribed resolution, but that is not necesarily true. Situations may occur where the required processing column is so wide and β (guard band) is so large that more than two processing columns are required within a single parallelogram. An example of such a situation is shown in Figure 38. In the case depicted in the figure, none of the processing columns produce any valid data in the adjacent parallelogram. In general, this happens when

$$G < \frac{N}{2}, \text{ i.e.,}$$

$$1-\beta - \frac{\sigma N k}{B^2} < \frac{1}{2}, \text{ or}$$

$$\beta > \frac{1}{2} - \frac{\sigma N k}{B^2}. \qquad (84)$$

If a substitution involving the resolution ρ_a, is given by

$$\rho_a = \frac{1.4VB}{\sigma N k}, \qquad (85)$$

where V is the velocity of the radar, is made in (84), the inequality can be written as

$$\beta > \frac{1}{2} - \frac{1.4V}{B\rho_a} . \qquad (86)$$

Note in (85) that N is restricted to integer powers-of-two. This places limits on the permissible values ρ_a may assume.

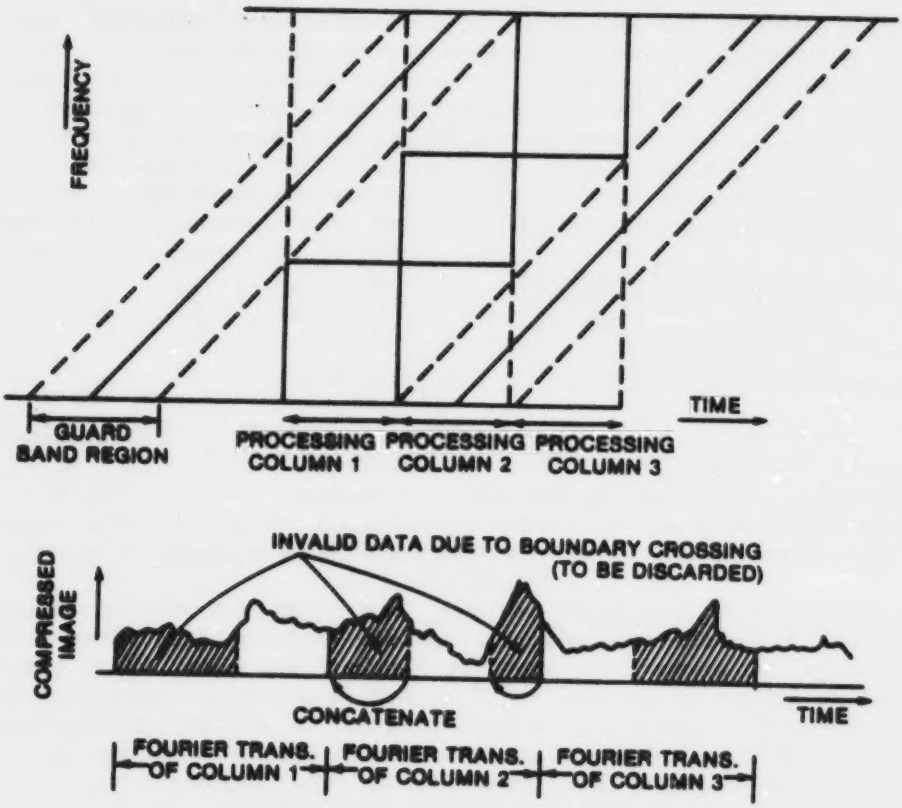

Fig. 38 - Placement of processing regions for a case with large guard band.

Major drawbacks of this method include: cubic phase errors and range curvature cannot be compensated easily, it is difficult to achieve full resolution efficiently, and there is a variation of signal-to-noise ratio over the image due to the fact that different sections of the scene are illuminated by different portions of the antenna pattern.

8.2 Step Transform

The aim of the step transform technique is to reduce the energy loss encountered with high resolution deramp processing, while maintaining a high processing efficiency and efficient memory utilization. This is done by conforming the processing path to the trend of the signal ramp, thereby avoiding the problem of having to use multiple full length, highly

overlapped reference signals. This method is efficient for compressing linear FM signals in a minimal memory space, but it lacks on inherent capability for accommodating cubic or other non-linear phase characteristics of the frequency chirp. In the next section, the effect of the cubic phase term will be investigated, and a means for avoiding image degradations caused by cubic errors, suggested.

In the step transform, the multiple references in the frequency versus time plane are replaced by a continuous sawtooth reference function, as shown in Figure 39. The sawtooth reference will overlap an incoming signal more evenly, regardless of its time of arrival, and thus

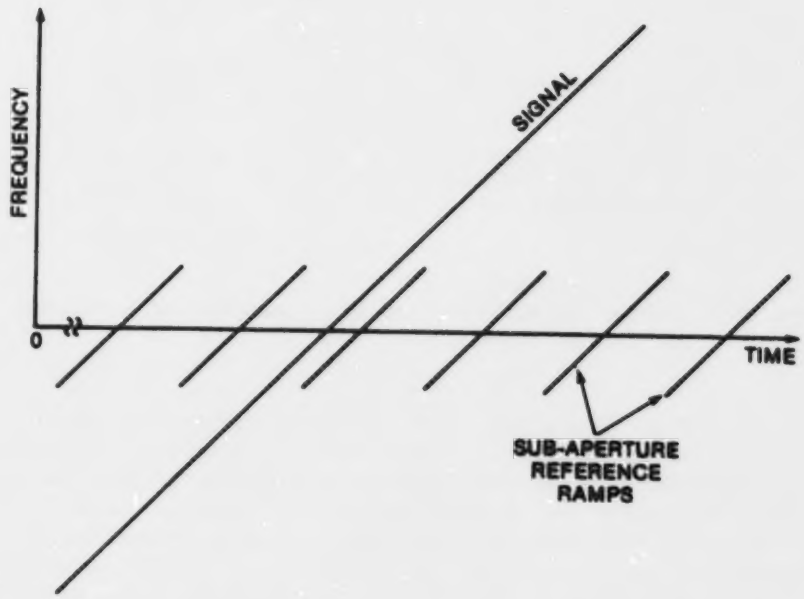

Fig. 39 - Step transform processing using a continuous sawtooth reference function.

reduce the energy loss to almost zero. Mixing an incoming ramp with the sawtooth reference gives a step-like waveform, in the frequency versus time plane, as shown in Figure 40. The horizontal part of each step is a CW waveform. The vertical parts of the steps are of equal size and are spaced evenly in time. This step-wise partitioning of the full aperture return signal is similar to the sub-aperture processing described in the previous sections. In the matched filtering case, the look extraction was performed by a combination of FIR and matched filter in the frequency domain. Hence each extracted look consists of scenes illuminated by the same portion of the antenna pattern. In the step transform, each look extraction is performed by a Hamming weighted conjugate ramp in the time domain. Hence each extracted look consists of scenes illuminated by a different part of the antenna pattern.

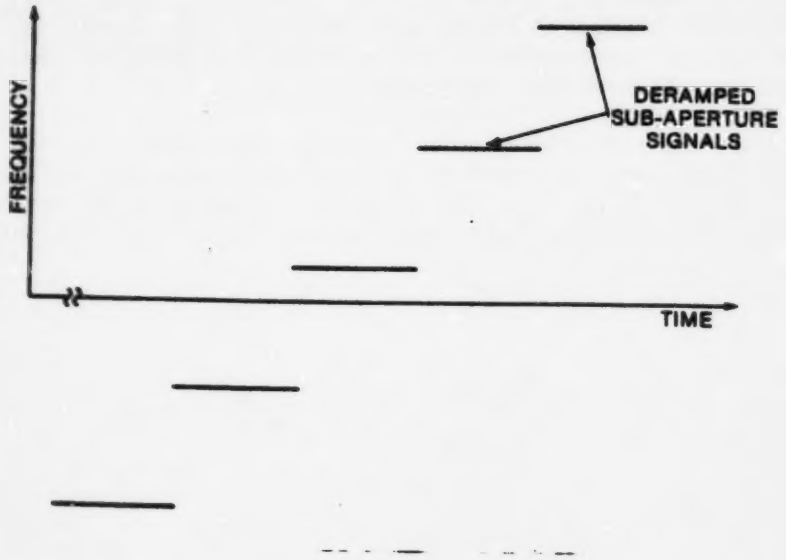

Fig. 40 - Signal after deramped by a continuous sawtooth reference function.

In the step transform, as in the basic deramping technique previously described, different targets will generate different Doppler frequencies depending on their locations relative to the sub-ramps. If part of the signal data for several different targets falls into the same sub-ramp, the extracted look will be composed of an ensemble of CW signals whose frequencies are directly proportional to the locations of the targets on the sub-ramps. The frequency produced by mixing the signal with the reference will also be directly related to position in the azimuth antenna pattern. Thus, it can be seen that different targets in the sub-aperture are acquired from different portions of the antenna pattern. This is the basic difference between the matched filter and the step transform approaches. The scenario for the step transform is illustrated in Figure 41. The image formed by the first stage of the step transform is of low resolution because only a small fraction of the target energy is contained in each sub-aperture. The remaining portions of the signal energy are embedded in the other sub-apertures that together make up the full aperture. In order to regain the original resolution, the sub-apertures must be added coherently.

The case of an input signal consisting of one point target is shown in Figure 42. The spectrum associated with the target moves to a higher frequency as it climbs each step up the frequency staircase. In addition, there is a step increment in linear phase, which depends on the separation in time of the signal and the reference tooth. These two properties can be used to regain the original high resolution of the input signal.

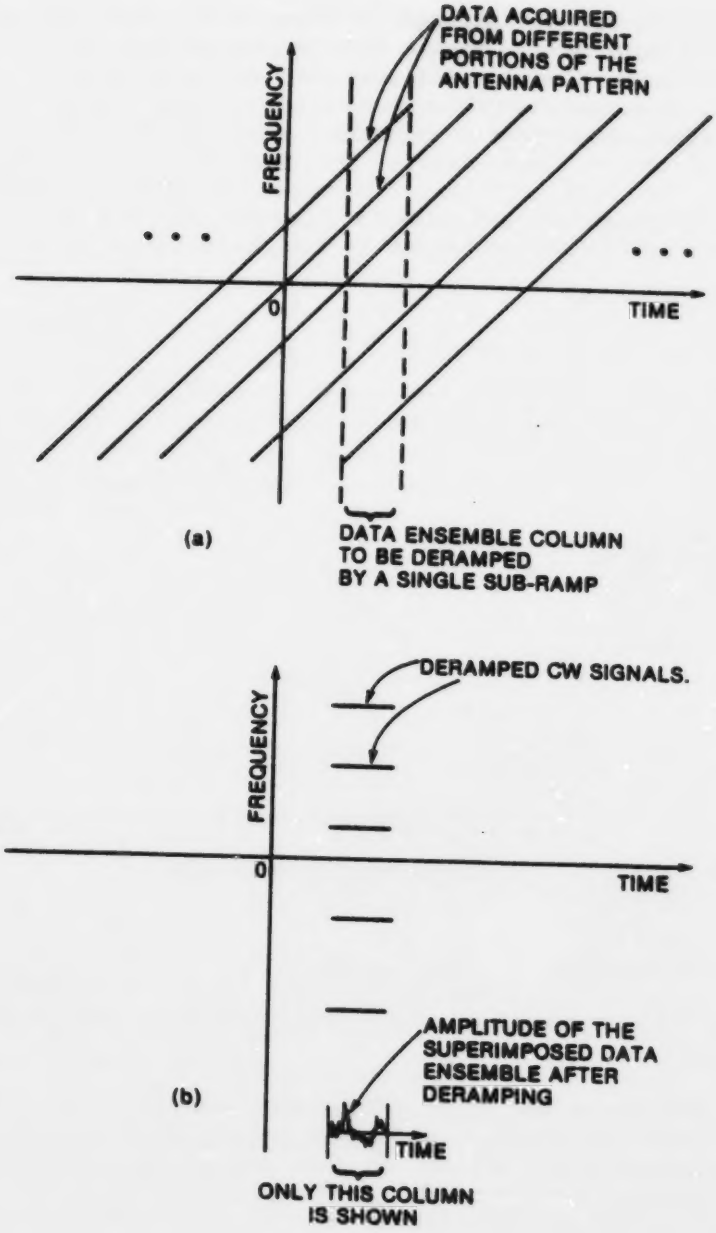

Fig. 41 - Deramping of multiple targets.

The frequency step in a sub-aperture (see Figure 41(b)) can be segregated from the superimposed ensemble data by utilising a DFT as a filter bank. The frequency stepping behaviour necessitates a two-dimensional processing scheme indexed by spectral frequency and sub-

aperture number, as illustrated in Figure 42. All the spectral energy associated with a single target can be recaptured by coherently summing the sub-apertures along a diagonal line. Each line of the diagonally arranged spectra associated with a point target contains a linear phase whose frequency is linearly dependent on its distance from the nearest sub-aperture on the time axis. The form of this phase term will be derived in the next section. Because of this intimate relationship between local frequency and time, a diagonal DFT can be used to sort out the fine details which are hidden in the first set of DFTs.

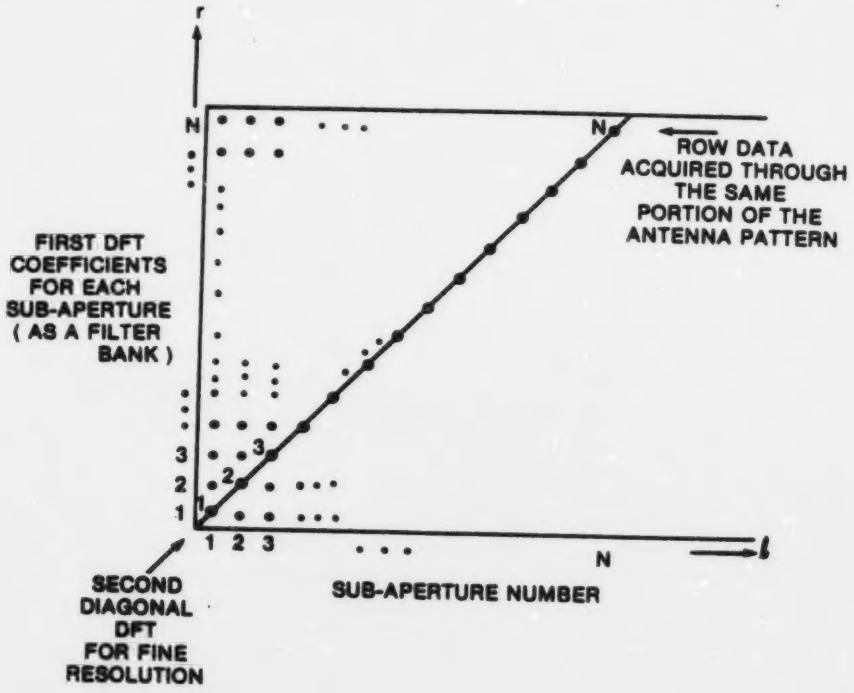

Fig. 42 - Processing matrix after the first set of DFTs.

In performing the first DFT on each sub-aperture, windowing must be applied in order to suppress sidelobes and spectral leakage. It is essential to suppress these effects so that energy spill-over onto the neighbouring diagonals is minimized. One major negative aspect of the windowing is that the spectrum is broadened. Since the first DFT is regarded as a filter bank, a broadened spectrum due to windowing means a wider band-pass filter element (wider than one cell). The widened bandwidth will undoubtedly let in energy from the adjacent diagonals. These intruders, which are further away from the diagonal under consideration, contain higher frequency components. These higher frequency components exceed the sampling rate along the diagonal. If a DFT is taken along the diagonal data array, the intruding components will fold into the desired region. In order to avoid aliasing, the sampling frequency along the diagonal direction must be increased. In order to do this, the dimension of the

processing matrix, i.e., the spacing between the first DFTs must be decreased. Since a minimum size DFT is required for adequate resolution from the first processing stage, the first DFTs become overlapped when the spacing is decreased. The above explanation is summarized in Figure 43 [7]. A block diagram of the step transform processing is shown in Figure 44.

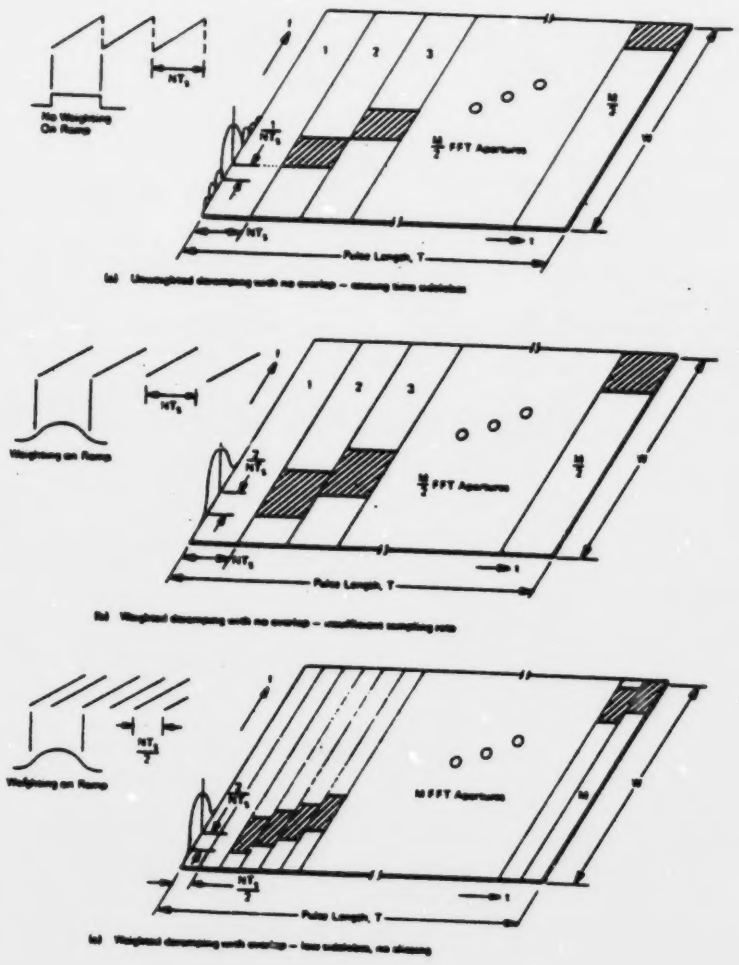

Fig. 43 - Time weighting and overlap to reduce time sidelobes and time aliasing [7].

8.2.1 Formulation of the Step Transform

In this section, which follows [6], the step transform is described mathematically. Figure 45 shows the frequency versus time diagrm for the received linear FM signal,

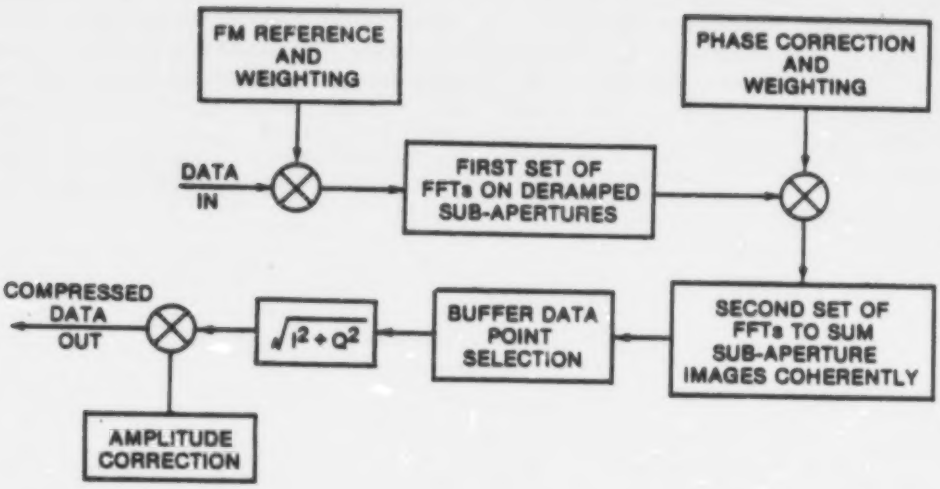
FM REFERENCE AND WEIGHTING
PHASE CORRECTION AND WEIGHTING
DATA IN
FIRST SET OF FFTs ON DERAMPED SUB-APERTURES
COMPRESSED DATA OUT
$\sqrt{I^2+Q^2}$
BUFFER DATA POINT SELECTION
SECOND SET OF FFTs TO SUM SUB-APERTURE IMAGES COHERENTLY
AMPLITUDE CORRECTION

Fig. 44 - Step transform processing procedure [6].

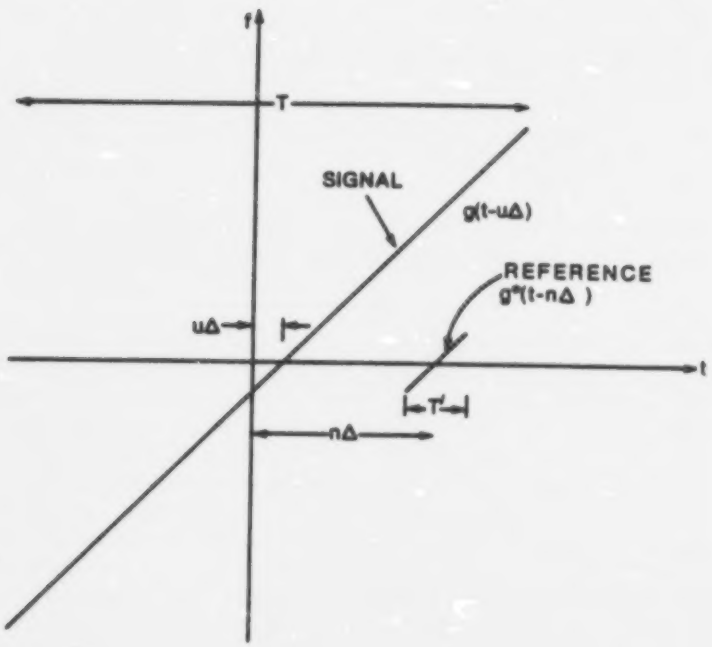

Fig. 45 - Mixing a point target signal with a reference ramp.

$$g(t-u\Delta) = e^{j\frac{\pi B}{T}(t-u\Delta)^2}, \qquad (87)$$

where $t = u\Delta$ is the time of arrival of the received signal, B is its bandwidth, and T is its duration. Also shown in the diagram is a segment of the sawtooth reference signal used to deramp the input signal. The reference segment located at $t = n\Delta$ is given by

$$g^*(t-n\Delta) = e^{-j\frac{\pi B}{T}(t-n\Delta)^2}. \qquad (88)$$

It has a duration of T', i.e.,

$$-\frac{T'}{2} + n\Delta < t < \frac{T'}{2} + n\Delta .$$

After performing the deramping within this duration, we have

$$g(t-u\Delta)g^*(t-n\Delta) = e^{j\frac{\pi B}{T}(t-u\Delta)^2} e^{-j\frac{\pi B}{T}(t-n\Delta)^2}. \qquad (89)$$

Since the processing is performed in discrete form,

$$t = (n\Delta - \frac{T'}{2}) + k\Delta, \qquad 0<k< \frac{T'}{\Delta} -1,$$

where the term in parenthesis is the beginning of the reference segment, k is the sampling index, and Δ is the sampling interval. The discrete form of (89) is

$$g\left[(n+k-u)\Delta - \frac{T'}{2}\right].g^*\left(k\Delta - \frac{T'}{2}\right)$$

$$= e^{j\frac{\pi B}{T}\left[(n+k-u)\Delta - \frac{T'}{2}\right]^2} e^{-j\frac{\pi B}{T}\left(k\Delta - \frac{T'}{2}\right)^2}$$

$$= e^{j\frac{\pi B}{T}(u^2\Delta^2+u\Delta T')} e^{j\frac{\pi B}{T}(n^2\Delta^2-n\Delta T')} e^{j\frac{2\pi B\Delta^2}{T}(n-u)k} e^{-\frac{2\pi B}{T}\Delta^2 un} \qquad (90)$$

This output is then Fourier transformed, with respect to k, to extract an image with a resolution corresponding to the bandwidth of the reference segment.

The interpretation of each exponential factor in (90) is as follows:

i) The first exponential factor is independant of the location of the sub-aperture reference n, and is solely a function of the location of the input signal u, therefore this term will not be affected by the first or subsequent Fourier transforms.

ii) The second exponential factor is an undesirable term since it does not relate n to the input signal location, u. This term is deterministic and must be cancelled out before the second Fourier transform is taken.

iii) The third exponential factor is a linear phase term, which determines where the signal spectrum is located in the frequency dimension after the first DFT is taken with respect to k. The first DFT can be regarded as a filter bank which segregates the spectral components in the sub-aperture. The spectral locations are determined by the corresponding locations relative to the sub-aperture reference.

iv) The fourth exponential factor is a phasor whose frequency of rotation depends on the location u. In order to recover the precise target location, another Fourier transform can be applied.

The DFT of (90) with respect to k, (ignoring the first exponential factor) is,

$$
\begin{aligned}
X(r,n) &= e^{j\frac{\pi B}{T}(n^2\Delta^2 - n\Delta T')} \; e^{-j\frac{2\pi B}{T}\Delta^2 un} \; \mathcal{F}\{e^{j\frac{2\pi B\Delta^2}{T}(n-u)k}\}, \\
&= e^{j\frac{\pi B}{T}(n^2\Delta^2 - n\Delta T')} \; e^{-j\frac{2\pi B}{T}\Delta^2 un} \sum_{k=0}^{N-1} e^{j\frac{2\pi B\Delta^2}{T}(n-u)k} \; e^{-j\frac{2\pi rk}{N}}, \\
&= e^{j\frac{\pi B}{T}(n^2\Delta^2 - n\Delta T')} \; e^{-j\frac{2\pi B}{T}\Delta^2 un} \sum_{k=0}^{N-1} e^{j2\pi\left[\frac{NB\Delta^2}{T}(n-u)-r\right]\frac{k}{N}}, \\
&= e^{j\frac{\pi B}{T}(n^2\Delta^2 - n\Delta T')} \; e^{-j\frac{2\pi B}{T}\Delta^2 un} \; \mathrm{sinc}\left[r - \frac{NB\Delta^2}{T}(n-u)\right],
\end{aligned}
\tag{91}
$$

where $\mathcal{F}\{\}$ is a Fourier transform operator, $N = \frac{T'}{\Delta}$ is the number of points in the DFT, r is the frequency variable corresponding to the temporal variable k, and sinc(.) is a cyclic sinc-function defined as $\mathrm{sinc}(x) = \sin(\pi x)/\sin(\pi x/N)$.

The location of the sinc-function depends on the spatial separation between the target and the reference ramp, $(n-u)\Delta$, i.e. the target is located at $r = r'$

$$
r' = \frac{NB\Delta^2}{T}(n-u), \tag{92}
$$

relative to the sub-aperture reference located at $t = n\Delta$.

Assuming tht the input signal is sampled at the Nyquist rate, we have $B\Delta=1$. If the signal is oversampled (i.e. $B\Delta<1$), as is normally done in practice, some of the Fourier coefficients in r will be small, containing only noise and leakages, but this will not affect our analysis. Hence, (92) becomes

$$r' = \frac{N\Delta}{T}(n-u),$$

$$= \frac{T'}{T}(n-u). \qquad (93)$$

Furthermore, if we set the number of sub-apertures that can be fit into a full aperture to also be N, i.e. $T/T' = N$, then (93) can be simplified to

$$r' = \frac{n}{N} - \frac{u}{N} \qquad (94)$$

In summary, the aperture data is divided into N sub-apertures of N samples each, which gives a total of N^2 points for a full aperture data set. Equating (92) and (94) gives the value of N

$$N^2 = \frac{T}{B\Delta^2},$$

$$= \frac{1}{(\text{FM rate})\Delta^2}. \qquad (95)$$

Since adjacent sub-aperture references are separated by n=N cells, the sub-apertures can be indexed by a new parameter ℓ, defined as $\ell = n/N$. Equation (94) then becomes,

$$r' = \ell - \frac{u}{N} \qquad (96)$$

Substituting (95) and (96) into (91), we have

$$X(r,\ell) = e^{j\pi(\ell^2-\ell)}\, e^{-j\frac{2\pi u\ell}{N}}\, \text{sinc}\left[r-\ell+\frac{u}{N}\right]. \qquad (97)$$

Thus, (95) ensures that the signal history associated with a point target lies on a line with unit slope (in the r versus ℓ plane) and passing through the ℓ axis at u/N, as denoted in (96). This arrangement makes the processing more efficient since further processing can proceed along successive diagonal lines with unit slope, and no interpolation is needed. If FFTs are to be used to perform DFTs, N must be a power-of-two integer. Unfortunately, this imposes a stringent restriction on the signal characteristic, namely the FM rate and the sampling interval, upon which a step transform can be accurately applied. This restriction can be partially relieved by overlapping the sub-aperture reference ramps as will

be described in Section 8.2.2.

To obtain the full resolution, the sub-aperture data represented by (91) must be added coherently over the entire aperture. The processing is two-dimensional (across aperture, 'ℓ', and within aperture, 'r'). The coherent summation is performed via an IDFT with respect to ℓ(=n/N) along the diagonal line r=ℓ, i.e.

$$Y(q) = \sum_{\ell=-N/2}^{N/2-1} \left[X(\ell,\ell)\, e^{-j\pi(\ell^2-\ell)} \right] e^{j\frac{2\pi q\ell}{N}}, \qquad (98)$$

where q is the time domain equivalent of the sub-aperture number 'ℓ'. The exponential factor in parentesis cancels the first exponential term in (97). Before the second DFT is taken in (99a), X(r,ℓ) should be rotated over r by half a cycle (i.e. N/2) in order to ensure that the negative axis in r precedes the positive axis in a linear continuous manner. In practice, this can be achieved by embedding an appropriate linear phase term in the reference ramp. If we substitute X(ℓ,ℓ) from (97) into (98), we get

$$Y(q) = \sum_{\ell=-N/2}^{N/2-1} e^{-j\frac{2\pi u\ell}{N}}\, \mathrm{sinc}\left[\frac{u}{N}\right] e^{j\frac{2\pi q\ell}{N}},$$

$$= \mathrm{sinc}\left[\frac{u}{N}\right] \sum_{\ell} e^{-j\frac{2\pi u\ell}{N}}\, e^{j\frac{2\pi q\ell}{N}}, \qquad (99a)$$

$$= \mathrm{sinc}\left[\frac{u}{N}\right] \mathrm{sinc}[q-u],$$

$$= \mathrm{sinc}\left[\frac{q}{N}\right] \mathrm{sinc}[q-u]. \qquad (99b)$$

Hence after both DFTs (forward and inverse DFTs are collectively referred to as DFTs since they do not bear the usual connotations of the Fourier transforms), a target located at t=uΔ is recovered as a compressed pulse denoted by the second sinc function in (99b) at q=u. The first sinc-function in (99b) is an envelope modulation function inherited from the rectangular window in the first DFT.

As mentioned previously, the input data are assumed to be adequately sampled, therefore there is no aliasing effect in the first DFT. However, as described in (99a), the Nyquist criterion is violated in the second DFT. The width of the mainlobe of the envelope function is 2N, whereas the sampling rate is only N, i.e. the DFT length is only N. Hence, areas of the mainlobe corresponding to $|u| > \frac{N}{2}$ are folded back into

unambiguous region of the DFT resulting in heavy degradation of the radar image. The aliasing effect is shown in Figure 46. Three point targets A, B and C are shown. The top diagram shows that A, B and C are unambiguously resolved as if there is no aliasing problem in the second DFT. The bottom diagram shows the realistic case where the function is circularly periodic, with period q.

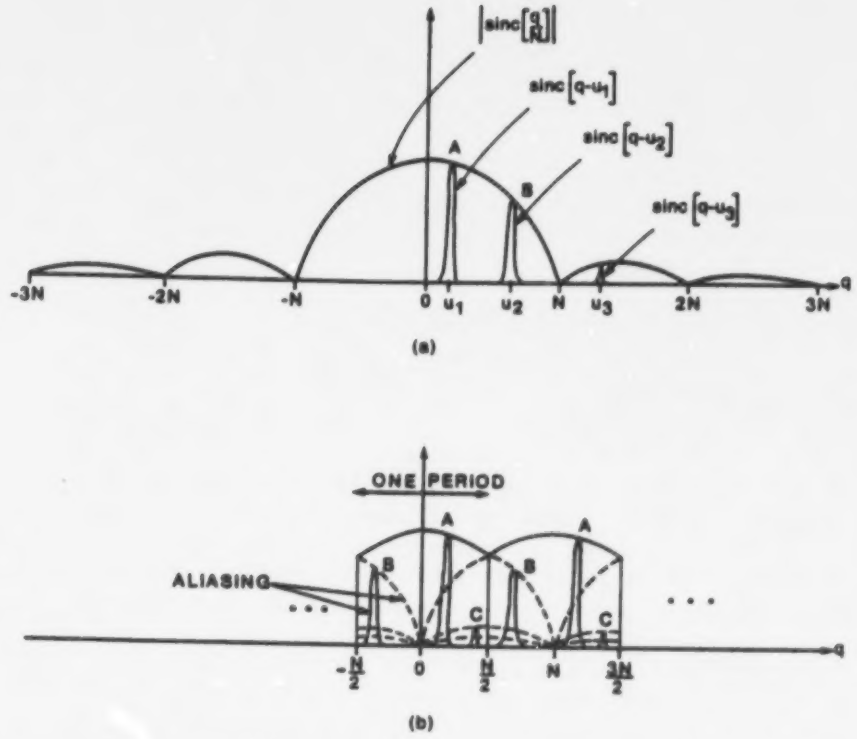

Fig. 46 - Compressed image after coherent summation of sub-aperture images along a diagonal line in the processing matrix. Three point targets A, B and C are shown, (a) assuming no aliasing, (b) with aliasing.

8.2.2 Effects of Windowing and Sub-aperture Overlap on the Step Transform

In order to avoid the aliasing effect, the signal, $\exp\{-\frac{2\pi ui}{N}\}$ in (99a), must be adequately sampled in 'i', and the point target response of the first DFT, i.e. the sinc-function in (99a) must be replaced by one with a negligible sidelobe level.

To suppress the sidelobe level of the target response of the first DFT, windowing can be imposed on the sub-aperture data before the DFT is

taken. In practice, a Hamming window is used to suppress the sidelobes to less than -43dB. In such a case, (91) becomes

$$X(r,n) = e^{j\frac{\pi B}{T}(n^2\Delta^2 - n\Delta T')} \; e^{-j\frac{2\pi B}{T}\Delta^2 un}$$

$$F\left\{\left[0.54-0.46\cos\left(2\pi\frac{k+0.5}{N_\xi}\right)\right] e^{j\frac{2\pi B\Delta^2}{T}(n-u)k}\right\},$$

$$= e^{j\frac{\pi B}{T}(n^2\Delta^2 - n\Delta T')} \; e^{-j\frac{2\pi B}{T}\Delta^2 un} \; W\left[r-\frac{N_\xi B\Delta^2}{T}(n-u)\right], \quad (100)$$

N_o is now replaced by N_ξ to signify the effects of windowing and overlapped sub-apertures, and W(r) is the Fourier transform of the Hamming window, which is given by

$$W(r) = 0.54D(r) + 0.23\left[D(r-1)+D(r+1)\right],$$

and

$$D(r) = e^{j\frac{\pi r}{N}} \frac{\sin(\pi r)}{\sin(\pi r/N_\xi)} .$$

To increase the sampling rate in 'ℓ', the spacing between adjacent sub-aperture references needs to be smaller than N. This implies that they have to overlap. Let ξ be the ratio of the number of cells overlap to the number of cells in a sub-aperture. The sub-aperture index 'ℓ' is redefined as

$$\ell = \frac{n}{N_\xi(1-\xi)} , \quad (101)$$

where the factor $N(1-\xi)$ represents the sub-aperture reference spacing in number of cells.

If the processing efficiency for the second DFT is to be maintained, the locus of the envelope function of $X(r,\ell)$, $W(r,\ell)$, given by (100) needs to lie on a diagonal line parallel to $r=\ell$, as in the previous case, otherwise interpolation would be required. This discrete space arrangement can be achieved by modifying (95) to

$$N_\xi^2 = \frac{T}{(1-\xi)B\Delta^2},$$

$$= \frac{1}{(1-\xi)(\text{FM rate})\Delta^2}. \quad (102)$$

Substituting (101) and (102) into (100), we have

$$X(r,\ell) = e^{j\pi\ell[(1-\xi)\ell-1]}\, e^{-j\frac{2\pi u\ell}{N_\xi}}\, W\left[r-\ell+\frac{u}{N_\xi(1-\xi)}\right]. \qquad (103)$$

Note that the diagonality property (r-ℓ for the signal position) is maintained in the argument of W[.].

We can perform coherent summation along the diagonal line r=ℓ via an IDFT with Hamming window:

$$Y(q) = \sum_{\ell=N/2}^{N/2-1} \left[0.54-0.46\cos\left(2\pi\frac{\ell+0.5}{N_\xi}\right)\right] X(\ell,\ell)\, e^{-j\pi\ell[(1-\xi)\ell-1]}\, e^{j\frac{2\pi u\ell}{N_\xi}}, \qquad (104a)$$

$$= W\left[\frac{u}{N_\xi(1-\xi)}\right] \sum_{\ell} \left[0.54-0.46\cos\left(2\pi\frac{\ell+0.5}{N_\xi}\right)\right] e^{-j\frac{2\pi u\ell}{N_\xi}}\, e^{j\frac{2\pi q\ell}{N_\xi}},$$

$$= W\left[\frac{u}{N_\xi(1-\xi)}\right] W[q-u],$$

$$= W\left[\frac{q}{N_\xi(1-\xi)}\right] W[q-u], \qquad (104b)$$

This result is analogous to the previous case without windowing and sub-aperture overlap, as described by (99b). The sinc-functions are now replaced by the Fourier transform of Hamming window. The compressed pulse is represented by the second W-function located at q=u. The first W-function represents an envelope due to the Hamming window in the first DFT. The W-function offers a much lower sidelobe level (<-43dB) than the sinc-function (-13dB). Hence in most cases the W-function can be regrarded as sidelobe free.

A minor penalty introduced by the W-function is that its mainlobe width (null-to-null) is four cells wide, whereas that of the sinc-function is two cells wide. The mainlobe would cause more mainlobe aliasing, if it were not for the overlapping of the sub-apertures. Assuming the sidelobe level is negligibly low, the W-function in (104a) limits u to the region $-2 \text{ cells} < \frac{u}{N_\xi(1-\xi)} < 2 \text{ cells}$, recalling that the Fourier transform of the Hamming windowing has a null-to-null mainlobe width of four cells. The N-point Fourier transform allows $-\frac{N_\xi}{2} \le u < \frac{N_\xi}{2}$. Equating thes inequalities gives a sub-aperture overlap ratio, $\xi = 0.75$. For point targets lying outside the region, i.e. $\left|\frac{u}{N_\xi(1-\xi)}\right| > 2$, the W-function attenuation

becomes so large (>43dB) that aliasing becomes unimportant. The above aliasing mechanism is illustrated in Figure 47.

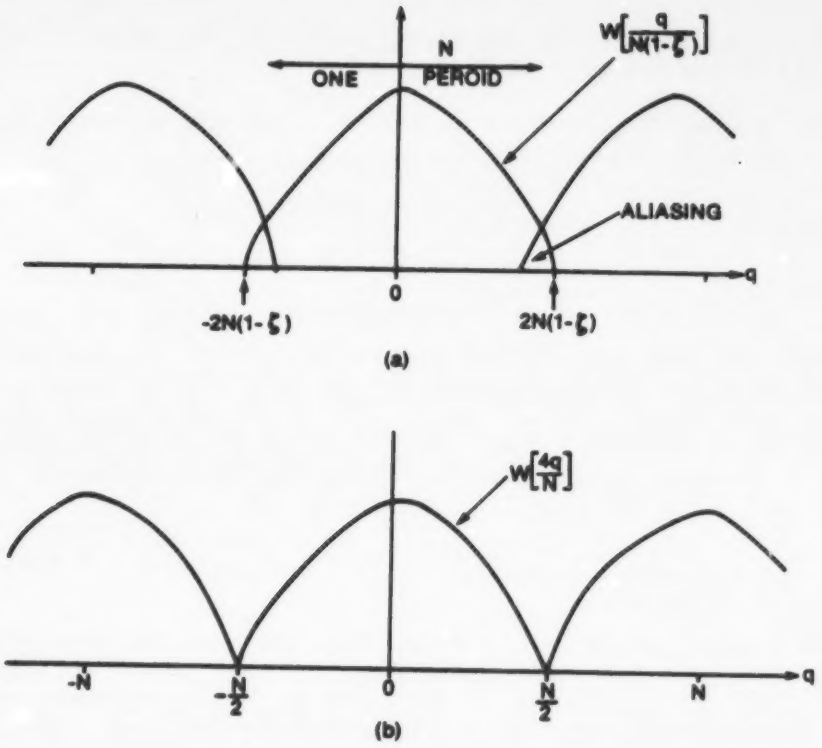

Fig. 47 - Aliasing mechanism due to the envelop function of the Hamming window, (a) with aliasing for $\xi < 0.75$, (b) minimum condition with no aliasing, $\xi = 0.75$.

The processing efficiency can be further improved by minimizing the sub-aperture overlap, and hence reducing the processing of duplicate data. The amount of overlap can be reduced by allowing aliasing in the portion of the data tht will be thrown away. The alias free region is defined as the width of the separation between adjacent sub-aperture references, i.e., $-\frac{N_\xi(1-\xi)}{2} \leq u < \frac{N_\xi(1-\xi)}{2}$. Targets falling in the aliased regions, namely, $-2N_\xi(1-\xi) \leq u < -\frac{N_\xi(1-\xi)}{2}$ and $\frac{N_\xi(1-\xi)}{2} \leq u < (1-\xi)$, are recovered from the unaliased regions of adjacent diagonal DFTs. Figure 48 illustrates how allowing aliasing in the throwaway region can reduce the amount of sub-aperture overlay. In the diagram, the envelope modulation function (the first term in (104b)) is partitioned into five regions (A to E). The unambiguous width in q is kept at N_ξ. Region C represents an unaliased region, from which valid processed data are derived. The other regions produce duplicate (invalid) processed data.

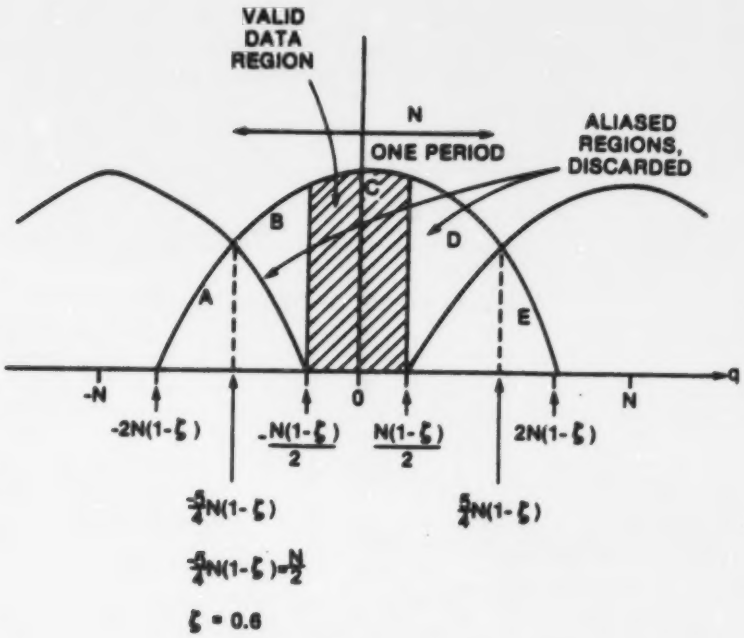

Fig. 48 - Improved processing efficiency by allowing aliasing into discarded regions.

It is desirable to let region A to fold into region D, and region E to fold into region B, in order to pack all regions compactly within N cells. Regions B and D now contain aliased data and will be discarded. In this case, as shown in the diagram, the optimum value of is 0.6. Data from region C is retained as valid data. The valid data are amplitude corrected by multiplying by the inverse of the envelope function (i.e. $\frac{1}{W[\frac{q}{N\xi(1-\xi)}]}$). The process is repeated for all diagonal data, and then all valid data are concatenated to form an image.

In cases where $0.2<\xi<0.6$ for a selected value of N_ξ, the data, which lie on a diagonal after the first set of FFTs, are undersampled as just described. This can be remedied by using another set of sub-aperture references to interpolate the original diagonal data array. The method is illustrated in Figure 49. The top diagram shows the signal of a point target with the original sub-aperture reference. The middle diagram shows the signal with another sub-aperture reference. The new sub-aperture reference is so designed that it is delayed by half a period from the original sub-aperture sawtooth, and has a negative frequency offset corresponding to half a resolution cell. This offset reference provides an additional sampling process to obtain the in-between value of the

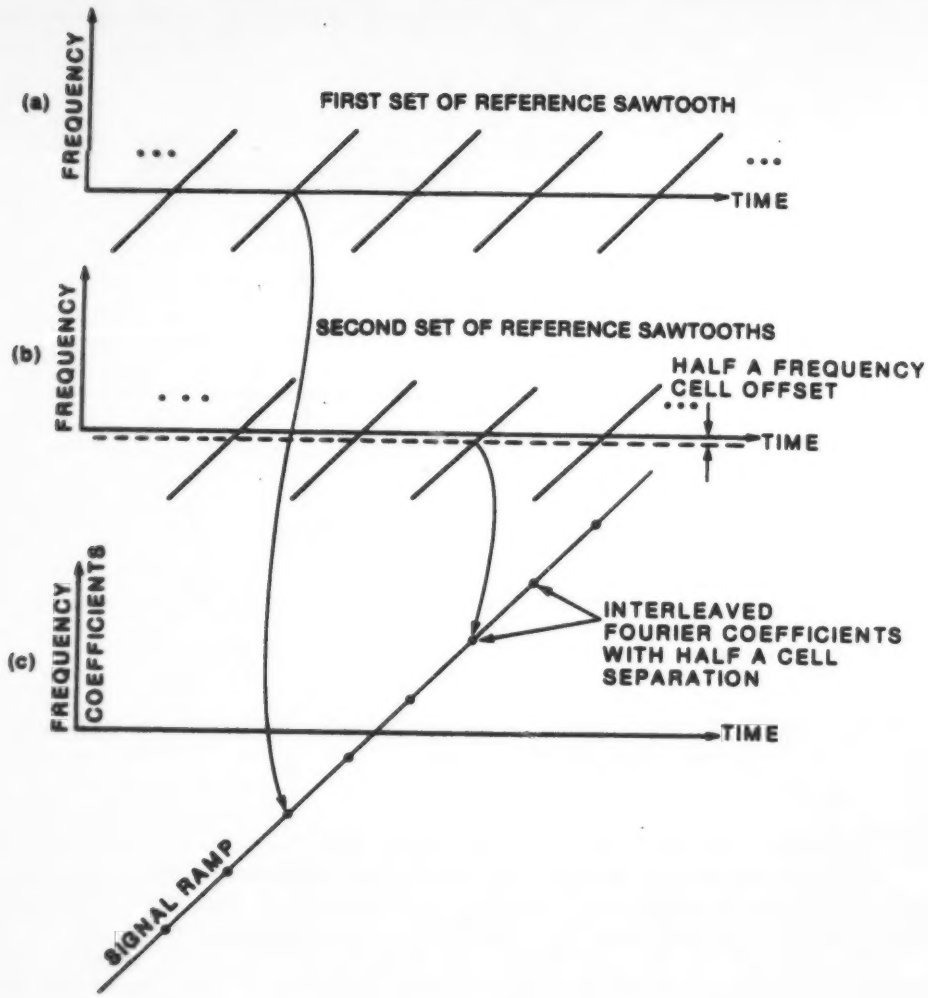

Fig. 49 - Two sets of reference ramps for cases with $0.2 < \xi < 0.6$.

original diagonal data array. Phase correction is then imposed on both diagonal arrays as described in (47). Because of the additional frequency offset in the second diagonal data array, an additional phase correction factor, $\exp\{-j\frac{\pi B}{T}\frac{T'}{2}\}$, is required. This is done to maintain phase coherency between the two diagonal arrays. The data from the arrays are interleaved (as shown in the bottom diagram) before the second FFT of length $2N$ is taken.

In cases where $0 < \xi < 0.2$, one has to choose a larger value of N or tolerate a fair amount of degradation.

8.2.3 Computer Simulation Results

Figure 50 shows the result of a computer simulation for a point target, which had a time-bandwidth product of 384, and which was processed

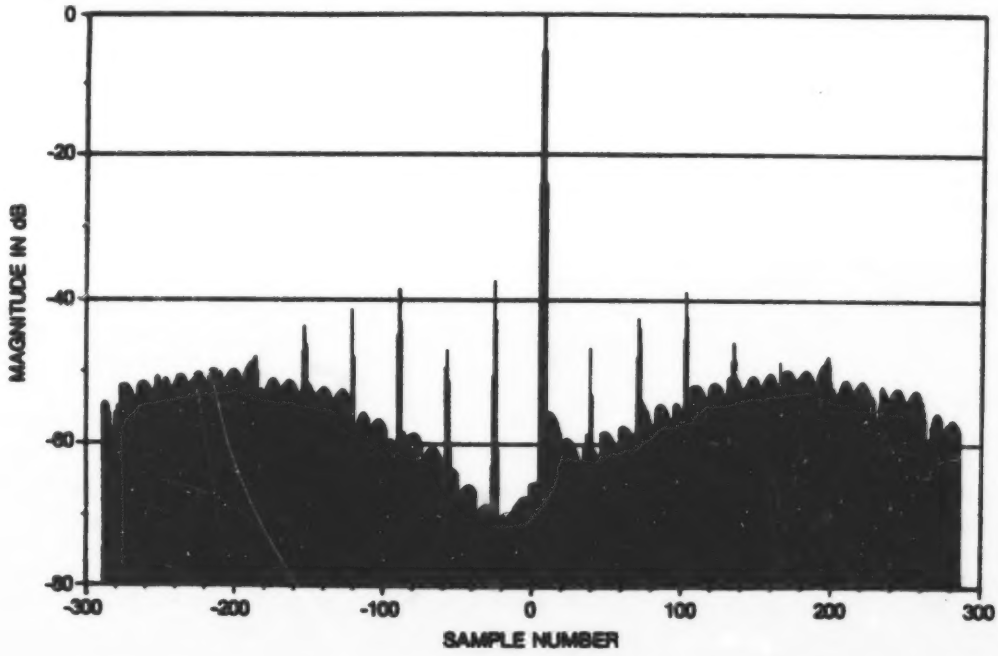

Fig. 50 - Compressed pulse of a point target processed with step transform.

with a sub-aperture of length of 32 cells, overlapped with the other sub-apertures by 20 cells (62.5%). The prominent main peak has been normalized to 0dB. Artifacts are noticeable but are mostly at least -40dB down from the main peak. These artifacts originate from the sidelobe structure of the first W-function given in (104b).

The humps on each side of the mainlobe are due to spectral leakage from the incompletely filled sub-apertures at both extreme ends of the diagonal, i.e. the data starts and ends part way through those sub-aperture. These partially filled sub-apertures have lower resolution than the rest, and the data corresponding to the target is spread widely over the 'r'-dimension after the first DFT is taken. This data does not get properly incorporated in the Fourier transform along the diagonal, but instead it contributes to the integrated sidelobe ratio. The shapes of the humps are determined by the window used in the diagonal DFT. The peaks of the humps are located at approximately $\frac{N\xi^2(1-\xi)}{2}$ from either side of the main peak, where ξ is the portion of sub-aperture overlap.

8.2.4 Effects of the Cubic Term on the Step Transform

The foregoing description of the step transform assumes that the input signal is strictly linear FM. It is thelinearity (in frequency versus time) of a linear FM signal that allows the step transform, which follows the trend of the linear FM slope in a step-wise fashion, to be used to perform pulse compression. The introduction of cubic and higher order phase terms destroys the desirable linear relationship, and results in unequal deramped frequency step intervals, and other abnormalities, such as defocussing in the output of the first DFT. In this section, as was done for the matched filter approach, we will consider the effect of the cubic phase term, and seek ways to remedy the problem it causes.

In the following analysis, we assume the form of the received signal to be

$$g(t-u\Delta) = e^{j\frac{\pi B}{T}(t-u\Delta)^2 + j2\pi\varepsilon(t-u\Delta)^3}, \quad -\frac{T}{2}+u\Delta \leq t \leq \frac{T}{2}+u\Delta, \tag{105}$$

where $t=u\Delta$ is the time of arrival of the mid-point of the received signal, Δ is the sampling interval, B is the second-order signal bandwidth, and T is the second-order signal duration. The first phase factor represents the second-order azimuth signal (i.e., a linear FM signal). The second phase factor represents the third-order azimuth signal, seen at extreme adar squint angles [2]. The coefficient ε is in cycles/sec^3.

A segment of the sawtooth reference, centred at $t=n\Delta$, is used to deramp the input signal. The reference is shown in Figure (8.21), and is given by,

$$g^*(t-n\Delta) = e^{-j\frac{\pi B}{T}(t-n\Delta)^2}. \tag{106}$$

It has a duration of T', i.e.,

$$-\frac{T'}{2} + n\Delta \leq t \leq \frac{T'}{2} + n\Delta. \tag{107}$$

After multiplying the input signal by the reference function, we have,

$$g(t-u\Delta)\, g^*(t-n\Delta) = e^{j\frac{\pi B}{T}(t-u\Delta)^2+j2\pi\varepsilon(t-u\Delta)^3} \; e^{-j\frac{\pi B}{T}(t-u\Delta)^2}. \tag{108}$$

Because the processing is performed in discrete form, t must be replaced by

$$t = (n\Delta - \frac{T'}{2}) + k\Delta, \quad 0 \leq k \leq N_\xi - 1, \quad N_\xi = \frac{T'}{\Delta}, \tag{109}$$

where the term in parenthesis is the beginning of the reference segment, and k is the sampling index within the sub-aperture. The discrete form of (108) is

$$g\left[(n+k-u)\Delta - \frac{T'}{2}\right] g^*(k\Delta - \frac{T'}{2})$$

$$= e^{j\frac{\pi B}{T}(u^2\Delta^2+u\Delta T')} \; e^{j\frac{\pi B}{T}(n^2\Delta^2-n\Delta T')} \; e^{j\frac{2\pi B\Delta^2}{T}(n-u)k}$$

$$e^{-j\frac{2\pi B\Delta^2}{T}un} \; e^{j2\pi\varepsilon\left[(n+k-u)\Delta - \frac{T'}{2}\right]^3}. \quad (110)$$

The first factor in (110) is solely dependent on u and is of no importance to the image processing. It will therefore be dropped. With this change (110) becomes

$$g\left[(n+k-u)\Delta-\frac{T'}{2}\right] g^*(k\Delta-\frac{T'}{2})$$

$$= e^{j\frac{\pi B}{T}(n^2\Delta^2-n\Delta T')} \; e^{j\frac{2\pi B\Delta^2}{T}(n-u)k} \; e^{-j\frac{2\pi B\Delta^2}{T}un} \; e^{j2\pi\varepsilon\left[(k\Delta-u\Delta-\frac{T'}{2})+n\Delta\right]^3}.$$

(111)

The last exponential factor in (111) is solely due to the cubic phase term. The k-dependancy in this factor signifies that the error caused by the cubic term is proportional to the duration of a sub-aperture. In practice, the sub-aperture length is much shorter than the full aperture, and the variation in the phase factor as k changes from one end of the practice, the sub-aperture length is much shorter than the full aperture, and the variation in the phase factor as k changes from one end of the sub-aperture to the other is very small. An expansion of this factor gives

$$e^{j2\pi\varepsilon\left[(k\Delta-u\Delta-\frac{T'}{2})+n\Delta\right]^3} = e^{j2\pi\varepsilon(k\Delta-u\Delta-\frac{T'}{2})^3} \; e^{j2\pi\left[3\varepsilon(k\Delta-u\Delta-\frac{T'}{2})^2 n\Delta\right]}$$

$$e^{j2\pi\varepsilon(n\Delta)^3} \; e^{j2\pi\left[3\varepsilon(k\Delta-u\Delta-\frac{T'}{2})(n\Delta)^2\right]}. \quad (112)$$

The significance of these phase terms is depicted in Figure 51, and is explained as follows:

i) The first exponential factor is independent of n. It represents the phase deviation due to the cubic term of the input signal within the sub-aperture located nearest to the centre of the full aperture. This term is extremely small and is of the order of less than 0.5° for highly-squinted (e.g. 6° from flight direction), high resolution (e.g. 1 metre), and long slant range (e.g. 100 km) cases operating at x-band.

ii) The second exponential factor, which is a function of n, represents the additional phase error within a deramped sub-aperture. This phase error is rather small under most stringent circumstances, it is less than 10° for sub-apertures located at the ends of the full aperture.

iii) The third exponential factor depends solely on n. Itdescribes the global phase error along the input data. Its magnitude may be rather significant and it must be cancelled before the second DFT is performed.

iv) The fourth exponential factor, dependent on k, u, and n, is the amount of frequency offset from the normal deramped CW signal. This frequency offset shows up as a shift in the spectrum produced by the first DFT.

In summary, the first two exponential factors describe the local residual phase errors within a sub-aperture. Their magnitudes are normally too small to affect the final result. The last two exponential factors describe the global residual phase error and the frequency offset respectively. Their effect on the final result is worth further consideration.

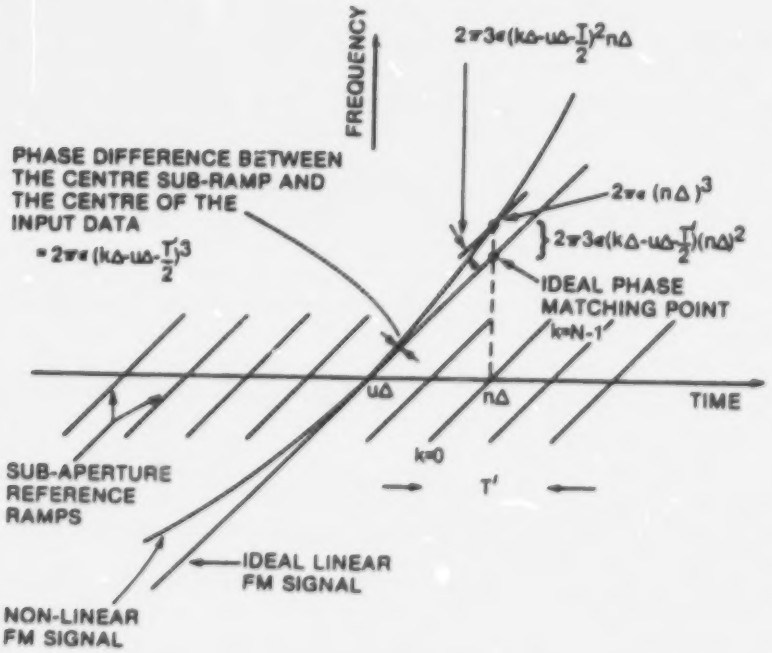

Fig. 51 - Deramping a non-linear FM signal with cubic phase. All errors are shown for the case in which an ideal sawtooth reference is applied.

With only the last two phase factors of the expansion included, the deramped signal of (8.30) can be written as

$$g\left[(n+k-u)\Delta-\frac{T'}{2}\right]\, g^*\left(k\Delta-\frac{T'}{2}\right)$$

$$= e^{j\frac{\pi B}{T}(n^2\Delta^2-n\Delta T')}\; e^{j\frac{2\pi B\Delta^2}{T}(n-u)k}\; e^{-j\frac{2\pi B\Delta^2}{T}un}\; e^{j2\pi\varepsilon(n\Delta)^3}$$

$$e^{j2\pi\left[3\varepsilon(k\Delta-u\Delta-\frac{T'}{2})(n\Delta)^2\right]}. \qquad (113)$$

The image is produced from (113) by using the modified step transform. First a Hamming window is imposed on the sub-aperture in order to suppress sidelobe leakage, and a DFT is taken with respect to k; the result is

$$X(r,n) = e^{j\frac{\pi B}{T}(n^2\Delta^2-n\Delta T')}\; e^{j2\pi\varepsilon(n\Delta)^3}\; e^{-j6\pi\varepsilon(u\Delta+\frac{T'}{2})(n\Delta)^2}\; e^{-j\frac{2\pi B\Delta^2}{T}un}$$

$$\sum_{k=0}^{N-1}\left[0.54-0.46\cos\left(2\pi\frac{k+0.5}{N_\xi}\right)\right]$$

$$\left[e^{j\frac{2\pi B\Delta^2}{T}(n-u)k}\; e^{j2\pi 3\varepsilon k\Delta(n\Delta)^2}\right] e^{-j\frac{2\pi rk}{N_\xi}},$$

$$= e^{j\frac{\pi B}{T}(n^2\Delta^2-n\Delta T')}\; e^{j2\pi\varepsilon(n\Delta)^3}\; e^{-j6\pi\varepsilon(u\Delta+\frac{T'}{2})(n\Delta)^2}\; e^{-j\frac{2\pi B\Delta^2}{T}un}$$

$$W\left[r-\left(\frac{N_\xi B\Delta^2(n-u)}{T}+3N_\xi\varepsilon\Delta^3n^2\right)\right]. \qquad (114)$$

where W(r) is the Fourier transform of the Hamming window and is given by

$$W(r) = 0.54D(r)-0.23[D(r-1)+D(r+1)], \qquad (115)$$

and

$$D(r) = e^{j\frac{\pi r}{N_\xi}}\frac{\sin[\pi r]}{\sin[\frac{\pi r}{N_\xi}]}.$$

Substituting (101), (102) and $T' = N_\xi\Delta$ into (113) yields

$$X(r,\ell) = e^{-j6\pi\varepsilon N_\xi^2(1-\xi)^2\Delta^3u\ell^2}\; e^{j\pi B(\ell)}$$

$$e^{-j\frac{2\pi}{N_\xi}u\ell}\; W\left[r-\ell-3\varepsilon N_\xi^3(1-\xi)^2\Delta^3\ell^2+\frac{u}{N\xi(1-\xi)}\right], \qquad (116)$$

where $\beta(\ell) = 2\varepsilon\left[N_\xi(1-\xi)\Delta\right]^3\ell^3 + \left[1-\varepsilon-3\varepsilon N^3(1-\xi)^2\Delta^3\right]\ell^2-\ell$. We can see that the location of the spectrum is off by $[3\varepsilon N_\xi^3(1-\xi)^2\Delta^3\ell^2]$ cells from the normal diagonal position. If uncompensated this positional shift will result in amplitude tapering of the signal on both ends of the diagonal; moreover, the energy associated with one diagonal can curve into the adjacent diagonals. This intermixing of diagonals will introduce image blurring into the DFT of the adjacent diagonals.

If this amount of degradation is intolerable, then the curvature can be corrected by interpolation along the r-dimension after the first DFT.

The W-function in (116) represents a narrow bandpass filter moving along a locus described by $r = \ell + 3\varepsilon N_\xi^3(1-\xi)^2\Delta^3\ell^2$, in the r versus ℓ plane. To regain the original resolution, a coherent summation (DFT) over r needs to be performed along this locus.

The first exponential factor in (116)is dependant on the location of the target, u, and the sub-aperture location, ℓ. The maximum phase value of this term occurs at the above extreme values

$$|u| = \frac{N_\xi(1-\xi)}{2} \text{ and } |\ell| = \frac{N_\xi}{2}, \text{ i.e.}$$

$$\theta_{max} = 0.75\pi\varepsilon N^5\Delta_\xi^3(1-\xi)^3,$$

$$= \frac{0.75\pi\varepsilon T^3}{N_\xi}. \qquad (117)$$

The maximum tolerable θ_{max} value is 0.75π for a heavily weighted DFT (see (120) below). Therefore

$$N_\xi > \varepsilon T^3. \qquad (118)$$

Substituting the criterion in (118) into the cubic phase at the end of a full aperture as given in (105), gives

$$\theta_{cubic} = 2\pi\varepsilon\left(\frac{T}{2}\right)^3,$$

$$< \frac{\pi N_\xi}{4}. \qquad (119)$$

In other words, if the cubic phase at the end of the full aperture is $\pi N_\xi/4$ or less, then the first exponential factor in (116) is insignificant, and will be dropped henceforth. For example if $N_\xi = 32$, the maximum tolerable cubic phase at the end of the full aperture is 1440; a phase error which would otherwise be intolerable if no sub-aperture compensation is used.

Before proceeding with the coherent sub-aperture summation, namely, a second DFT, the second and third exponential factors in (116) should be cancelled. When this is done the second DFT with Hamming window becomes,

$$Y(q) = \sum_{\ell=-N_\xi/2}^{N_\xi/2-1} X(r,\ell)\left[0.54-0.46\cos\left(2\pi\frac{\ell+0.5}{N_\xi}\right)\right] e^{-j\pi\beta(\ell)} e^{j\frac{2\pi q\ell}{N_\xi}},$$

$$= W\left[\frac{u}{N_\xi(1-\xi)}\right] \sum_{\substack{\text{along}\\ r=\ell+\beta\xi N_\xi^2(1-\xi)^2\Delta^3\ell^2}} \left[0.54-0.46\cos\left(2\pi\frac{\ell+0.5}{N_\xi}\right)\right] e^{-j\frac{2\pi u\ell}{N_\xi}} e^{j\frac{2\pi q\ell}{N_\xi}}$$

$$= W\left[\frac{u}{N_\xi(1-\xi)}\right] W[q-u]. \qquad (120)$$

After both DFTs, a target located at $t = u\Delta$ is recovered as a compressed pulse, $W[q-u]$. The first W-function in (120) represents an undesired amplitude modulation function inherited from the Hamming weighting in the first DFT, and should be corrected.

8.2.5 Range Curvature Compensation

Range curvature can be compensated in a similar fashion to the matched filtering case described in Section 7.1. In the step transform, the range curvature compensation should take place after the first set of DFTs. Referring back to Figure 42, each row of data indexed in ℓ have the same frequency characteristic and are acquired through the same portion of the antenna pattern. Thus each row of data in the processing matrix suffers the same amount of curvature, whereas the data in a column, which are each acquired from different angles, suffer different amounts of curvature. To perform the interpolation a number, based on the length of the interpolator, of processing matrices from consecutive ranges are collected (see Figure 52). Interpolation is then performed across the matrices on a set of corresponding data (ℓ,r), one from each processing matrix.

9. COMPUTATIONAL REQUIREMENTS

In this section, we attempt to give an assessment of the computational requirements for the foregoing SAR data processing algorithms. SAR data processing is often characterized by its voluminous data size, and the stringent requirement for arithmetic operations. Thus the design of a SAR processor should be optimized in terms of arithmetic complexity and control-function complexity. The predominant factors for consideration are the throughput rate, the pulse-compression ratio, and the number of looks. A desirable algorithm for SAR data processing should be selected by making the necessary tradeoffs between these factors. Because of a large number of parameters, the computational rates of

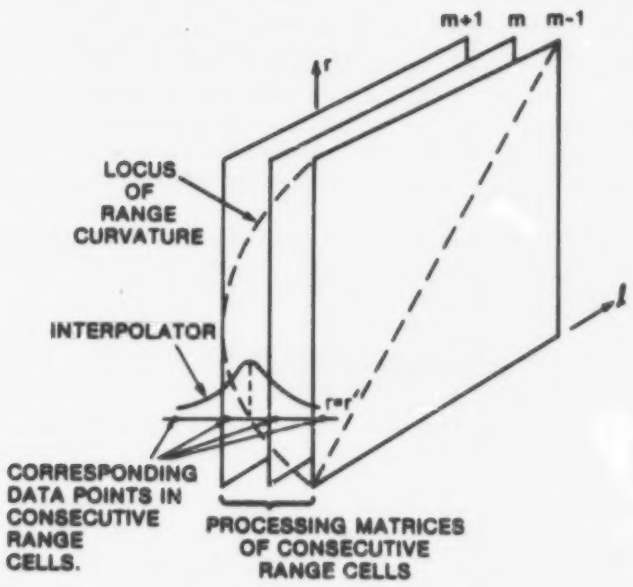

Fig. 52 - Range curvature compensation in step transform.

generalized optimal processing schemes are not easily compared. In general, the matched filtering approach requires less control-function complexity and provides more flexibility and exactness in tailoring the matched filter to fit the data. On the other hand, the deramping technique demands less memory and can proceed in a continuous rather than batch fashion, and is thereby more suited to real-time processing. In the present assessment, we express the computational requirements in terms of numbers of complex multiplications and additions (including subtractions), in the hope that the quantity, when considered with other factors, will help in the refinement of the overall processing configuration. It is assumed in the following that the matched filters, or the deramp references, and the phase-magnitude correction factors are pre-computed, and that the effort required to synthesize them is small compared with the actual processing of the data.

Unless otherwise redefined, the symbols used in the following evaluations are the same as those used in their respective descriptions given earlier. In order to use the FFT algorithm, the variables N_T, N_ξ and N need to be power-of-two integers.

9.1 Computational Requirements for Single Look Cases without Range Curvature and Cubic Phase Term Compensation

The computational requirements for the three pulse compression techniques are evaluated. It is assumed that the complications due to range curvature and the cubic phase term are negligible.

a) Computational requirement for the matched filtering approach (via fast convolution)

For complex multiplications

-Forward FFT on a set of N_T input data	$\frac{N_T}{2}\log_2 N_T$
-Matched filtering with windowing included	N_T
-Inverse FFT on N_T matched filtered data	$\frac{N_T}{2}\log_2 N_T$
-Total number of complex multiplications	$N_T\log_2 N_T+N_T$

For Complex Additions

-Forward FFT on N_T input data	$\frac{N_T}{2}\log_2 N_T$
-Inverse FFT on N_T matched filter data	$\frac{N_T}{2}\log_2 N_T$
-Total number of complex additions	$N_T\log_2 N_T$
-Matched filter length in time domain	M
-Valid output data length	N_T-M
-Number of complex multiplications per valid output point	$\frac{\log_2 N_T+1}{1-\frac{M}{N_T}}$
-Number of complex additions per valid output point	$\frac{\log_2 N_T}{1-\frac{M}{N_T}}$

b) Computational requirement for the step transform

Let ξ be the sub-aperture overlap and N_ξ be the number of sub apertures, so that $N_\xi^2 = \frac{1}{(1-\xi)(\text{FM rate})\Delta^2}$.

For cases with $\xi>0.6$
For complex multiplications

-Deramp input signal with N_ξ sub-apertures and use N_ξ data points for each sub-aperture	N_ξ^2
-First FFT for one sub-aperture	$\frac{N_\xi}{2}\log_2 N_\xi$
-Do the above for N_ξ sets of sub-aperture FFTs which results in a $N_\xi X N_\xi$ matrix containing N_ξ complete diagonals	$\frac{N_\xi^2}{2}\log_2 N_\xi$
-Number of multiplications to form one complete diagonal	$\frac{N_\xi}{2}\log_2 N_\xi + N_\xi$
-Phase correction and windowing on one diagonal	N_ξ
-Second FFT (along diagonal)	$\frac{N_\xi}{2}\log_2 N_\xi$
-Total number of complex multiplications (not including the final amplitude correction)	$N_\xi \log_2 N_\xi + 2N_\xi$

For complex additions

-Number of additions in the first and second FFTs that are required to form the output from one diagonal	$N_\xi \log_2 N_\xi$
-Number of valid data produced from one FFT along the diagonal	$(1-\xi)N_\xi$
-Number of complex multiplications per valid output point	$\frac{\log_2 N_\xi + 2}{1-\xi}$
-Number of complex additions per valid output point	$\frac{\log_2 N_\xi}{1-\xi}$

For cases with $0.2<\xi<0.6$

These cases require two sets of sub-aperture references, see Section 8.2.2 for details.

For complex multiplications

-Deramp input signal with $2N_\xi$ sub-apertures and use N_ξ data points for each sub-aperture.	$2N_\xi^2$
-First FFT for one sub-aperture	$\frac{N_\xi}{2}\log_2 N_\xi$
-Do the above for $2N_\xi$ sets of sub-aperture FFTS which results in $2N_\xi$ X N_ξ matrix containing N_ξ complete diagonals	$\frac{2N_\xi^2}{2}\log_2 N_\xi$
-Number of multiplications to form one complete diagonal	$N_\xi\log_2 N_\xi+2N_\xi$
-Phase correction and windowing on one diagonal	$2N_\xi$
-Second FFT (along diagonal)	$\frac{2N_\xi}{2}\log_2 2N_\xi$ $=N_\xi(1+\log_2 N_\xi)$
-Total number of complex multiplications (not including the final amplitude correction)	$2N_\xi\log_2+5N_\xi$

For complex additions

-Number of additions in the first and second FFTs that are required to form the output from one diagonal	$N_\xi\log_2 2N_\xi^2$ $=2N_\xi\log_2 N_\xi+N_\xi$
-Number of valid data produced from one FFT along the diagonal	$(1-\xi)N_\xi$
-Number of complex multiplications per valid output point	$\frac{2N_\xi\log_2 N_\xi+5}{1-\xi}$

-Number of complex additions per valid output point

$$\frac{2\log_2 N_\xi + 1}{1-\xi}$$

c) Computational requirements for the spectral analysis method

In the present treatment, we assume that the guard band, β, and the DFT length, N, depend on the required resolution, and that they are sufficiently large that the number of processing columns within a parallelogram is not less than two (see for example, Figure 38). The number of processing columns required for each parallellogram can be calculated, by using (82), as

$$L = \text{INTEGER}\left[\frac{N}{(1-\beta-\frac{\sigma N k}{B^2})N}+1\right],$$

$$= \text{INTEGER}\left[\frac{1}{1-\beta-\frac{\sigma N k}{B^2}}+1\right].$$

Let N_p be the recorded data length before presumming, therefore

$$N_p = BT - \frac{B^2}{k}.$$

For complex multiplications

-Deramp input signal (including windowing to form L processing columns within a parallelogram) LN

-FFTs for L processing columns $L\frac{N}{2}\log_2 N$

-Total number of complex multiplications for one parallelogram $\frac{LN}{2}\log_2 N + NL$

For complex additions

-Number of additions in the L FFTs $\frac{LN}{2}\log_2 N$

-Number of valid data given by one parallelogram N

-Number of complex multiplications per valid data output

$$\frac{L}{2}\log_2 N+L$$

-Number of complex additions per valid data output

$$\frac{L}{2}\log_2 N$$

9.1.1 **Examples for Cases without Range Curvature and Cubic Phase Term Compensation**

The following examples are intended to provide some insight into the computational requirements of the processingalgorithms. Two cases are given, both have a presum factor of 8.

Examples for typical resolution (3.5m)

Parameters:

-Raw data length	16,384
-Data length after presum, N_T	2,048
-Slant range	100 km
-Matched filter length, M (>Time-bandwidth product in cycles)	557

a) Matched filtering approach

Number of complex multiplications per valid data point

$$\frac{(\log_2 2048)+1}{1-\frac{557}{2048}}$$

$$= \underline{16.5}$$

Number of complex additions

$$\frac{\log_2 2048}{1-\frac{557}{2048}}$$

$$= \underline{15.1}$$

b) Step transform (assuming (8.21) is satisfied)

The computational requirement depends heavily on the FM rate and the sampling interval as given in (8.21), or equivalently, the oversampling factor. According to the Nyquist criterion, $B\Delta<1$, we have

$$N_\xi > \frac{TB}{1-\xi}$$

and

$$\leq 1 - \frac{TB}{N\xi^2}$$

where TB is the time-bandwidth product. Setting TB = 557, ξ = 0.6, we have,

$$N\xi > \sqrt{\frac{557}{0.4}} = 37.3,$$

we choose $N\xi$ = 64, and

$$\xi \leq 1 - \frac{557}{(64)^2}$$

$$\leq 0.864.$$

which gives the number of overlapped points = 27.6 = 27, ξ is recalculated as 0.844.

To calculate the computational requirement with ξ = 0.844, we have

-Number of complex multiplications per valid data point $\frac{\log_2 64+2}{1-0.844}$

$$= \underline{52}$$

-Number of complex additions per valid data point $\frac{\log_2 64}{1-0.844}$

$$= \underline{39}$$

c) <u>The spectral analysis method</u>

Since N = 557, we choose N = 1024, this makes the resultant resolution proportionally finer.

The number of processing columns is

$$L = \text{INTEGER}\left[\frac{1}{1.-0.4 - \frac{0.4 \times 1024}{16384}} + 1\right], \text{ where } \beta=0.4,\ 0=0.4,$$

$$= \text{INTEGER}\,[2.7],$$

$$= 2.$$

-Number of complex multiplications per valid data point

$$\frac{2}{2}\log_2 1024+2$$

$$= \underline{12}$$

-Number of complex additions per valid data point

$$\frac{2}{2}\log_2 1024$$

$$= \underline{10}$$

Examples for fine resolution (1.75 m)

Parameters:

-Raw data length 16,384

-Data length after presum 2,048

-Slant range 100 km

-Matched filter length 1,116

a) **Matched filtering approach**

-Number of complex multiplications per valid data point

$$\frac{(\log_2 2048)+1}{1-\frac{1116}{2048}}$$

$$= \underline{26.4}$$

-Number of complex additions per valid data point

$$\frac{\log_2 2048}{1-\frac{1116}{2048}}$$

$$= \underline{24.2}$$

b) **Step transform (assuming (102) is satisfied)**

$$N_\xi^2 \geq \frac{TB}{1-\xi}$$

$$N_\xi \geq \sqrt{\frac{1116}{0.4}}$$

$$\geq 52.8$$

choose $N_\xi = 64$

$$\xi < 1 - \frac{TB}{N_\xi^2}$$

≤ 0.728

which gives the number of overlapped points = 2.33 ≈ 23. ξ is recalculated as 0.719.

To calculate the computational requirement with $\xi = 0.719$, we have

-Number of complex multiplications per valid data point

$$= \frac{\log_2 64+2}{1-0.719}$$

$$= \underline{29}$$

-Number of complex additions per valid data point

$$= \frac{\log_2 64}{1-0.719}$$

$$= \underline{22}$$

c) Spectral analysis method

N = 1116
choose N = 2048
The number of processing columns is

$$L = \text{INTEGER}\left[\frac{1}{1-0.4-\frac{0.4\times 2048}{16384}} + 1\right], \text{ with } \beta = 0.4,\ \sigma = 0.4.$$

$$= \text{INTEGER}\,[2.8]$$

$$= 2$$

-Number of complex multiplications per valid data point

$$= \frac{2}{2}\log_2 2048+2$$

$$= \underline{13}$$

-Number of complex additions per valid data point

$$= \frac{2}{2}\log_2 2048$$

$$= \underline{11}$$

In practice, the matched filtering method and the step transform require the raw data be presummed before being processed. The presumming can be accomplished by using a two-stage low-pass filter with 15 coefficients each. Therefore, an additional 30 multiplications and additions per input data point should be added on top of the computation requirements. In the case of the spectral analysis method, the presumming process is done by selectively deramping and windowing the desired

processing column, thus no additional presumming is required. However, the output product is not as well controlled, with respect to aliased energy, as the cases in which a presumming filter is used.

9.2 Computational Requirements for Single Look Cases with Range Curvature Compensation

The above computational evaluations are now extended to include cases with range curvature. The spectral analysis method is not included since it cannot accommodate range curvature.

a) Computational requirements for the matched filtering approach (via fast convolutional) with range curvature compensation

The range curvature compensation is accomplished by interpolation, in the range dimension, along the curvature. A four-point interpolator is assumed here. The procedure has been described in Section 6.2

For complex multiplications

-4-point interpolator $4N_T$

-Other computations $N_T \log_2 N_T + N_T$

-Total number of complex multiplications $N_T \log_2 N_T + 5N_T$

For complex additions

-4-point interpolator $3N_T$

-Other computations $N_T \log_2 N_T$

-Total number of complex additions $N_T \log_2 N + 3N_T$

-Valid output data length $N_T - M$

-Number of complex multiplications per valid data output point

$$\frac{\log_2 N_T + 5}{1 - \frac{M}{N_T}}$$

-Number of complex additions per valid data output point

$$\frac{\log_2 N_T + 3}{1 - \frac{M}{N_T}}$$

b) Computational requirements for the step transform with range curvature compensation

The range curvature compensation is accomplished by interpolation of the corresponding elements in the processing matrices from different ranges, as described in Section 8.6. A four-point interpolator is assumed here also.

For cases with $\xi > 0.6$
For complex multiplications

-Interpolation to form one complete diagonal $4N_\xi$

-Other computations $N_\xi \log_2 N_\xi + 2N_\xi$

-Total number of complex multiplications $N_\xi \log_2 N_\xi + 6N_\xi$

For complex additions

-Interpolation to form one complete diagonal $3N_\xi$

-Other computations $N_\xi \log_2 N_\xi$

-Total number of complex additions $N_\xi \log_2 N_\xi + 3N_\xi$

-Number of valid data given by one diagonal FFT $(1-\xi)N_\xi$

-Number of complex multiplications per valid data output point

$$\frac{\log_2 N_\xi + 6}{1-\xi}$$

-Number of complex additions per valid data output point

$$\frac{\log_2 N_\xi + 3}{1-\xi}$$

For cases with $0.2 < \xi < 0.6$

For complex multiplications

-Interpolation to form one complete diagonal	$8N_\xi$
-Other computations	$2N_\xi \log_2 N_\xi + 5N_\xi$
-Total number of complex multiplications	$2N_\xi \log_2 N_\xi + 13N_\xi$

For complex additions

-Interpolation to form one complete diagonal	$6N_\xi$
-Other computations	$2N_\xi \log_2 N_\xi + N_\xi$
-Total number of complex additions	$2N_\xi \log_2 N_\xi + 7N_\xi$
-Number of valid data given by one diagonal FFT	$(1-\xi)N_\xi$
-Number of complex multiplications per valid data output point	$\frac{2\log_2 N_\xi + 13}{1-\xi}$
-Number of complex additions per valid data output point	$\frac{2\log_2 N_\xi + 7}{1-\xi}$

9.3 Computational Requirements for the Coherent Multi-look Cases with Range Curvature and Cubic Phase Compensations

The computational requirements for the severe combination of range curvature, cubic phase, and high resolution are encompassed in the following.

a) Computational requirements for the multi-look matched filtering approach (via fast convolution)

No additional computation is required for the cubic phase compensation, since the cubic phase term can be pre-calculated and embedded in the matched filter when it is synthesized. If sub-aperture summation is performed in the time-domain, the inverse Fourier transform of each sub-aperture has to be the same length as the overall original data length (N_T). This is accomplished by appending zeroes to the unoccupied portion of a sub-aperture spectrum. If sub-aperture summation is performed in the frequency domain during compression, the sub-aperture spectra are concatenated (except in the transition bands) to the original bandwidth, before the inverse Fourier transform is taken. Thus the amount of computation is very much the same as that for the single look case. In the following analysis, post-compression sub-aperture summation in the time domain is assumed.

For complex multiplications

-Forward FFT on a set of N_T input data	$\frac{N_T}{2}\log_2 N_T$
-Interpolation for all sub-apertures (with a 4-point interpolator)	$\approx 4N_T$
-Matched filtering with extraction filter and windowing for L sub-apertures	$\approx N_T$
-L inverse FFTs with N_T data	$\frac{LN_T}{2}\log_2 N_T$
-Total number of complex multiplications	$\frac{N_T(L+1)}{2}\log_2 N_T + 5N_T$

For complex additions

-Forward FFT on a set of N_T input data	$\frac{N_T}{2}\log_2 N_T$
-Interpolation for all sub-apertures	$\approx 3N_T$
-L inverse FFTS with N data each	$\frac{LN_T}{2}\log_2 N_T$
-Coherent summation of L sub-apertures in the spatial domain	$(L-1)N_T$

-Total number of complex additions

$$\frac{N_T(L+1)}{2}\log_2 N_T + (L+2)N_T$$

-Valid output data length

$$N_T - M$$

-Number of complex multiplications per valid output point

$$\frac{\frac{(L+1)}{2}\log_2 N_T + 5}{1-\frac{M}{N_T}}$$

-Number of complex additions per

$$\frac{\frac{(L+1)}{2}\log_2 N_T + L + 2}{1-\frac{M}{N_T}}$$

b) Computational requirements for the step transform with range curvature and cubic phase

If the cubic phase term is significant compared to the quadratic phase term, then the data array for the second DFT will no longer lie along the diagonal of the array. This phenomenon has been described in Section 8.6. To remedy this, interpolation is used to straighten out the curvature of the diagonal, before the computation of the second DFT. In the following analysis, we assume that all the diagonal data are interpolated using a four-point interpolator.

For cases with $\xi > 0.6$

For complex multiplications

-Interpolation for the diagonal data $4N_\xi$

-Other calculations (including range curvature computation) $N_\xi \log_2 N_\xi + 6N_\xi$

-Total number of complex multiplications $N_\xi \log_2 N_\xi + 10N_\xi$

For complex additions

-Interpolation for the diagonal data $3N_\xi$

-Other calculations (including range curvature compensation) $N_\xi \log_2 N_\xi + 3N_\xi$

-Total number of complex additions $N_\xi \log_2 N_\xi + 6N_\xi$

-Number of valid data given by one diagonal FFT $(1-\xi)N_\xi$

Number of complex multiplications per valid data output point $\dfrac{\log_2 N_\xi + 10}{1-\xi}$

Number of complex additions per valid data output point $\dfrac{\log_2 N_\xi + 6}{1-\xi}$

For cases with $0.2<\xi<0.6$

For complex multiplications

-Interpolation for the diagonal data $8N_\xi$

-Other calculation (including range curvature computation) $N_\xi \log_2 2N_\xi^2 + 12N_\xi$

-Total number of complex multiplications $N_\xi \log_2 2N_\xi^2 + 20N_\xi$

For complex additions

-Interpolation for the diagonal data $6N_\xi$

-Other calculations (including range curvature compensation) $N_\xi \log_2 2N_\xi^2 + 6N_\xi$

-Total number of complex additions $N_\xi \log_2 2N_\xi^2 + 12N_\xi$

-Number of valid data given by one diagonal FFT $(1-\xi)N_\xi$

-Number of complex multiplications per valid data output point $\dfrac{\log_2 2N_\xi^2 + 20}{1-\xi}$

-Number of complex additions per valid data output point $\dfrac{\log_2 2N_\xi^2 + 12}{1-\xi}$

10. SUMMARY

A general theory of coherent sub-aperture processing for SAR, has been presented. The problems encountered in applying a one-dimensional matched filter on SAR azimuth data have been reviewed and characterized. A piecewise solution for the one-dimensional matched filter has been formulated and it has been shown how this solution can be used to combat the processing problems without resorting to memory intensive two-dimensional filtering. The solution has been thoroughly tested by computer simulations, and an error analysis of the effects of the phase and amplitude distortions, caused by the piecewise approximation, has been given. In addition, the basic deramping techniques have been overviewed, and the step transform technique discussed in detail. In particular, the step transform method has been extended to include compensation for phase errors and range curvature. Finally, the computational requirements for different cases and processing techniques have been evaluated.

11. ACKNOWLEDGEMENT

This work was supported by the Department of National Defence, Research and Development Branch under Project No. 33C06.

12. REFERENCES

[1] J.R. Klauder, A.C. Price, S. Darlington, and W.J. Albersheim, "The Theory and Design of Chirp Radars", BSTJ, Vol. XXXIX, No. 4, pp.745-809, July 1960.

[2] M.R. Vant and G.E. Haslam, "A Theory of 'Squinted' Synthetic Aperture Radar", CRC Report, No. 1339, November 1980.

[3] A. Papoulis, "Signal Analysis", p.271, McGraw-Hill, New York, 1977.

[4] F.J. Harris, "On the Use of Windows for Harmonic Analysis with Discrete Fourier Transform", Proceedings of the IEEE, Vol. 66, No.1, pp.51-83, January 1978.

[5] S. Shlien, "Geometric Correction Registration and Resampling of Landsat Imagery", Canadian Journal of Remote Sensing, Vol.5, No.1, pp.74-89, May 1979.

[6] R.P. Perry and L. Martinson, "Radar Matched Filtering", in Chapter 11, "Radar Technology", edited by E. Brookner, pp.163-169, Artech House, Dedham, MA, 1977.

[7] L. Martinson, "A Programmable Digital Processor for Airborne Radar", pp.186-191, IEEE International Radar Conference, 1975.

[8] R.P. Perry and H.W. Kaiser, "Digital Step Transform Approach to Airborne Radar Processing", pp.280-287, NAECON, 1973.

[9] C. Elachi, T. Bicknell, R.L. Jordan, and C. Wu, "Spaceborne Synthetic Aperture Imaging Radars: Applications, Techniques, and

Technology", Proceedings of the IEEE, Vol.70, No. 10, pp.1174-1209, October 1982.

[10] "The Design of a Digital Breadboard Processor for the RSA Remote Sensing Satellite Synthetic-Aperture Radar", Final Report, MacDonald, Dettwilar & Associaters Ltd., Richmond, B.C., July 1981.

[11] J.R. Bennett, I.G. Cumming, and R.A. Deane, "The Digital Processing of Seasat Synthetic-Aperture Radar Data", IEEE International Radar Conference Proceedings, pp.168-175, 1980.

[12] L.R. Rabiner, and B. Gold, "Theory and Application of Digital Signal Processing", Prentice-Hall, New Jersey, 1975.

APPENDIX A

Polynomial Truncations of the Taylor Expansion of the Radar Received Signal

To illustrate that the quartic (and higher order) phase terms are insignificant, we go through the following numerical example.

We assume a high squint angle, high resolution case, which represents the worst possible operating conditions:

Resolution (ρ)	=	1.358 m,
Wavelength (λ)	=	0.0321 m ,
Squint angle (η_o)	=	6°,
Slant range (r_o)	=	100 km.

The half aperture length is given by

$$s_{max} = \frac{\lambda r_o}{4\rho \sin\eta_p}.$$

With these parameters, the quadratic, cubic and quartic phase terms at the end of the full aperture are given by

$$\text{quadratic phase} = \frac{4\pi}{\lambda} a_2 s_{max}^2,$$

$$= \frac{\pi\lambda r_o}{8\pi^2},$$

$$= \underline{31.1\pi \text{ rad}},$$

$$\text{cubic phase} = \frac{4\pi}{\lambda} a_3 s_{max}^3,$$

$$= \frac{\pi\lambda^2 r_p}{32\rho^3 \tan\eta_p},$$

$$= \underline{12.2\pi \text{ rad}},$$

$$\text{quartic phase} = \frac{4\pi}{\lambda} a_4 s_{max}^4,$$

$$= \frac{\pi\lambda^3 r_p}{512\rho^4}\left(\frac{4}{\tan^2\eta_p} - 1\right),$$

$$= \underline{0.686\pi \text{ rad.}}$$

In practice, the overall phase error, with a heavily weighted aperture, should not be more than 0.75π rad. It can be seen then, that even in this extreme case, the contribution due to the quartic phase term can be ignored.

APPENDIX B

Azimuth Resolution

The azimuth resolution is mainly determined by the second order phase term given in (3.2).

Let

$$\theta = \frac{4\pi}{\lambda} a_2 s^2.$$

The Doppler bandwidth (BW) is given by

$$BW = \frac{1}{2\pi} \frac{d\theta}{ds}\Big|_{s=N_p\Delta S_A},$$

$$= \frac{4}{\lambda} a_2 N_p \Delta S_A,$$

$$= \frac{2\sin\eta_F}{\lambda r_F} N_p \Delta S_A,$$

where all variables are defined in Section 3.

The resolution, ρ', in the flight direction is given by

$$\rho' = \frac{1.4}{BW} = \frac{1.4\lambda r_F}{2N_p\Delta S_A \sin^2\eta_F},$$

where the factor of 1.4 is due to the broadening effect of the Hamming window.

The azimuth resolution in the direction perpendicular to the antenna pointing vector is

$$\rho = \rho'\sin\eta_F = \frac{1.4\lambda r_F}{2N_p\Delta S_A \sin\eta_F}.$$

Unclassified

Security Classification

DOCUMENT CONTROL DATA - R & D

(Security classification of title, body of abstract and indexing annotation must be entered when the overall document is classified)

1. ORIGINATING ACTIVITY Communications Research Centre
P.O.Box 11490, Station H
Ottawa, Ontario, Canada K2H 8S2

2a. DOCUMENT SECURITY CLASSIFICATION
Unclassified

2b. GROUP

3. DOCUMENT TITLE

Coherent Sub-Aperture Processing Techniques for Synthetic Aperture Radar.

4. DESCRIPTIVE NOTES (Type of report and inclusive dates)
CRC Report, 1982 - 1983.

5. AUTHOR(S) (Last name, first name, middle initial)
WU, Kam Hung
VANT, Malcolm R.

6. DOCUMENT DATE
January 1984.

7a. TOTAL NO. OF PAGES
99

7b. NO. OF REFS
12

8a. PROJECT OR GRANT NO.
Defence R&D Program Task No. 33C06.

8b. CONTRACT NO.

9a. ORIGINATOR'S DOCUMENT NUMBER(S)
CRC Report No. 1368.

9b. OTHER DOCUMENT NO.(S) (Any other numbers that may be assigned this document)

10. DISTRIBUTION STATEMENT
Approved for Public Release; Distribution Unlimited.

11. SUPPLEMENTARY NOTES

12. SPONSORING ACTIVITY
Directorate of Radar Research
Communications Research Centre for CRAD
under the Defence R&D Program in DOC.

13. ABSTRACT

Coherent sub-aperture techniques for processing synthetic aperture radar (SAR) signals are described. The techniques involve partitioning the full aperture data, in either the time or the frequency domain. Each partition or sub-aperture is then processed independently by the application of a conventional matched filter, or the equivalent. The low resolution images formed by this process are then coherently recombined to form a full resolution image. Such a processing scheme has the advantage of high computational efficiency and provides the capability for the compensation of low frequency spurious motions, even when the SAR is operating in a highly squinted, high resolution imaging situation.

A detailed description of two coherent sub-aperture techniques namely, the multi-look matched filtering approach and the step transform, are presented. The techniques are characterized and the normal computational requirements are evaluated. Computer simulations, which were performed to vertify the feasibility of the processing schemes, are also described.

DSIS
77-465

Security Classification

KEY WORDS

Synthetic Aperture Radar
Sub-Aperture Processing
Coherent Processing

INSTRUCTIONS

1. **ORIGINATING ACTIVITY**: Enter the name and address of the organization issuing the document.

2a. **DOCUMENT SECURITY CLASSIFICATION**: Enter the overall security classification of the document including special warning terms whenever applicable.

2b. **GROUP**: Enter security reclassification group number. The three groups are defined in Appendix 'M' of the DRB Security Regulations.

3. **DOCUMENT TITLE**: Enter the complete document title in all capital letters. Titles in all cases should be unclassified. If a sufficiently descriptive title cannot be selected without classification, show title classification with the usual one-capital-letter abbreviation in parentheses immediately following the title.

4. **DESCRIPTIVE NOTES**: Enter the category of document, e.g. technical report, technical note or technical letter. If appropriate, enter the type of document, e.g. interim, progress, summary, annual or final. Give the inclusive dates when a specific reporting period is covered.

5. **AUTHOR(S)**: Enter the name(s) of author(s) as shown on or in the document. Enter last name, first name, middle initial. If military, show rank. The name of the principal author is an absolute minimum requirement.

6. **DOCUMENT DATE**: Enter the date (month, year) of Establishment approval for publication of the document.

7a. **TOTAL NUMBER OF PAGES**: The total page count should follow normal pagination procedures, i.e., enter the number of pages containing information.

7b. **NUMBER OF REFERENCES**: Enter the total number of references cited in the document.

8a. **PROJECT OR GRANT NUMBER**: If appropriate, enter the applicable research and development project or grant number under which the document was written.

8b. **CONTRACT NUMBER**: If appropriate, enter the applicable number under which the document was written.

9a. **ORIGINATOR'S DOCUMENT NUMBER(S)**: Enter the official document number by which the document will be identified and controlled by the originating activity. This number must be unique to this document.

9b. **OTHER DOCUMENT NUMBER(S)**: If the document has been assigned any other document numbers (either by the originator or by the sponsor), also enter this number(s).

10. **DISTRIBUTION STATEMENT**: Enter any limitations on further dissemination of the document, other than those imposed by security classification, using standard statements such as:

    (1) "Qualified requesters may obtain copies of this document from their defence documentation center."

    (2) "Announcement and dissemination of this document is not authorized without prior approval from originating activity."

11. **SUPPLEMENTARY NOTES**: Use for additional explanatory notes.

12. **SPONSORING ACTIVITY**: Enter the name of the departmental project office or laboratory sponsoring the research and development. Include address.

13. **ABSTRACT**: Enter an abstract giving a brief and factual summary of the document, even though it may also appear elsewhere in the body of the document itself. It is highly desirable that the abstract of classified documents be unclassified. Each paragraph of the abstract shall end with an indication of the security classification of the information in the paragraph (unless the document itself is unclassified) represented as (TS), (S), (C), (R), or (U).

    The length of the abstract should be limited to 20 single-spaced standard typewritten lines; 7½ inches long.

14. **KEY WORDS**: Key words are technically meaningful terms or short phrases that characterize a document and could be helpful in cataloging the document. Key words should be selected so that no security classification is required. Identifiers, such as equipment model designation, trade name, military project code name, geographic location, may be used as key words but will be followed by an indication of technical context.